Institute of Process Engineering
Chinese Academy of Sciences

KT-IPE PhD Book 2018

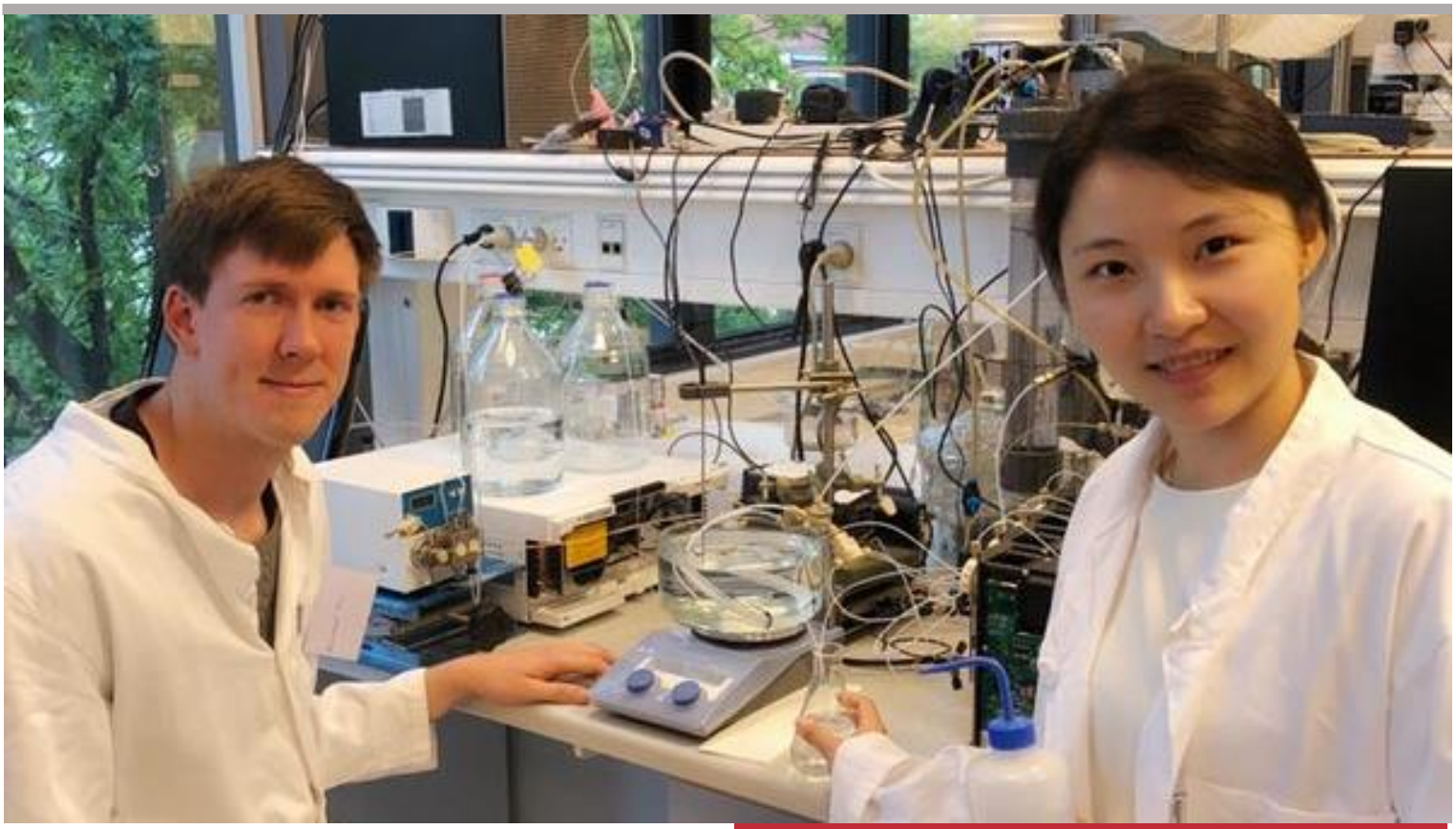

Editors:

Professor Kim Dam-Johansen
Head of Department of Chemical and Biochemical Engineering, DTU

Professor Suojiang Zhang
Director of Institute of Process Engineering, CAS

Professor Weigang Lin

DTU Chemical Engineering
Department of Chemical and Biochemical Engineering

序言

中国科学院过程工程研究所（IPE）是国内独具特色的从事过程工程科学研究的综合性研究所，历经六十年的建设与发展，研究所在介科学、绿色化学过程、生物质工程和分离技术以及生物材料等领域积累了丰富的经验，取得丰硕的成果。与此同时，研究所与众多世界知名院校及化工企业开展合作 ，积极推动科研技术成果的转移转化。丹麦科技大学（DTU）是欧洲顶尖的理工大学之一，也是北欧地区最好的工科大学，在世界范围内享有盛誉，是丹麦培养高级工程技术人员的最主要学府。多年来，双方紧密合作、优势互补，为推动中丹两国的科研教育事业发展而不懈努力，并取得了显著成效。

为顺应科研教育全球化发展趋势，2013 年起，双方依托中国科学院大学、中丹中心和中丹学院平台共同开办了化工与生物化工研究生课程，已在可再生能源领域培养出五十余名硕士和十余名博士。在此基础上，IPE 和 DTU 深入地探索了科研合作模式、拓宽了科研合作范围，开创了以联合培养博士生方式加强科研合作的新模式，并取得了一系列有价值的科研成果。现将合作以来联合培养博士项目情况汇编成册，包括正在进行或已经结题的 28 个项目，内容涵盖化工、能源、环境、生物化工、材料、纳米等多个领域。

教育是一项面向未来的事业，而科学研究是造福全人类的伟大工程。感谢中国科学院大学、中丹中心、中丹学院的各级领导对 CBE 项目的关心和帮助，使项目 5 年来顺利运行。感谢丹麦科技大学的信任与支持，使双方的合作亲密无间，感谢参与项目的中丹双方教师和研究生的努力探索和辛勤付出。我相信，随着双方科研教育合作的继续深入，我们一定会培养出一大批具有国际视野和国际竞争力的优秀科研人才，并在未来取得更多具有世界引领性的科研成果。

我们欢迎更多的海内外优秀学生加入我们的交流项目，为中丹两国之间的科研教育事业发挥更积极的作用!

张锁江

中国科学院院士

中国科学院过程工程研究所所长

Preface

Institute of Process Engineering (IPE), Chinese Academy of Sciences is one of the leading institution on chemical engineering in China. With 60 years development, IPE has accumulated substantial research experience and achievement on Meso-Science, Green Chemical Engineering, Biochemical Engineering, Mineral Process as well as Environment Technology and Engineering. At the same time, we actively cooperate with well-known chemical enterprises to promote technology transfer and achievement transformation. The Technical University of Denmark (DTU) is one of the European top universities on science and technology as well as the best university on engineering in northern Europe. DTU is the most important institution to train engineers in Denmark. For many years, IPE and DTU have been closely working together and have made great efforts to promote education cooperation between both sides.

To comply with the rapid development of the globalization of scientific research and higher education, IPE and DTU have been jointly working on the master program in the field of Chemical and Biochemical Engineering (CBE) under the framework of Sino-Danish Center (SDC) for education and research. Since 2013, more than 50 master students and more than 10 PhD students have been and graduated from UCAS and Sino-Danish Center. Moreover, IPE and DTU applied several new ways of cooperative PhD projects which has broadly extended the range of their cooperation and trained many excellent young researchers who have made a series of valuable scientific research achievements. In this brochure, we compiled their main cooperation achievement on education and research, including 28 outstanding dissertation covering chemical, energy, environmental, biological, chemical, material, and other fields.

Education is a future career, while scientific research benefits all mankind. Thanks to the support from Sino-Danish College of UCAS and Sino-Danish center, the project CBE has been smoothly carried out for 5 years. We appreciate the trust and support from DTU, which make the close cooperation of both sides a great success. I would like to thank all the involved professors and colleagues for their hard work and contribution on this project. I believe that with the further of our collaboration, we will cultivate a large number of talents with international vision and competitiveness and make more leading research achievement in the future.

We sincerely welcome more and more excellent students to join our joint projects and contribute to the education and research in China and Denmark.

Suojiang Zhang
Academician of Chinese Academy of Sciences
Direactor of Institute of Process Engineering (IPE)
Chinese Academy of Sciences

Preface

At Department of Chemical and Biochemical Engineering, Technical University of Denmark, it is a tradition that a PhD yearbook is published each year to describe the current PhD project. Since DTU Chemical Engineering and Institute of Process Engineering (IPE) decided to participate in the cooperation in the Sino-Danish Center for Research and Education (SDC), collaborative PhD projects were also initiated in different formats: SDC PhD projects supported by SDC, CSC PhD projects supported by China Scholarship Council, and joint KT-IPE PhD projects supported by both organizations. The cooperation between the two organizations through the collaborative PhD projects is very successful. Up to now, 28 collaborative PhD projects have started, 8 have completed. In this book, you can read about all collaborative PhD projects, which show the close cooperation between DTU Chemical Engineering and Institute of Process Engineering in many disciplines.

We hope you will find the book interesting, and we invite all readers to contact us for further details.

Kim Dam-Johansen
Professor
Head of Department of Chemical and Biochemical Engineering (KT)
Technical University of Denmark

Contents

Božidar Aničić

Phone: +4525 2837
E-mail: boza@kt.dtu.dk

Type: SDC (KT)
Supervisors: Kim Dam-Johansen
Weigang Lin
Hao Wu
Wei Wang, Bona Lu, IPE, China

PhD Study
Started: August 2015
Completed: July 2018

Agglomeration in Fluidized Bed at High Temperature

Abstract

The PhD project focuses on agglomeration in fluidized bed combustion of biomass. Bed agglomeration, as one of the main operational problems, is studied in order to understand the fundamental mechanisms, and to develop modelling tools and countermeasures that can be applied to minimize the problem.

Introduction

Fluidized bed combustion is a promising technology for efficient and flexible utilization of biomass to produce heat and power. However, bed agglomeration is one of the major operational problems that can influence bed hydrodynamics, change fluidization regime, and in severe cases cause defluidization [1]. It is primarily caused by interactions between bed material and biomass ash [2].

Objectives

The objectives of the PhD project:

- Understanding the fundamental bed agglomeration mechanism during biomass combustion at different operation conditions.
- Develop modeling tools to analyze agglomeration.
- Propose and evaluate the countermeasures to reduce bed agglomeration tendency.

Methodology

A small-scale fixed bed reactor and a thermogravimetric analyzer (TGA) are used to investigate the reactions between model potassium salts and model bed material (silica sand) under various conditions. Moreover, a lab-scale fluidized bed reactor is applied to study defluidization induced by model potassium compounds, and combustion of different types of biomass. The agglomerate samples are characterized by scanning electron microscopy coupled with energy-dispersive x-ray spectroscopy (SEM-EDX) and x-ray diffraction (XRD). In addition, CFD simulation of particle segregation in a fluidized bed is performed in order to evaluate the impact of continuous agglomerates formation on bed hydrodynamics.

Progress

Reaction between K_2CO_3 and silica sand

The interactions between sand particles and model potassium compounds (KCl, K_2CO_3, K_2SO_4) have been studied in the fixed bed reactor. It was found that K_2CO_3 is able to react with silica sand forming agglomerates, and the other potassium species acts as physical glue to bind silica sand particles. Thus, the reaction between K_2CO_3 and silica sand was further investigated in the TGA. Figure 1 shows K_2CO_3 conversion rate under different conditions.

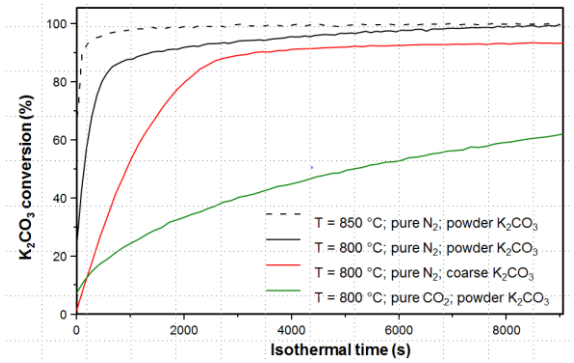

Figure 1: *K_2CO_3 conversion under different operating conditions. K_2CO_3:sand ratio = 0.03:1 wt.:wt.; premixing of reactants; 500 K/min heating rate.*

The results show that the reaction rate increases with increasing temperature. With a large K_2CO_3 particle size the initial reaction rate was significantly reduced, and the final K_2CO_3 conversion degree reached 0.9. The presence of CO_2 strongly inhibited the reaction rate and reduced the final conversion degree. Based on the SEM-EDX results a plausible reaction mechanism is proposed. The reaction starts at the contact points between reactants and it is initially dominated by surface diffusion of the salt molecules into the silica sand surface. This leads to the formation of a molten

thin product layer that may cover complete sand surface. The reaction proceeds further by diffusion through the formed product layer.

Defluidization

Defluidization induced by different potassium species (KCl, K_2SO_4, K_2CO_3 and $K_2Si_4O_9$) and their mixtures has been investigated in a lab-scale fluidized bed reactor. K-species were added to a sand bed and the reactor was heated up at a constant heating rate of 10 K/min, and with a constant gas flow until defluidization occurs (indicated by a sudden decrease of pressure drop over the bed). The temperature, at which defluidization occurs, is defined as defluidization temperature (DT). Figure 2 presents selected experimental results.

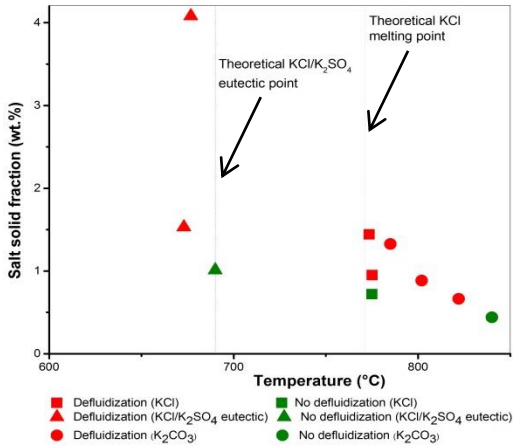

Figure 2: *Defluidization temperature as a function of potassium content*

A minimum weight ratio of salt to sand necessary for defluidization is 0.95 and 1.53 wt.% when adding KCl and KCl/K_2SO_4 eutectic mixture up to 800°C, respectively. In these cases, DT corresponded to either KCl melting temperature (771 °C) or KCl/K_2SO_4 eutectic point (690 °C). SEM-EDX analyses of the agglomerate samples reveal that the sand particles are covered by molten K-salts. However, addition of K_2CO_3 results in defluidization induced by reaction between K_2CO_3 and silica sand, as indicated by CO_2 release. The formation of potassium silicates is indicated by SEM-EDX analyses. The minimum salt content is 0.72 wt.% and the corresponding DT is 822 °C. As the salt content is increased to 1.5 wt.% DT decreases to 785 °C. When $K_2Si_4O_9$ is added, no defluidization is observed up to 850 °C for a high silicate content of 9.8 wt.%. The results of this work imply that defluidization can be induced by both, molten K-salts with low-viscosity and high-viscous K-silicates formed in reaction between potassium carbonate and sand.

CFD modeling of particle segregation

CFD simulation of particles segregation in a lab scale system has been carried out based on multi-fluid model. Experimental data from literature [3] are used for model validation. Different gas-solid drag, radial distribution and, solid pressure models are tested. It was found that the fitting between experimental and simulation results is very poor when using standard gas-solid (Symalal O´Brien), and standard radial distribution and solid pressure models (Lun), as indicated at Figure 3. On the other hand, implementation of EMMS gas-solid drag force model [4], together with Ma-Ahmadi radial distribution and solid pressure models [5] improved simulation results and fitting to experimental data.

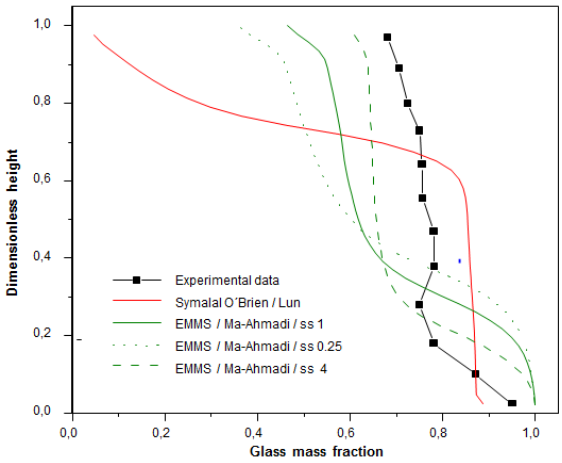

Figure 3*: Comparison between simulation and experimental results*

Furthermore, simulation results are very sensitive to solid-solid interaction, meaning that it is necessary to consider further modification or development of novel solid-solid interaction models in order to overcome general limitations of multi-phase approach and to improve the fitting between simulation and experimental results.

Future work

Biomass combustion experiments will be carried out in the lab-scale fluidized bed combustor. The impact of different types of biomass on bed agglomeration under well-defined operating conditions will be investigated. Countermeasures to reduce agglomeration will be evaluated.

Acknowledgment

This project is funded by Innovation Fund Denmark (DANCNGAS), Sino-Danish Center for Education and Research, and Technical University of Denmark.

References

[1] M. Bartels, W. Lin, J. Nijenhuis, F. Kapteijn, and J. R. van Ommen, *Progress in Energy and Combustion Science*, vol. 34, no. 5. pp. 633–666, 2008.

[2] B. Gatternig and J. Karl, *Energy & Fuels*, vol. 29, no. 2, pp. 931–941, 2016.

[3] G. G. Joseph, J. Leboreiro, C. M. Hrenya, and A. R. Stevens, *AIChE J.*, vol. 53, no. 11, pp. 2804–2813, 2007.

[4] W. Wang and J. Li, *Chem. Eng. Sci.*, vol. 62, no. 1–2, pp. 208–231, 2007.

[5] G. Ahmadi and D. Ma, *Multiph. Flow*, vol. 16, no. 2, pp. 323–340, 1990.

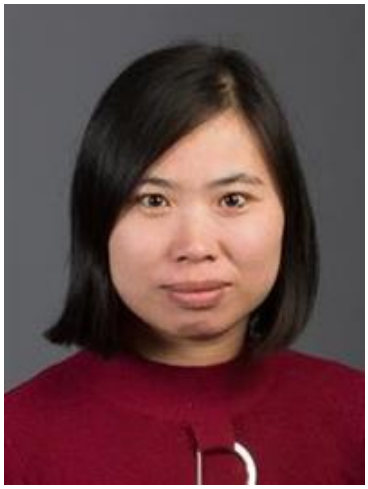

Yingjun Cai

Phone: +45 4525 2821
E-mail: ycai@kt.dtu.dk

Type: CSC
Supervisors: Kaj Thomsen
Nicolas von Solms
Suojiang Zhang

PhD Study
Started: February 2017
To be completed: February 2020

Physicochemical Properties of Binary Mixtures (1-vinyl-3-acetamido imidazole bis(trifluoromethylsulfonyl) imide+acetonitrile)

Abstract

Pure ionic liquid 1-vinyl-3-acetamido imidazole bis(trifluoromethylsulfonyl)imide was synthesized. The physicochemical and electrochemical properties of the pure ionic liquid 1-vinyl-3-acetamido imidazole bis(trifluoromethylsulfonyl) imide ([VAIM][TFSI]) and its binary liquid mixtures with acetonitrile were measured at temperatures from (298.15 to 333.15) K and at pressure of 0.1 MPa over the whole composition range.

Introduction

High-voltage and fast-charging lithium-ion batteries (LIB) are being considered as attractive power sources for portable electric devices, electric vehicles and energy storage systems [1-3]. Electrolytes used as a medium for charge transfer in lithium batteries greatly influence the performance with respect to cycle life, charging/discharging rate, and safety. Current state-of-art electrolytes are highly flammable，volatile and have low conventional voltage limitation (~4.2V) based on organic carbonate. This feature prohibits the development of batteries with safe and wide operating temperature range.

Ionic liquids were intensively studied as one component of the electrolyte in LIB, owing to their perfect characteristics of having low melting-temperature, being non-volatile, having high specific conductivity and having a wide ranging electrochemical window. Development of ionic liquids as solvents of the LIB electrolyte was limited by: i) the high viscosity reduces the specific conductivity, ii) the incompatibility of ionic liquids and electrodes decreases the cyclic lifetime [4]. Fortunately, many experts are committed to develop new types of functionalized ionic liquids to enhance the performances of new LIB.

Acetonitrile has a convenient liquid range and a high dielectric constant of 38.8, which is often used as solvent in electric devices such as LIB and supercapacitors [5,6]. Acetonitrile can easily dissolve solutes exhibiting excellent ionic conductivity that may contribute to fast-charging lithium batteries.

In this research, a new type of functional ionic liquid 1-vinyl-3-imidazole bis(trifluoromethylsulfonyl) imide ([VAIM][TFSI]) was synthesized. The physicochemical and electrochemical properties of pure ionic liquid and binary mixture of [VAIM][TFSI] and acetonitrile were measured at temperatures from 298.15 to 333.15 K and at pressure of 0.1 MPa.

Objective

The objective of this study is to evaluate physicochemical and electrochemical properties of [VAIM][TFSI] and AN to check if they can be used in the lithium-ion batteries. The goal is to create one kind of electrolyte for fast-charging or high voltage lithium-ion batteries.

Results and discussion

The functional ionic liquid was synthesized in two-step procedures as follow:

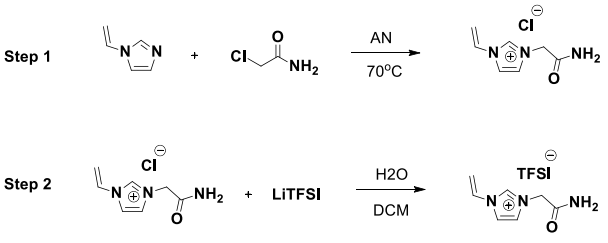

The chemical shifts (DMSO, δ/ppm relative to TMS) appear as follows: 1H NMR (600 MHz, DMSO) δ 9.41 (s, 1H), 8.19 (t, J = 1.8 Hz, 1H), 7.87 (s, 1H), 7.83 (t, J = 1.6 Hz, 1H), 7.59 (s, 1H), 7.37 (dd, J = 15.6, 8.7 Hz, 1H), 5.98 (dd, J = 15.6, 2.5 Hz, 1H), 4.99 (s, 2H). The chemical shift of the peaks corresponded to the structure of [VAIM][TFSI], and no impurity peaks were observed in the 1H NMR spectrum.

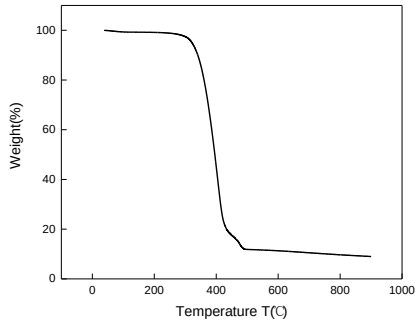

Figure 1: The TGA of [VAIM][TFSI]

The thermal stability of [VAIM][TFSI] was evaluated by Thermal Gravimetric Analyzer (TGA). Figure 1 shows the TGA curve of the IL [VAIM][TFSI], which exhibits outstanding thermal stability up to about 300 °C.

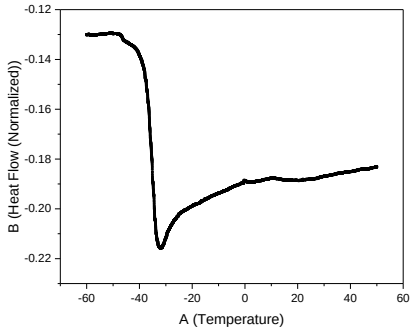

Figure 2: The DSC of [VAIM][TFSI]

The phase transition of [VAIM][TFSI] investigated by Differential Scanning Calorimetry (DSC) is shown in Fig.2. The melting point of [VAIM][TFSI] obtained from the DSC curve is -35.443 ℃. The DSC in combination with TGA analysis shows that the ionic liquid has a large convenient liquid range which suggests a wide temperature adaptability in lithium-ion batteries.

Conductivity plays an important role for fast-charging lithium-ion batteries, and the higher the better. The conductivities of binary mixtures of [VAIM][TFSI] and AN were measured using a three-electrode flow cell by impedance analyzer (CHI 660E) at different temperatures from 298.15 to 333.15 K. From figure 3, it can be seen that the conductivities of the mixture increased with the increase of temperature. Meanwhile, the conductivities of the mixture increased at first with the adding of ionic liquid, and reached the maximum value at a mole fraction of about 0.07 at all temperatures. Then, the conductivities decreased sharply as shown in figure 3. This phenomenon was detected in other mixed solvent [7]. The explanation is that the ionic liquid exists in the solvent as a "salt in solvent" at low concentration, the higher the concentration, the higher the conductivities. However, when the concentration of the ionic liquid reached a mole fraction 0.07, the viscosity of the mixture become higher and the ionic liquid gradually associated into huge clusters, which results in the decrease of the conductivity.

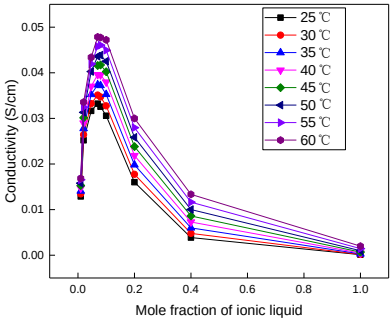

Figure 3: The conductivities of binary mixture of [VAIM][TFSI] and AN.

Conclusion and future works

A new type of functional ionic liquid [VAIM][TFSI] has been synthesized in a two-step method. The ionic liquid has high thermal stability and wide temperature adaptability. In combination with acetonitrile, the mixture display excellent conductivity.

In the future, more physicochemical and electrochemical properties will be evaluated, such as density, viscosity, diffusion of lithium-ion in the mixture, and the charge-discharge performance in lithium batteries.

Achnowledgements

The PhD project is supported by China Scholarship Council.

References

1. P. G. Bruce, S. A. Freunberger, L. J. Hardwick, J. -M. Tarascon, Nature Materials 11 (2012) 19−29.
2. M. Armand, J.-M. Tarascon, Nature 451 (2008) 652−657.
3. J. B. Goodenough, Y. Kim, Chemistry of Materials 22 (2010) 587−603.
4. M. Egashira, H. Todo, N. Yoshimoto, M. Morita, J. I. Yamaki, Journal of Power Sources 174 (2) 2007 560-564.
5. F. Mizuno, S. Nakanishi, A. Shirasawa, K. Takechi, T. Shiga, H. Nishikoori, H. Iba, Electrochemistry 79 (2011) 876−881.
6. Z. Peng, S. A. Freunberger, L. J. Hardwick, Y. Chen, V. Giordani, F. Bardé, P. Novák, D. Graham, J.-M. Tarascon, P. G. Bruce, Angewandte Chemie International Edition 123 (2011) 6475−6479.
7. A. Guerfi, M. Dontigny, P. Charest, M. Petitclerc, M. Lagacé, A. Vijh and K. Zaghib, Journal of Power Sources 195 (2010) 845-852.

Yuan Chen
Phone: +45 9185 5084
E-mail: yuache@kt.dtu.dk

Type: SDC (IPE)
Supervisors: Weigang Lin
Peter Arendt Jensen

PhD Study
Started: September 2016
To be completed: June 2020

Study on dual fluidized bed gasification of antibiotic mycelial dregs

Abstract
The disposal and utilization of antibiotic mycelial dregs (AMDs), which have been identified as a hazardous waste in China, are a serious concern and in great urgent because of the residual antibiotics and huge annual output. Dual fluidized bed gasification (DFBG) technology is an excellent method to treat AMDs due to the characteristics of both AMDs and DFBG. Thus, the objective of this PhD project is to innocent dispose AMDs using DFBG technology. To achieve this goal, the elimination of antibiotics contamination of AMDs will be investigated, as well as the release and distribution of nitrogen and phosphorus. Finally, the DFBG of AMDs on pilot scale will also be investigated. The results of current research suggest that the antibiotics contamination was eliminated after DFBG process and DFBG is feasible to dispose AMDs.

Introduction
Antibiotic mycelial dregs (AMDs), which have an annual production of 1.3 million tonnes in China, is a kind of typical bio−wastes generated from biopharmaceutical processes of antibiotics [1]. It mainly consists of mycelia, surplus fermentative substrates, flocculant agent, intermediate metabolites and residual antibiotics. Therefore, AMDs is characterized by high content of nutrients (like proteins, nucleic acids, lipids, polysaccharides and nutrient salts) and little heavy metals, as well as a certain amount of residual antibiotics which can reach to approximately 0.6 wt.% [2]. Serious environmental problems can be caused by AMDs if it is improper disposed, such as water pollution, odors and particularly resistant genes development. As a result, AMDs has been classified as hazardous waste in China since 2008 [3]. Thus it is of great necessary and urgent to find an adequate method to manage AMDs, especially based on the reality that the output of AMDs keeps increasing at the rate of about 10% per year [4].

The foremost concern associated with AMDs disposal is antibiotics contamination. Moreover, the reuse of nutrients in AMDs should also be considered when developing novel disposal methods. According to Chinese standard (GB 5104−2014), the disposal of AMDs should follow the principles of reduction, recycling and harmlessness. Therefore, an efficient disposal method that can eliminate antibiotics contamination and simultaneously recycle the nutrients in AMDs is desired. In the past, AMDs were broadly used as feedstuff and fertilizer due to the high nutrients content. However, this behavior was forbade by related regulations, because the residual antibiotics can easily accumulate in animals' bodies to cause drug resistance [5]. Currently, AMDs are primarily disposed via incineration and safe landfill. Unfortunately, incineration and safe landfill are high cost and waste of resources and can cause serious secondary environmental pollution.

Dual fluidized bed gasification (DFBG) technology is an excellent method for the conversion of biomass resources because of the high fuel flexibility, high heat and mass transfer rate, high intensity, high carbon conversion, and high quality of resulted gas. Given the high nutrients content in AMDs, DFBG can be an effective method to dispose AMDs.

Specific objectives
This PhD project aims to innocent dispose AMDs through DFBG technology. Therefore, the antibiotics contamination of AMDs must be eliminated, which can be effectively achieved by eliminating the residual antibiotics. In addition, the release and distribution of nitrogen and phosphorus, which is largely retained in AMDs, should be investigated too, because nitrogen and phosphorus are not only environmental sensitivity elements but also important resources, especially phosphorus which is non−renewable and becoming scarce in the near future [6]. Besides, the DFBG of

AMDs on pilot scale should also be investigated for the sake of finding out the optimized conditions to obtain high quality gas.

Results and discussion

It is well known that pyrolysis is the first step of gasification. Thus, in order to verify that the antibiotics contamination of AMDs was eliminated after the DFBG process, the pyrolysis of AMDs was conducted followed by the detection of antibiotic residue on the resulted biochar using HPLC. The obtained HPLC detecting curves are shown in Figure 1. According to Figure 1, there is no peak at the AMDs retention time, which means no antibiotics was retained in biochar, indicating that the antibiotics contamination of AMDs will be eliminated after DFBG process.

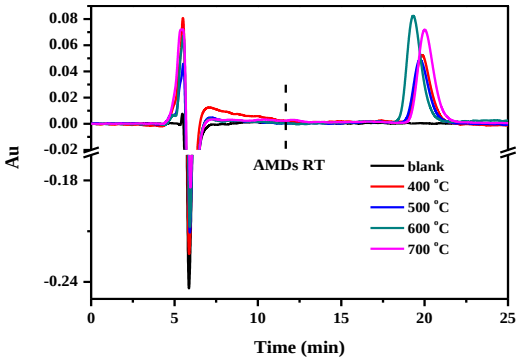

Figure 1. The HPLC detecting curve of antibiotic on the biochars obtained at different pyrolysis temperature. The AMDs RT means the retention time of AMDs.

The DFBG of AMDs on pilot scale was roughly conducted. Air was used as the gasifying agent. Figure 2 gives the temperature records of riser, dilute phase and dense phase of gasifier during the gasification process. As observed in Figure 2, the temperature of riser is stable at 900 ºC, while dilute phase increased from 600 ºC to 700 ºC, and dense phase decreased from 700 ºC to 520 ºC. The big temperature variation of dilute phase and dense phase should be ascribed to the progressive decreasing of the amount of circulating ash, which can be solved by add ash into the system.

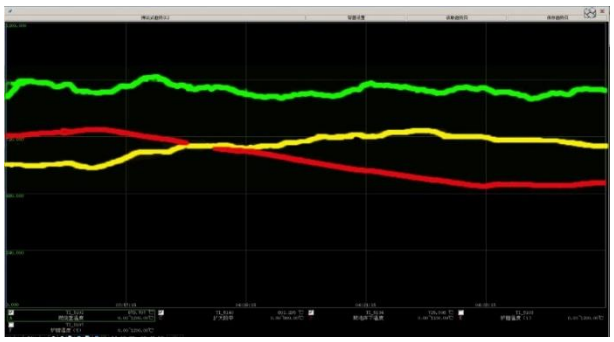

Figure 2. The temperature records during the DFBG of AMDs on pilot scale. The green, red and yellow curves recorded the temperature of riser, dense phase and dilute phase of gasifier.

Three parallel gas samples at intervals of 15 min were token and then analyzed. The results are shown in Table 1. From Table 1, the composition of the three parallel gas samples were similar, indicating the stability of gasification process. However, the carbon conversion (25.98−29.02%) and the low heating value (2.04−2.36 MJ/Nm^3) are quite low, which should be attributed to the low gasification temperature (520−700 ºC) and the dilution of nitrogen in gasifying agent to the resulted gas.

Table 1: Analysis result of three parallel sample gas.

Compositions	Samples		
	1#	1#	3#
CO_2	15.10	15.52	13.78
C_2H_4	1.12	1.44	1.20
H_2	2.58	3.97	2.90
N_2	70.61	67.88	69.90
CH_4	1.99	2.35	2.46
CO	8.33	8.65	8.48
Tar + water / (kg/Nm^3 dried gas)		0.341	
C conversion rate / %	26.23	29.02	25.98
Dried gas / (Nm^3/h)	38.60	40.15	38.99
LHV / (MJ/Nm^3)	2.04	2.36	2.26

In general, the antibiotics contamination can be eliminated through DFBG process, and the DFBG of AMDs on pilot scale is relatively stable, indicating the feasibility of the AMDs disposal by DFBG technology.

Conclusion and future work

The current research results show that the antibiotics contamination can be eliminated after DFBG process and DFBG is feasible to dispose AMDs.

In the future, the release and distribution of nitrogen and phosphorus, together with the optimization of gasification conditions to obtain high quality gas and the utilization of ash, should be investigated.

References

1. C. Cai, H. Liu, B. Wang. J Hazard Mater 331 (2017) 265-272.
2. D. Ma, G. Zhang, C. Areeprasert, C. Li, Y. Shen, K. Yoshikawa, G. Xu. Chemical Engineering Journal 284 (2016) 708-715.
3. X. Jiang, Y. Feng, G. Lv, Y. Du, D. Qin, X. Li, Y. Chi, J. Yan, X. Liu. Environ Sci Technol 46 (2012) 13539-13544.
4. D. Ma, G. Zhang, P. Zhao, C. Areeprasert, Y. Shen, K. Yoshikawa, G. Xu. Chemical Engineering Journal 273 (2015) 147-155.
5. C. Li, G. Zhang, Z. Zhang, D. Ma, L. Wang, G. Xu. Chemical Engineering Journal 279 (2015) 530-537.
6. C. Adam, B. Peplinski, M. Michaelis, G. Kley, F.G. Simon. Waste Manag 29 (2009) 1122-1128.

Ping Feng

Phone: +86 13810271558
E-mail: feng.ping@outlook.com

Type: CSC
Supervisors: Kim Dam-Johansen
Weigang Lin
Wenli Song, IPE, CAS

PhD Study
Started: September 2012
Completed: July 2016

Effect of Temperature on Gasification of Coal/Bio-Oil Slurries

Abstract
Coal/bio-oil slurry is a new partial green fuel for bio-oil utilization. CBS reacts with gasification agents at high temperatures and converts into hydrogen and carbon monoxide. This research provides a feasibility study for the gasification of CBS in an atmospheric entrained flow reactor for syngas production. Experiments have shown that CBS can be successfully processed and gasified in the entrained flow reactor to produce syngas with almost no tar content and low residual carbon formation. High reactor temperature is favorable for H_2 production. At 1400 ºC with steam/carbon ratio of 5, the syngas components are similar with that in equilibrium.

Introduction
Biomass is paid much attention in recent years as an alternative CO_2 neutral energy resource. However, due to its low energy density and high transportation cost, a method to utilize the biomass is to convert it to a pyrolysis oil (bio-oil) that has a high energy density. Bio-oil is difficult to utilize directly owing to its high acidity and oxygen content, thus the Institute of Process Engineering, Chinese Academy of Sciences proposed a novel technology of coal/bio-oil slurry (CBS) for bio-oil utilization[1]. This new kind of slurry fuel is a partial green fuel because of the utilization of the energy content in the bio-oil. Furthermore, the CBS has a higher volumetric heating value than bio-oil due to the addition of coal and could be used as slurry fuels to produce heat or syngas through gasification.

Specific Objectives
The objective of this work is to evaluate the gasification behaviors of CBS under various operation conditions and compare with the commercial coal water slurries. In the present research, the gasification behavior of coal/bio-oil slurries was investigated in a continuous feeding atmospheric pressure entrained flow gasifier for syngas production. The effect of reactor temperature on gas and solid residual yields was be investigated to clarify the gasification performance of CBS.

Experimental
Figure 1 shows the electrically heated entrained flow gasification unit configured for slurry feeding. CBS were gasified at high temperature in the entrained flow reactor which contained a SiC tube with 80 mm in inside diameter and 2 m in length. Fuels and gasification agents were injected from the top of the reactor. The fuels and atomizing gas were kept at room temperature before injecting into the reactor, while steam and secondary gas (mainly nitrogen) were preheated to 1200 °C by a preheater located on the top of the reactor. The entrained flow reactor operated from 1200 °C to 1400 °C which is in the temperature range in industrial reactors.

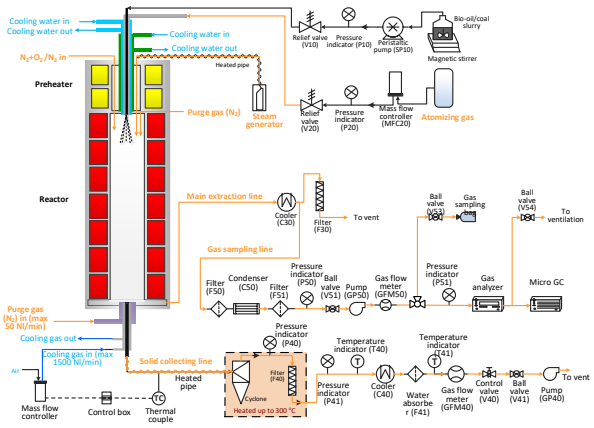

Figure 1 Schematic of the slurry fed entrained flow gasification system

Syngas and solid products were introduced into a quench section at the exit of the reactor. Part of the syngas and solid residuals were sucked out by a probe for solid collection, and the rest syngas and solids flowed into a water-cooled chamber for gas analysis. To

prevent water and tar condensation in sampling system, the filter and cyclone were kept at 300 °C. The reactor with a solid feeding system has previously been applied for biomass gasification experiments[2-3].

Results and Discussion

The gasification experiments were conducted under temperature from 1200 ºC to 1400 ºC with CBS of 20% coal concentration (CBS20) and CBS of 30% coal concentration (CBS30). The effect of reactor temperature on gaseous components and residual carbon yields in CBS gasification are showed in Figure 2. The carbon conversion increased from 85% to 99% with reactor temperature rising from 1200 ºC to 1400 ºC for CBS20. At 1400 ºC, the carbon conversion for CBS is quite close to the carbon conversion of CWS in industry. At 1400 ºC, CBS also yielded more syngas with 1.7 Nm^3/kg compared with 1.25 Nm^3/kg at 1200 ºC. The gas components differ with temperature changes. The H_2 and CO content increased with temperature increasing while CO_2 and CH_4 went by contraries. The increased H_2 and CO content might be attributed to the promotion of methane cracking reaction and the inhabitation of water gas shift reaction at high gasification temperature. Figure 9 (d) shows the residual carbon yield of CBS gasification from 1200 °C to 1400 °C. The slurry yielded less unconverted carbon under 1400 °C. In particular for residual carbon in cyclone, it is 0.004 g/g slurry at 1400 ºC, which is only one fourth of the amount of residual carbon produced at 1200 °C. Thus, high gasification temperature strongly reduces the residual carbon yields.

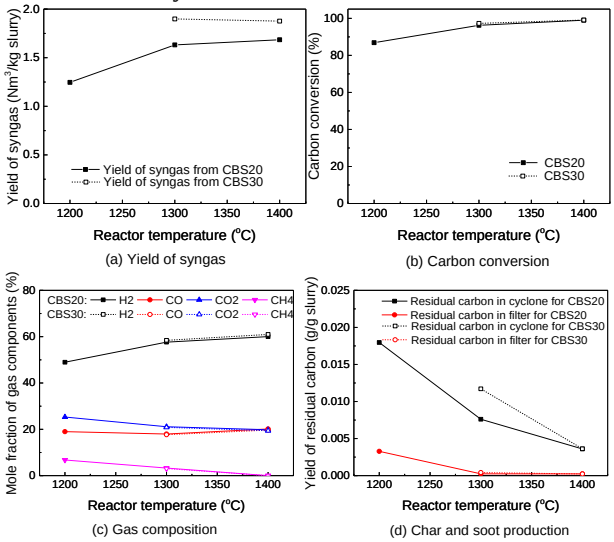

Figure 2 Effect of temperature on gasification performance of CBS20 and CBS30 at H_2O/C=5: (a) yield of syngas, (b) carbon conversion, (c) syngas composition, (d) residual carbon in cyclone and filter

Since the gasification were carried out at relatively high temperature (1200 ºC-1400 ºC), the experimental results were compared with thermodynamical equilibrium values to see if the experiments can be predicted by equilibrium calculations. The equilibrium syngas composition of CBS gasification was calculated at experimental conditions assuming no residual carbon or C_2+ compounds produced. So the syngas includes H_2, CO, CO_2, CH_4, NH_3, H_2S and H_2O. The main gas products in experiments and equilibrium were compared in Table 1.

Table 1 Comparison of the gas mole fractions between experiment and equilibrium calculation

Components	H_2	CO	CO_2	CH_4
Run	%	%	%	%
T1	48.95	18.99	25.30	6.76
T1*	59.14	19.37	21.49	0.00
T2	57.49	17.96	21.23	3.32
T2*	58.60	20.92	20.47	0.00
T3	60.01	20.16	19.83	0.00
T3*	58.14	22.28	19.58	0.00
T4	58.43	17.68	20.86	3.04
T4*	59.62	20.98	19.40	0.00
T5	60.95	19.68	19.38	0.00
T5*	59.18	22.31	18.51	0.00

*means equilibrium calculation results

At 1200 ºC, the experimental and equilibrium values were of great difference. When temperature increased 1300 ºC, the syngas components are similar except CH_4 content. At 1400 ºC, CH_4 was not detected in syngas in experiments and the syngas components are similar with that in equilibrium. In addition, the carbon conversion at this condition is as high as 99%. Thus, at this condition it could be regarded that the experiments have almost achieved the thermodynamical equilibrium.

Conclusions

In this study, A slurry feeding system fitted for atmospheric entrained flow gasifier was developed and the spray was even and continuous without blockage inside and outside the atomizer. The characteristics of gasification of coal/bio-oil slurry was evaluated in a lab scale entrained flow gasifier. At 1400 ºo. the gasification of CBS is very close to the thermaldynamical equilibrium state.

Acknowledgements

This study is supported by Danish Strategic Research Council, Technical University of Denmark, China Scholarship Council, International S&T Cooperation Program of China (2013DFG62640) and The National Natural Science Foundation of China (51104137).

References

1. P. Feng, L. Hao, C. Huo, Z. Wang, W. Lin, W. Song, Energy 66 (1) (2014) 744-749.
2. K. Qin, W. Lin, P.A. Jensen, A.D Jensen, Fuel 93 (2012) 589-600.
3. K. Qin, P.A. Jensen, W. Lin, A.D. Jensen, Energy & Fuels 26 (9) (2012) 5992-6002.

List of Publications

1. P. Feng, W. Lin, P.A. Jensen, W. Song, L. Hao, K. Raffelt, K. Dam-Johansen, Energy 111 (15) (2016) 793-802

Jie Gao

Phone: +45 5020 8886
E-mail: jgao@kt.dtu.dk

Type: CSC
Supervisors: Kim Dam-Johansen
Weigang Lin
Hao Wu

PhD Study
Started: May 2018
To be completed: May 2021

Flame Synthesis for Nanoparticles

Abstract
It is well known that the combustion of proper precursor sprays pyrolysis (FSP) process is a highly diverse and scalable technique for the synthesis of nanostructural materials with commercial exploitation. My PhD project will focus on preparation of nanoparticles in high temperature reactors with various techniques.

Introduction
Flame aerosol technology have found to be practiced with painting on cave wall and in ink artwork by Chinese, Egyptians and Greeks[1] and is widely used in producing large scale nanoparticles by many industry leader company, for example, DuPont, Cabot, Aerosil and Ishihara which totally valued more than 15 USD billion/year (Table 1). And products cover catalysts (eg. Al_2O_3, SiO_2 and TiO_2), photocatalysts (eg. TiO_2), pigments (eg. TiO_2), major flowing aid in pharmaceuticals and cosmetics industry (eg. Fumed SiO_2) and for chemical mechanical polishing purpose in microelectronics (eg. fumed Al_2O_3 as solutions).

Table 1: Aerosol manufacturing of nanoparticles[2]

Product particles	Volume (Mt/year)	Value (B$/year)	Industrial Process
Carbon black	8	8	Flame
Titania	2	4	Flame
Zinc oxide	0.6	0.7	Evap./oxid.Zn
Fumed silica	0.2	2	Flame

In recent 20 years, the flame technology creates more applications in wider field. Countless nanoparticles have been prepared for the sensors, fuel cells, electronics, biomaterials, lighting and medical applications etc..

Specific Objectives
The objectives of the PhD project:

- Understanding the fundamental FSP working principle during the combustion process
- Guiding all the recent research conducted in FSP or related technique with a review article.
- Improving reactors functions to get various nanoparticles for different application
- Using diverse analyzation method for products characterization

Results and Discussions
The results from the literature research on the fundamental of FSP technique will be presented in this section.

History of Aerosol Flame Reactors

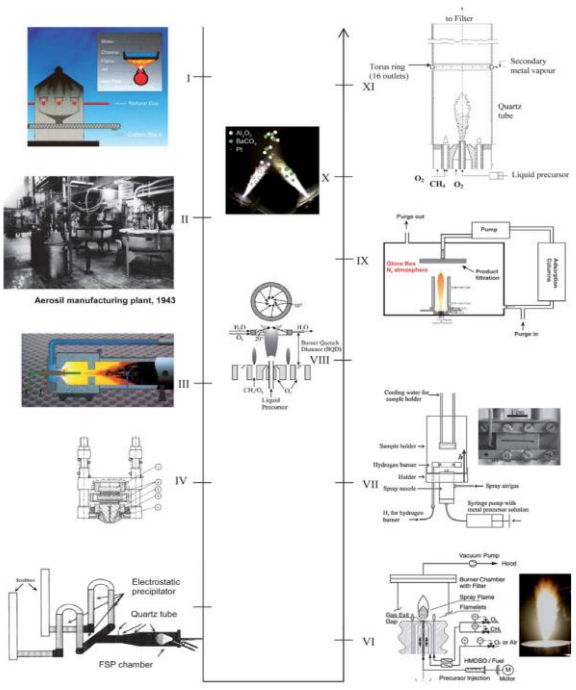

Fig. 1. Evolution of aerosol flame reactors, including FSP reactor and its modifications. (I) 1940s: Early

industrial-scale production of carbon blacks as commodity particles – 'channel black process'. (II) 1940-50s: Production of fumed SiO_2 (1943) from the flame hydrolysis of metal halide vapours (picture showing the first Aerosil production plant, source: courtesy of Evonik Degussa GmbH). The process further led to the manufacture of other commodity oxide ceramics such as Al_2O_3 (1953) and TiO_2 (1954) using the same vapour-type flame technique. (III) 1970s: Furnace black process using a modern 'jet-type' flame reactor. (IV) 1977: First reported development of ultrasonic-assisted Flame Spray Pyrolysis by Sokolowski et al., where metal acetylacetonate in organic solvent was used as the liquid precursor. (V) 1996/97: Gas-assisted atomizer FSP reported by Bickmore et al. and Karthikeyan et al. mark the pioneering of systematic studies in FSP. (VI) 2002: Pressure-assisted FSP reported by Mädler et al. that further led to systematic studies of various simple to complex metal oxides and metal/metal oxide systems using similar type reactor. (VII) 2004: A one-step film deposition technique by thermophoretic coating that further led to a series of supported catalysts and gas-sensor fabrications. (VIII) 2005: A flame height-selective rapid-quenching technique to control precisely the metal deposit size on metal oxide support. (IX) 2006: Reducing FSP by limiting the ambient O_2 in flame reactor that allows production of metallic and carbon-coated nanoparticles. (X) 2006: A multi-nozzle FSP to synthesis multi-component particles with controllable phase segregation. (XI) 2008: In situ sequential coating of preformed FSP nanoparticles by introducing secondary metal vapour via a torus pipe ring with multiple hollow openings[3].

Classification of Aerosol Flame Reactors

Depending on different state of the supplied precursors, the aerosol flame reactors can be classified by the following types[4]: Vapour-fed aerosol flame synthesis (VAFS) and Liquid-fed aerosol flame synthesis (LAFS).

VAFS: the volatile precursors combusted in a gas phase, such as hydrocarbon, hydrogen or halide flame and then formed particles. It is a nucleation reaction and the particles could experience surface reaction, coagulation and subsequent coalescence to grow larger. It could be used in producing pigmentary titania and fumed silica.

The other one is LAFS. Compared with VAFS, LAFS does not need to evaporate precursor from liquid/solid into gas therefore it has little limitation and a reasonable cost. Through an air-assisted or ultrasonic nozzles, spraying could be achieved by solution atomization. LAFS was used to produce carbon black in industry.

Acknowledgements

This Ph.D. project is conducted at the Combustion and Harmful Emission Control (CHEC) Research Centre at the Department of Chemical and Biochemical Engineering at the Technical University of Denmark.
The author would like to express her gratitude to the China Scholarship Council (CSC) with grant ID: 201704910988 and the Chemical Engineering Department of DTU for funding this project.

References

1. Ulrich, G. D. Flame synthesis of fine particles. *Chem. Eng. News Arch.* **62,** 22–29 (1984).
2. Wegner, K. & Pratsinis, S. E. Scale-up of nanoparticle synthesis in diffusion flame reactors. *Chem. Eng. Sci.* **58,** 4581–4589 (2003).
3. Teoh, W. Y., Amal, R. & Mädler, L. Flame spray pyrolysis: An enabling technology for nanoparticles design and fabrication. *Nanoscale* **2,** 1324–1347 (2010).
4. Strobel, R. & Pratsinis, S. E. Flame aerosol synthesis of smart nanostructured materials. *J. Mater. Chem.* **17,** 4743 (2007).

Anders Jaksland
Phone: +45 4010 1875
E-mail: andjaks@kt.dtu.dk

Type: SDC (KT)
Supervisors: John M. Woodley
Manuel Pinelo
Yinhua Wan, IPE, China

PhD Study
Started: September 2017
To be completed: September 2020

Membrane-based in-situ product removal

Abstract
In-situ product removal is a promising technology in the pursuit of making biorefineries competitive with traditional refinery technology. Especially membrane based methods have proven successful. In-situ product removal works by selectively removing product from the bioreaction increasing both productivity and product concentration. In this project in-situ product removal will be applied to value-added chemicals for a future bioeconomy, but also the lack of targets for the research field will be addressed.

Introduction
To overcome the problem of global warming the chemical industry has to move away from fossil feedstocks and instead utilize sustainable feedstocks such as biomass in biorefineries. In the future all platform and bulk chemicals will have to be produced in this way, however for many processes either the yield, productivity or product concentration is insufficient for commercialization. A solution to this problem is in-situ product removal (ISPR) where especially membrane technology shows promising results. In-situ product removal via membrane technology overcomes several problems in current fermentation technology by 1) continuously removing the product eliminating product inhibition on the cell, 2) increasing the product concentration of the broth before the downstream processing, and 3) removing the product without removing the cells from the fermentation and thus potentially improving the yield.

Membrane-based ISPR technology
ISPR is defined as fast selective removal of products from the vicinity of the cells. [1] It thus works by selectively removing the products from the fermentation or biocatalysis process and keeping the product concentration at or below the toxicity limit to increase the product productivity. At the same time the product is removed selectively to the downstream process at an increased titer, thus reducing the cost of downstream separation. The ISPR membrane module can be configured internally and externally. If configured internally the selective removal happens inside the bioreactor straining the cells as little as possible, but is more predisposed to clogging and fouling. An illustration of internal configuration can be seen in figure 1.

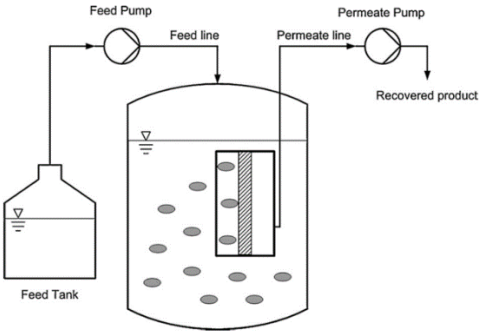

Figure 1: ISPR with internal configuration with the membrane module submerged into the bioreactor.[2]

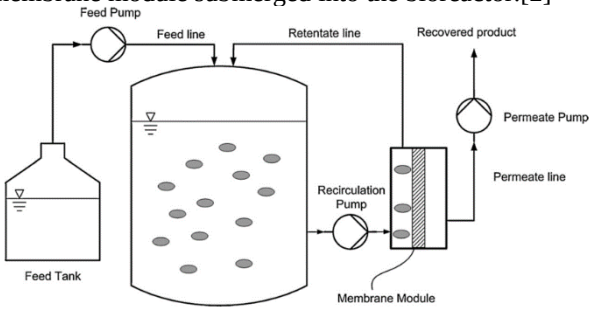

Figure 2: ISPR with external configuration with the membrane module connected in an external loop.[2]

If configured externally the selective removal happens in a recycle connected to the bioreactor. By circulating the broth past the membrane module externally the flow

is parallel to the membrane thus straining the cells more, but also reducing the potential for clogging and fouling. An illustration of external configuration can be seen in figure 2.

ISPR historically and state-of-the-art

Applications of ISPR with membrane technology exist as far back as 1984 by Groot et al.[3] Back then ISPR was introduced to a butanol/isopropanol system to overcome product inhibition. The fermentation was done with a clostridium bacteria and the ISPR with pervaporation through a silicon tubing. The experiment proved the concept with batch fermentation improving the glucose consumption from 20 g/L to 30 g/L while the productivity improved from 1.0 g/L/hr to 1.7 g/L/hr. In 1991 Qureshi et al.[4] applied ISPR to a system of immobilized cells producing acetone/butanol/ethanol (ABE). The system showed productivity of 3.5 g/L/hr and 97.9% lactose utilization in continuous fermentation. In 2011 Liu et al.[5] used an asymmetric membrane of PDMS with composite support. This increased the flux of the solvents hundred fold compared to the earlier studies significantly reducing the required membrane area. Neither yield, productivity nor product concentration were reported. In 2014 Liu et al.[6] again reported ISPR with the same membrane this time reporting the productivity. The use of ISPR increased it from 0.2 g/l/hr ABE to 0.42 g/L/hr, a doubling in productivity by removing the inhibiting product continuously. Most recently other membranes than the thoroughly studied PDMS membrane has been investigated. In 2015 Shin et al.[7] reported use of a block copolymer achieving a productivity of 0.94 g/l/hr ABE with a flux through the membrane of 1634 $g/m^2/hr$, 2-4 times higher than the best reports of the PDMS membrane. In 2017 Van Hecke et al.[8] used a poly(octyl methyl siloxane) based pervaporation membrane reporting a productivity of 0.43 g/L/hr, yield of 0.33 and with concentrations in the permeate of over 200 g/L total ABE solvents. All the mentioned ISPR applications use pervaporation, but also perstraction has been reported with worse results and most recently vapor permeation with similar results to pervaporation by Sun et al.[9] in 2017 on an ethanol system.

Guiding the research through a review

The first goal of this PhD project is to guide all the research conducted in membrane-based ISPR with a review article. The article has several goals aside from reviewing the current state of the art.

Terminology used in ISPR applications

In the literature, there is no common terminology for talking about in-situ product removal. The last word removal is often interchanged with recovery, while in-situ product recovery is also used for the removal of product without any concentration of the product, e.g. through ultrafiltration, where the goal is simply to avoid removing the cells with the product stream. Another cause of confusion is whether externally configured product removal via a recycle loop is still called in-situ removal or should be classified as ex-situ. The goal is thus to clarify that the use of in-situ product removal is reserved for applications with fast selective removal of the products from the vicinity of the producing cells no matter the method, where improvement is observed for productivity and product concentration.

Setting targets for development

Another problem with the current research is that no targets for the development has been set. The yield, productivity and final product concentration is being increased without any published consensus on at what point the development is sufficient and without any priority between the three. A techno-economic analysis of the three with accompanying sensitivity analysis could help setting the targets and priority for future development.

Future experimental work

With targets set for the development of ISPR experimental work on applying membrane-based ISPR to products in the price-range of 2$/kg to 10$/kg will be carried out.

The experimental work will be done in several phases. The first phase is deciding on the product and establish the fermentation. The second phase is finding and investigating the removal of the product with membrane technology. The third phase is implementing the membrane and fermentation together in fermentation with ISPR. The last phase is modelling and economic analysis of the developed process.

The ultimate goal of the experimental work is to show how ISPR can be used for non-fuel value added chemicals, but also to develop a generic method for implementing and testing ISPR to evaluate the performance on any fermentation or biocatalytic process.

References

8. A. Freeman, J.M. Woodley, M. D. Lilly, Nat Biotechnol. 11 (1993) 1007-1012
9. F Carstensen, A. Apel, M. Wessling, J. Membr. Sci. 421 (2012) 39-50
10. W. J. Groot, G. H. Schoutens, P. N. Van Beelen, C. E. Van Den Oever, N. W. F Kossen, Biotech. Let. 6 (1984) 789-792
11. N. Qureshi, A. Friedl, I. S. Maddox, Biotechnol. Bioeng 38 (1991) 518-527
12. G. Liu, W. Wei, H. Wu, X. Dong, M. Jiang, W. J, J. Membr. Sci. 373 (2011) 121-129
13. G. Liu, L. Gin, S. Liu, H. Zhou, W. Wei, W. Jin, Chem. Eng. Process. 86 (2014) 162–172
14. C. Shin, Z. C. Baer, X. C. Chen, A. E. Ozcam, D, S. Clark, N. P Balsara, J. Membr. Sci. 484 (2015) 57-63
15. W. Van Hecke, H. De Wever, J. Membr. Sci. 540 (2017) 321-332
16. W. Sun, W. Jia, C. Xia, W. Zhang, Z. Ren, J. Membr. Sci. 530 (2017) 192-200

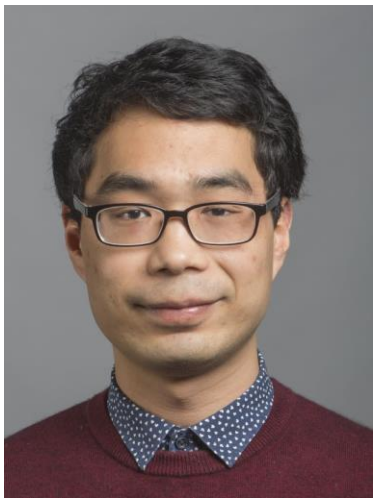

Mingbo Ji
Phone: +45 52909785
E-mail: minji@kt.dtu.dk

Type CSC
Supervisors: Manuel Pinelo
Anders Egede Daugaard
John Woodley
Yinhua Wan

PhD Study
Started: February 2018
To be completed: January 2021

The effect of chemical treatment on commercial polymeric membranes

Abstract
Ultrafiltration (UF) membranes are widely used in industrial purification and concentration. However, conventional UF membrane separation cannot satisfy all industrial requirements due to membrane fouling or low selectivity. Membrane pretreatment with solvents/chemicals may be exploited to develop high performance UF membranes because of its' simplicity and convenience. In present work, we treated polysulfone (PSf) and regenerated cellulose (RC) membranes with ethanol solution. Ethanol-treated PSf membranes shows much higher water permeability than pristine membrane, about 7 times, while ethanol-treated RC membrane displays little significant changes. Meanwhile, ethanol treatment decreased retention for both pepsin and BSA slightly for PSf membranes. However, it seems that ethanol-treated PSf membranes suffer more severe fouling during protein filtration, which need to be further studied.

Introduction
Previous research demonstrated that exposure to some solvents/chemicals would significantly change membrane property and impact membrane performance. For instance, Ross et al. [1] indicated that defluorination and oxygenation occurred on PVDF membrane with NaOH treatment, which would enhance the hydrophilicity of membrane. Navarro et al. [2] suggested that significant hydrolysis only and partial hydrolysis alone on H_3PO_4 and HF treated membrane, respectively. And an HF treatment increases flux due to higher hydrophilicity without a significant change in pore size, while the H_3PO_4 treatment substantially increases flux due to the wider pores, even with a reduction in hydrophilicity. Zhang et al. [3] treated the PSf and PVDF membrane with NaClO. And the result demonstrated that pore enlargement could be verified by a seemingly inconsistent result of dextran sieving experiments and the decreased HA rejection rate. Moreover, the increased negative charge on aged PSf membrane surface have a great impact on its sieving property and fouling propensity, especially for the charged and hydrophilic BSA.
Conclusion can be summarized that solvents/chemicals treatment will change the membrane property, such as hydrophilicity, pore size, charge, etc., severely affecting the membrane performance. Thus Solvent/chemicals treatment may be a promising way to develop high performance UF membranes.

Specific objectives
The objectives of the PhD project focuses on separating the proteins (which possess similar molecular weight) with high separation factor and further developing a novel, simple, universal and efficient modification protocol for membrane surface regulation to obtain high performance membranes. The scope of the PhD work includes:

- Membrane pretreatment with solvents/chemicals such as ethanol, NaOH, NaClO, etc.
- The membrane performance of water permeability, protein flux, retention, flux recovery ratio (FRR), pore size distribution, etc. will be studied in detail.
- Elucidating the mechanism of solvents/chemicals treatment with different membranes
- Based on mechanism of pretreatment, new modification method will be developed, such as surface chare regulation, which is producing lots of charge groups on membrane surface. Different groups and immobilization methods will be studied.
- Investigating the effect of surface charge on membrane separation performance as solvents/chemicals treatment

- Evaluating the protocol of commercial membranes modification, such as stability, reuse, cleaning, etc.

Results and discussion

As shown in Figure 1 and 2, ethanol-treated membranes shows seven times higher water permeability than PSf membrane. It can be seen that protein flux decreased tremendously during filtration and resulting low flux recovery ratio. It is interestingly that there is no significant changes in pepsin retention, which needs to be further studied.

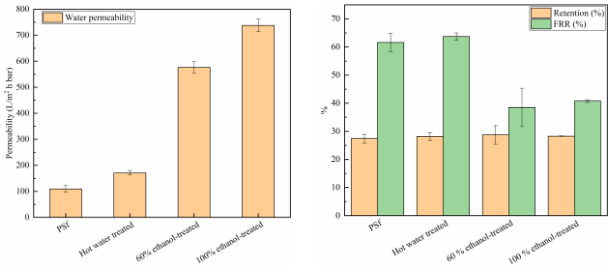

Figure.1 Water permeability, pepsin retention and flux recovery ratio (FRR) for pristine and ethanol-treated membranes, condition: 1 g/L, pH 4.7, stirring rate 100 rpm

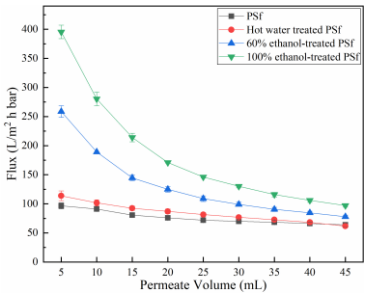

Figure.2 Pepsin flux for pristine and ethanol-treated membranes

To reduce concentration polarization on membrane surface, we increased the stirring ratio to 500 rpm during filtration. As shown in Figure 3, pepsin shows higher flux decline than BSA, which means that pepsin will foul membrane quickly. Pepsin has lower molecular and can block membranes pores easier. Furthermore, it can be seen that BSA and pepsin retention decreases slightly for ethanol-treated membranes.

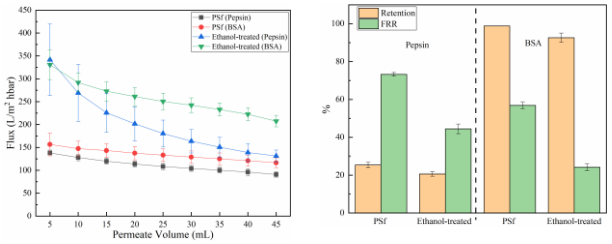

Figure.3 Flux, retention and FRR of pepsin and BSA filtration for pristine and ethanol-treated membranes, condition, 1 g/L, stirring rate 500 rpm

We can further studied the protein retention performance from Figure.4, which shows the permeate volume dependent retention. We hypotheses that during initial 0-10 mL, pepsin go through the membrane by sieving effect, leading to low retention; 10-25 mL, protein blocks membrane pores, leading to high retention; 25-45 mL, high concentration of residual solution results more protein go through the membrane, leading to low retention.

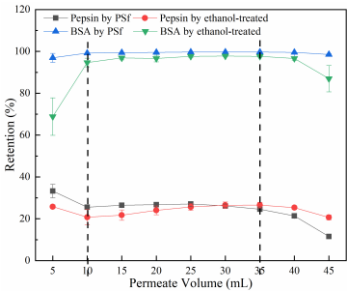

Figure.4 Permeate volume dependent retention of pepsin and BSA for PSf and ethanol-treated PSf membranes

As shown in Figure.5, ethanol treatment seems to have little effect on permeability and recovery for RC membrane. The possible reason is that RC membrane is hydrophilic intrinsically, leading to high flux recovery ratio. Furthermore, high FRR suggests that RC membrane mainly suffers surface fouling

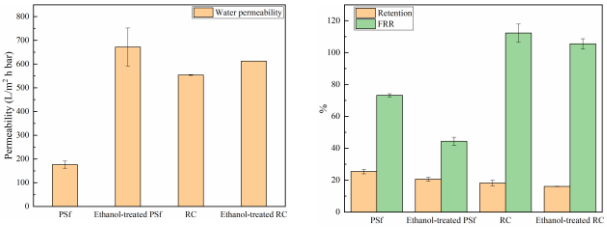

Figure 5: Water permeability, pepsin flux, retention and flux recovery ratio for PSf and regenerated membranes

Conclusions and Future work

Ethanol pretreatment significantly increases the water permeability of polysulfone membranes, approximately 7 times higher than pristine PSf. Ethanol-treated PSf membranes suffer more severe fouling than pristine membrane. Ethanol treatment decreased retention for both pepsin and BSA slightly for PSf membrane. However, due to hydrophilic intrinsically, ethanol treatment has little effect on regenerated cellulose membrane.

Future work mainly focus on the mechanism elucidation of solvents/chemicals on membrane and developing other modification method.

References

1. Ross, G. *Polymer (Guildf).* **2000**, *41*, 1685.
2. Navarro, R.; González, M. P.; Saucedo, I.; Avila, M.; Prádanos, P.; Martínez, F.; Martín, A.; Hernández, A. *J. Memb. Sci.* **2008**, *307*, 136.
3. Zhang, Y.; Wang, J.; Gao, F.; Chen, Y.; Zhang, H. *Water Res.* **2017**, *109*, 227.

Kristian Krum

Phone: +45 27509740
E-mail: krkkru@kt.dtu.dk
Type: SDC (KT)
Supervisors: Peter Glarborg
Hao Wu
Songgeng Li, IPE, China
Thomas Norman, BW-Vølund

PhD Study
Started: September 2017
To be completed: August 2020

NO_x Control in Combustion of Alternative Fuels

Abstract

Combustion of solid waste fuels in waste-to-energy (WtE) plants is a competitive method for conversion of waste to electrical energy and heat. The emission of nitrogen oxides (NO_x) from WtE plants continuous to be a major environmental concern. Additionally, the ash formed during combustion of waste causes severe practical issues due to deposition and corrosion in the boiler. In this project, it is of interest to study techniques for the simultaneous reduction of NO_x emissions, deposition and corrosion in the boiler section of WtE plants. A technique of interest is the commonly used selective non-catalytic reduction (SNCR) process using alternative additives, e.g. ammonium sulphate, ammonium phosphate and cyanuric acid. It is also of interest to study the impact of inorganic elements, released from the waste during combustion, on the SNCR process.

Introduction

The handling of municipal solid waste (MSW) that is produced daily in large amounts has become a significant challenge. An alternative to traditional landfilling is extraction of energy through combustion in waste-to-energy (WtE) plants.

Most of the waste fractions in MSW are nitrogen containing materials, and thus form nitrogen oxides (NO_x) during combustion. The emission of NO_x continuous to be a major environmental concern, as NO_x participates in the formation of acid rain and photochemical smog.

In Denmark, the most common technique to reduce NO_x emissions from grate-fired WtE plants is selective non-catalytic reduction (SNCR) using ammonia or urea as reducing agent. The SNCR process is governed by the overall reactions using ammonia and urea, respectively:

$$4NH_3 + 4NO + O_2 \rightarrow 4N_2 + 6H_2O \quad (1)$$

$$NH_2CONH_2 + 2NO + \tfrac{1}{2}O_2 \rightarrow 2N_2 + CO_2 + 2H_2O \quad (2)$$

The SNCR process is known to be very temperature dependent, and has a narrow temperature window of efficient NO_x reduction. It is therefore of practical interest to investigate the effect of different operating parameters, in order to study how the temperature window of effective NO_x reduction can be broadened.

The ash species formed from combustion of MSW have a high tendency to form sticky and corrosive ash deposits in the boiler, due to high amounts of inorganic elements and chlorine in MSW. In previous studies, it has been shown that addition of sulphur containing additives can reduce the extent of deposition and corrosion in the boiler [1]. Therefore, the use of alternative additives in the SNCR process, for simultaneous reduction of NO_x, deposition and corrosion, has recently become of interest. Potential additives include e.g. ammonium sulphate, ammonium phosphate and cyanuric acid. However, fundamental research on the decomposition behaviour of the additives, and their behaviour and performance in the SNCR process, is required in order to evaluate the viability of the additives.

Specific Objectives

The overall objective of this project is to obtain an improved understanding of the NO_x formation and reduction mechanisms during waste combustion. It is of interest to evaluate the use of alternative SNCR additives, such as urea, ammonium sulphate, ammonium phosphate and cyanuric acid, for simultaneous reduction of NO_x, deposition and corrosion. It is also desired to investigate the impact of inorganic elements released from MSW combustion on SNCR chemistry.

Experimental Investigation of the SNCR Process with Ammonium Sulphate as Reducing Agent

The SNCR performance of ammonium sulphate was studied in a bench-scale setup. The setup, shown in Figure 1, consists of a homogeneous flow reactor surrounded by an electrically heated oven, an FTIR analyzer and a novel feeding system capable of feeding micron sized liquid droplets. The feeding system consists of a storage tank for the aqueous solution of the additive of interest, in which a nebulizer is placed in

order to create a fine mist of micron sized droplets from the aqueous solution. A carrier nitrogen gas flow is used to transport the mist from the storage tank to the flow reactor.

SNCR experiments were performed for three aqueous ammonium sulphate solutions (2.5 wt%, 5 wt% and 10 wt%) at low and high oxygen concentration (1.25% and 8%). The typical water concentration was 3-5%. The temperature in each experiment was varied between 973 K and 1173 K. The inlet NO concentration to the flow reactor was approximately 370 ppm for each experiment. The residence time in the hot zone of the reactor was around 5-6 s depending on the flow rate and reactor temperature.

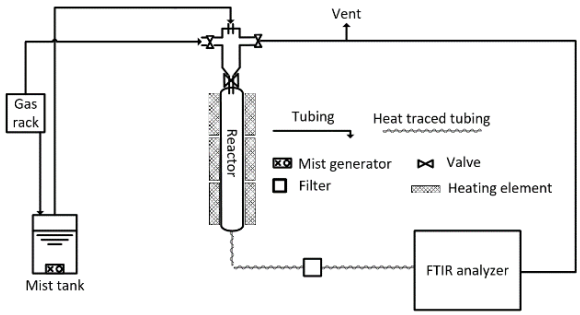

Figure 1: Schematic illustration of the bench-scale setup.

Kinetic Modeling of the SNCR Process with Ammonium Sulphate as Reducing Agent

A detailed chemical kinetic model (DCKM) has been developed for the SNCR process using ammonium sulphate as reducing agent, and Chemkin 17.1 has been used as modeling tool. The model is based on the mechanism developed by Glarborg et al. [2], consisting of a total of 150 species and 1389 reactions. The mechanism is constituted by different subsets for nitrogen chemistry, including subsets for NH_3, amine, H_2/O_2, H_2S/O_2, and S/N. In order to imitate the use of ammonium sulphate as reducing agent, the expected decomposition products from ammonium sulphate suggested by Halstead [3] has been implemented as inlet conditions in the model:

$$3(NH_4)_2SO_4 \rightarrow 4NH_3 + 3SO_2 + 6H_2O + N_2 \qquad (3)$$

The model was further modified by introducing a newly developed NH_2SO_2 subset constituted by 7 reactions, in an attempt to describe an observed inhibiting effect of SO_2 on NO reduction.

Results and Discussion

Through experiments with the developed bench-scale setup, it was generally observed that ammonium sulphate as an additive in the SNCR process yields comparatively low NO_x reductions compared to reference gas experiments using NH_3 gas, as reflected in Figure 2. The optimum temperature was typically observed to be around 1125 K. The low optimum temperature, as compared to other studies [4,5], may be explained by the significantly longer residence time in the present setup.

The experimental results shown in Figure indicate a strong dependency of SO_2 on the SNCR chemistry. However, the model does not capture this dependency satisfactorily.

The general trend of increasing the O_2 concentration was observed to be a downwards shift in the optimum temperature, while the NO reduction efficiency was decreased, which is in line with observations from other studies [6].

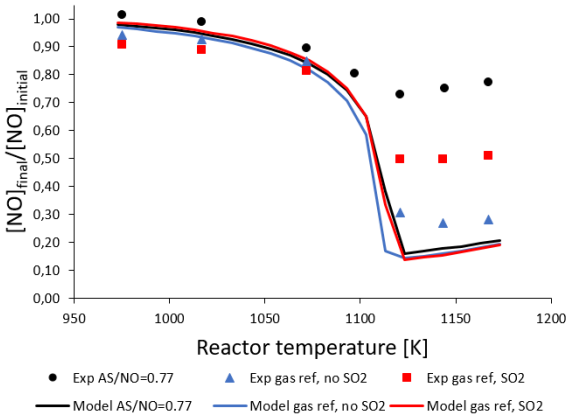

Figure 2: Comparison of experimental and simulation results of SNCR with ammonium sulphate (AS) with reference SNCR experiments using NH_3/NO=1.05 with an O_2 concentration of 1.25%.

References

1. M. Hupa et al., Proceedings of the Combustion Institute 000 (2016) 1–22.
2. P. Glarborg et al., Progress in Energy and Combustion Science 67 (2018) 31-68.
3. W. D. Halstead, Journal of Applied Chemistry 20 (1970) 129-132.
4. T. Nguyen et al., Chemical Engineering Journal 152 (2009) 36-43.
5. W. Hall, P. Williams, Waste Management & Research 24 (2006) 388-396.
6. Z. Lu, J. Lu, Combustion and Flame 156 (2009) 1303-1315.

He Liu

Phone: +86 18800176435
E-mail: liuhe1990@mail.tsinghua.edu.cn

Type: SDC (IPE)
Supervisors: Suojiang Zhang, IPE, CAS
Jakob Munkholt Christensen, DTU
Anker Degn Jensen, DTU

PhD Study
Started: Sept. 2012
Completed: July 2017

Catalyst for Catalytic Oxidation of Methane

Abstract
Methane slip from the exhaust of ship engine with methane as the fuels causes serious air pollution risks. The work attempts to exploit a highly efficient catalyst to catalytic oxidation of methane from the ship exhaust. Herein, a home-made supported catalyst was examined. This catalyst displays high activity with a light-off temperature of 375ºC. It also exhibits remarkable regenerative ability after sulfur poisoning at low temperature of 550ºC. These futures make this catalyst as attractive candidates in catalytic oxidation of methane.

Introduction
Methane is an attractive fuel to substitute the traditional fuels (such as diesel or bunker oil) for fuelling marine engines because it is cleaner and cheaper. However, methane slip from the exhaust of ship results in decrease of the efficiency of engine and causes huge risk to the environment since its impact on global warming is 20 times greater than that of carbon dioxide. The total catalytic oxidation of methane to carbon dioxide and water is considered as a technological option to reduce methane emissions from ship engine. Thus, the exploitation of high efficient catalysts to catalytic oxidation of methane at low temperature is urgently required.

The catalytic oxidation of methane has been investigated for at least the last 50 years.[1] Many types of catalysts, including transition metal oxides and noble metal oxides, are used for the complete oxidation of methane. Among these, supported noble-metal oxides are more active at lower temperature (below 400ºC), thus may function in the real working conditions of exhaust from ship engine. Notably, Pd-based catalysts exhibit highest catalytic activity for methane oxidation, but they do not have a good stability or high resistance to the loss of activity for long-term use in ship engine.[2] Additionally, Pd-based catalysts are very sensitive to sulfur poisoning.[3] In this respect, a new kind of catalyst for complete oxidation of methane with better long-term stability and higher sulfur tolerance and regenerative properties is urgently required.

Herein, catalyst A supported on X (A/X) was prepared and its performance for total oxidation of methane was studied. As the control sample, catalyst A supported on Y (A/Y) was also obtained to test the influence of specific supporters on the performance of methane oxidation. The light-off curves, sulfur poisoning resistance, and long-term stability of these catalysts were examined to evaluate their performance in catalytic oxidation of methane.

Experimental section
The experimental testing was carried out in a fixed bed catalytic reactor under the simulated exhaust of real ship engines as listed in Table 1.

Table 1: The specifications of feed for the experiments.

Specifications	Valus	Units
Total flow	300	NmL/min
Mass of catalyst	120	mg
CH_4 concentration	2500	ppm
O_2 concentration	10	vol%
H_2O concentration	5	vol%
SO_2 concentration (when added)	20	ppm
N_2 concentration	Rest	vol%

Results and Discussion
The light-off curves of A/X and A/Y catalysts were compared in Figure 1. The light-off temperature (T_{50}) is a criterion for evaluating the catalytic activity with respect to temperature, and it is defined as the temperature at which the given catalyst converts 50% of the reactant. A lower T_{50} indicates that the catalyst is more active at low temperature. T_{50} of 2% A/X catalyst is around 395°C in ignition curve and 375°C in extinction curve. Obviously, 2% A/X outperforms 2%

A/Y, and its activity can almost be comparable to 5% A/Y with T_{50} for ignition and extinction being 368°C and 396°C, respectively. This indicates the significance of supporter X in improving the performance of A-based catalyst. The better catalytic activity could be caused by the high dispersion and enhanced resistance to sintering of active species provided by supporter X.

Interestingly, compared with 1% A/Y, there is an activation occurring in the catalyst with higher A loading (2% and 5%), resulting in the activation shifting of T_{50} by 20~25°C. This could be rationalized by the removal of residual chlorine ions at higher temperatures, which act as inhibitors to the active materials.

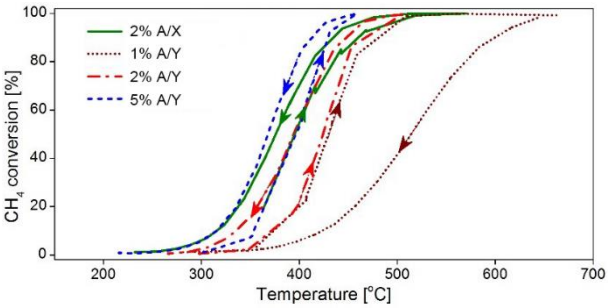

Figure 1: Comparison of light-off curves between different catalysts.

To gain knowledge on the sulfur resistance of catalyst A/X, 20 ppm SO_2 was imported into the feed gas. It can be observed that catalyst A/X deactivates completely by the SO_2 gas in a relatively short contact time (less than 2h) at 400°C (around T_{50}). However, after removing SO_2 from the feed and raising the temperature to 550°C, the conversion of methane almost fully recovers to 100% (Figure 2). This can be ascribed to the weak bond strength between sulphate species and A at relatively higher temperature, leading to the decomposition of sulphate species and regeneration of active sites. Notably, the regeneration temperature of catalyst A/X is low than 600°C, at which A-based catalysts are known to exhibit increased sintering. Thus, the thermal regeneration process would not cause damage to the activity of catalyst A/X. Additionally, thermal regeneration is comparatively easier to implement because the engine itself can be tuned to generate higher exhaust temperatures periodically.

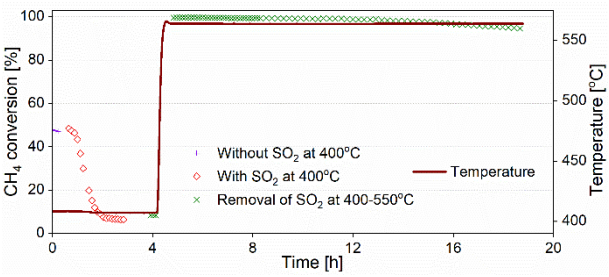

Figure 2: SO_2 poisoning of catalyst A/X at 400°C with 20 ppm SO_2. From t=0 to 0.7 h the SO_2 is diverted and from t=0.7 to 3.9 h, 20 ppm SO_2 is led into the reactor. From t=3.9 to 18.7 h the SO_2 is removing from the feed gas.

The long-term stability of catalyst A/X at different temperatures was also examined, and the results were illustrated in Figure 3. The conversion of CH_4 drops from 62% to 46% at 410°C and from 96% to 89% at 560°C for 15 h. This indicates that the long-term stability of catalyst A/X is not good as expected. This could be caused by the presence of water in the feed gas, which may form surface hydroxyls with low activity and accelerate sintering of active species.

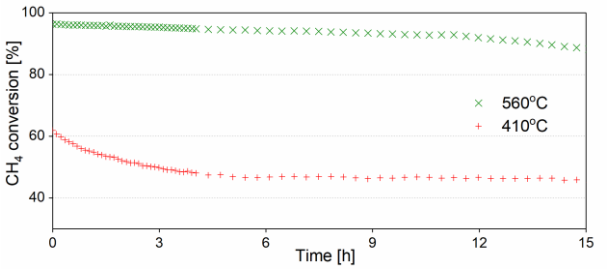

Figure 3: Long term deactivation (15 h) of catalyst A/X at 410°C and 550°C.

Conclusions

In conclusion, catalyst A/X was exploited to catalytic oxidation of methane. Catalyst A/X exhibits higher activity compared with catalyst A/Y, due to the high dispersion and enhanced resistance to sintering of active species provided by supporter X. The catalyst can be thermal regenerated from sulfur poisoning at low temperature of 550°C, inhibiting the increased sintering of active sites at high temperature. However, the long-term stability of catalyst A/X in the presence of water is not good, and this needs to be improved in the future work.

References

1. X. Jiang, D. Mira, D.L. Cluff, Prog. Energ. Combust. 66 (2018) 176-199.
2. J. Chen, H. Arandiyan, X. Gao, J. Li, Catal. Surv. Asia. 19 (2015) 140-171.
3. H.N. Sharma, V. Sharma, A.B. Mhadeshwar, R. Ramprasad, J. Phys. Chem. Lett. 6 (2015) 1140-1148.

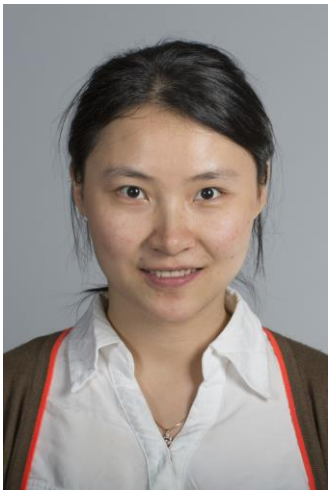

Xinyan Liu

Phone: +45 45256180
E-mail: xlin@kt.dtu.dk
Type: Joint KT-IPE

Supervisors: Georgios M. Kontogeorgis
Xiaodong Liang
Xiangping Zhang
Suojiang Zhang

PhD Study
Started: September 2016
To be completed: August 2019

Energy Efficient Hybrid Gas Separation with Ionic Liquid

Abstract

For most gas mixtures, the most common separation technology applied is distillation, which consumes large amounts of energy to give the high purity products. Hybrid gas separation processes, combining absorption and membranes together with distillation require less energy and have attracted much attention. With the property of non-volatility and good stability, ionic liquids (ILs) have been considered as new potential solvents for the absorption step. However, the enormous number of potential ILs that can be synthesized makes it a challenging task to search for the best one for a specific hybrid separation. In order to solve this problem, a systematic screening model for ILs is established by considering the needed properties for gas absorption process design. Rigorous thermodynamic model of IL-absorbed gas systems is established for process design-analysis. A strategy for hybrid gas separation process synthesis where distillation and IL-based absorption are employed for energy efficient gas processing is developed and its application is highlighted for a model shale gas processing case study.

Introduction

Gas separation process has been one of the most important technologies in the oil and gas related industries. For most gas mixtures, the most common separation technology applied is distillation, which consumes large amounts of energy to give the high purity products. These distillation columns operate at low temperatures and high pressures and therefore require high energy consumption, leading to negative environmental impacts. Therefore, an alternative scheme, taking advantage of the regions where each individual technology operate best, a hybrid gas separation scheme of combining distillation with absorption separation processes is considered.

Because of non-volatility, good stability, tunable viscosity and designable properties, ionic liquids (ILs) are considered as novel potential solvents and alternative media for gas absorption. Therefore, a strategy for hybrid gas separation process synthesis where distillation and IL-based absorption are employed for energy efficient gas processing has been developed. However, the potentially thousands of ILs that may be applicable, makes it a challenging task to search for the best one for specific gas absorptions in different raw gas systems. Therefore a selection-screening method for ILs is necessary for the development of novel hybrid gas separation process that can be designed.

Methodology

In this work, a three-stage methodology proposed for hybrid gas separation process design and evaluation will be highlighted. The first stage involves IL screening, where a systematic screening method together with a database tool is established to identify suitable ILs. The second stage is process design, where the important design issues are determined and the separation flowsheet is generated. The third stage involves verification and sustainability analysis based on rigorous process simulation of the generated hybrid gas separation process strategy. The gas separation problem for a model shale gas mixture is selected as a case study to highlight the application of this hybrid separation process design method.

This report will highlight the method, the data and applications of the method to generate novel, innovative and sustainable gas separation processes requiring significantly less energy than known processes.

Hybrid gas separation scheme

A generic representation of the natural or shale gas mixtures is developed, consisting of gases A, B, C, D and E, where a gas-A present in small amount is the lightest boiling, gas-B is in the largest amount, and the gases C-E are in small amounts and heavier boiling than gases A-B. A typical distillation train (scheme-1) for their separation is shown in Fig. 1 for a 5-gas mixture

requiring 3 separation steps. An alternative hybrid separation (scheme-2) is shown in Fig.2, where the distillation columns are replaced by absorption followed by flash-evaporation operations. Since the only energy requiring steps in the hybrid scheme of Fig 2 are the flash-evaporation steps, potentially a large reduction of energy consumption is possible by switching from scheme-1 to scheme-2.

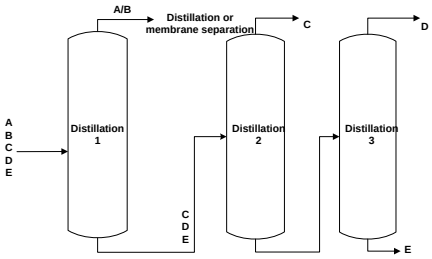

Figure 1: Gas separation with scheme-1

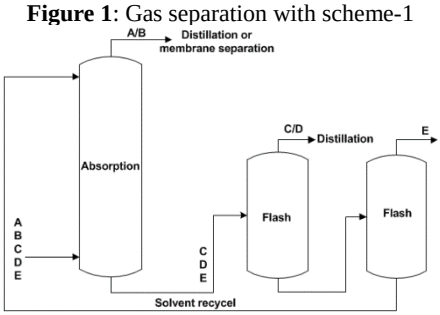

Figure 2: Gas separation with scheme-2

Scheme-2 is based on a new technology for removal of CO_2 from shale gas with IL as the solvent [1]. The first step for application of scheme-2 is the selection of an appropriate IL.

Database of ILs with measured solubility data

A database with collected measured solubility and Henry's law constant data of gases in ILs has been created. The collected data contains measured solubility data at different temperatures as well as Henry's law constant data of many gases in various ILs. It includes 14393 data points covering 16 gases and 136 ILs.

Model for Henry's law constant prediction

Because of the larger amount of data available for solubility of CO_2 in ILs, models to generate additional data were first developed for CO_2. The temperature dependence of the Henry's law constants was described by the following equation.

$$\mathrm{H} = \exp[a + b/T] \quad (1)$$

Where, H is Henry's law constant of CO_2 in ILs, in bar. T is the temperature, in K. *a* and *b* are coefficients which are regressed by using the experimental data.

Linear fitting of coefficients a and b as a function of carbon atom number on the alkyl chain of different anions of IL, the Henry's law constant model of CO_2 in a specific IL type is established (see Eq.2).

$$H = \exp[\mathrm{c1} + c2 \cdot Cn + \frac{c3 + c4 \cdot Cn}{T}] \quad (2)$$

Where, *Cn* is the carbon atom number on the alkyl chain of ILs. *c1, c2, c3* and *c4* are parameters estimated through regression. Through this model, solubility of CO_2 (or other gases with their corresponding models) in new IL can be predicted. In this case study, we established the model for imidazolium-based ILs with [Tf2N], [BF4] and [PF6] as anion.

Besides this group contribution model, other models such as UNIFAC and COSMO-RS model are also taken into consideration to be developed.

Application on database and model library

Based on the measured Henry's law constant data of CO_2 and CH_4, the Henry's law constant of CO_2 versus selectivity of CO_2/CH_4 under different temperature is plotted as in Figure 3.

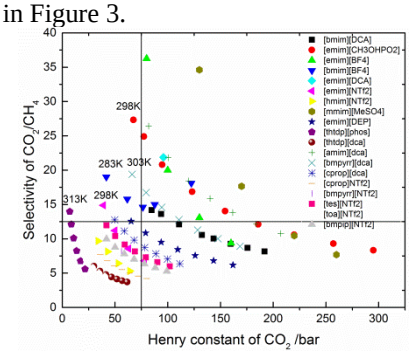

Figure 3 Henry's law constant of CO_2 versus selectivity of CO_2/CH_4 under different temperature

Then the optimal IL is the one which has the lowest Henry's law constant of CO_2 and highest selectivity of CO_2/CH_4. As the temperature increases, both the solubility of CO_2 and selectivity of CO_2/CH_4 decrease. Since [thtdp][phos] shows the lowest Henry constant among others at relative high temperature, which means it may have a lower Henry's law constant and higher selectivity when the temperature decreases, and it was, thus, chosen as the optimal one for the further study.

Conclusion and future work

This work provided a good basis for novel IL-based hybrid gas separation process design. All the predictive Henry's constant models have been found to be in good agreement with experimental data. On the basis of the database and models, a case study for selection of the potential IL-solvent for gas separation by absorption has been highlighted. An IL-based hybrid separation scheme for significantly reduced energy has been introduced and the potential benefits highlighted through a conceptual example.

Future work is necessary to develop a UNIFAC model in more gas-ILs systems. A better solvent and process for shale gas separation will be designed based on the database and model library. Rigorous gas separation simulation and evaluation will be also developed.

References

1. X. Liu, Y. Huang, Y. Zhao, R. Gani, X. Zhang, S. Zhang, Ionic liquid design and process simulation for decarbonization of shale gas. Industrial & Engineering Chemistry Research, 55(20) (2016) 5931-5944.

Xue Liu

Phone: +86 15101544706 /+45 5273 1868
E-mail: xliu@ipe.ac.cn / xuli@kt.dtu.dk

Type: Joint KT-IPE
Supervisors: Anne Ladegaard Skov
Suojiang Zhang
Yi Nie

PhD Study
Started: December 2017
To be completed: November 2020

Screen the optimal ionic liquid for dissolving keratin by COSMO-RS

Abstract

Wool keratin, which is polar, hydrophilic, biodegradable, is expected to enhance interaction responses between implantations and cells. But wool keratin is hard to reuse because it is difficult to dissolve in conventional solvents. An increasing interest has been manifested in the use of ionic liquids (ILs) as solvents for dissolution of wool keratin due to their tunable and excellent properties. However, it is nevertheless a challenge to identify the best ILs for keratin dissolution. Experimental measurement of all these systems is not practically feasible; hence a rapid and a priori screening method to predict the keratin solubility capacity for ILs is needed. Based on our previous work, we designed three keratin models for describing wool keratin, and 462 ILs formed from 21 cations and 22anions were selected for evaluation of their ability to dissolve wool keratin by COSMO-RS. From the prediction results of logarithmic activity coefficients (lnγ) of the three keratin models, it can be concluded that keratin dissolution capacity is mostly determined by the anion while the cation only has a moderate effect on the dissolution process. Ac^-, Dec^-, $HCOO^-$, Cl^-, BEN^-, DMP^-, DEP^-, DBP^-, TOS^- and $Br^-$with various cations studied in this work exhibited particularly good properties for keratin dissolution. The excess enthalpy calculations indicated that the main forces in the keratin dissolution in ILs are H-bonds, while the contribution of misfit forces and van der Waals forces are secondary. It lays a foundation for the research of keratin elastomer composites later.

Introduction

Dielectric elastomers (DEs), which are often referred to as “artificial muscles”, possess many excellent properties, such as large strains, high-energy densities, and fast responses [1]. Polydimethylsiloxane (PDMS) elastomers are one of the most used materials for DEs [2]. Unfortunately, most PDMS used in tissue engineering applications are nonpolar, inert and highly hydrophobic，which lead to the low biocompatibility and interaction responses between implantations and cells [3].

Keratin, which is polar, hydrophilic, biodegradable, is expected to enhance interaction responses between implantations and cells [3]. The biofunctions of silicone /keratin composites for tissue engineering could be achieved due to the special amino acid sequence in keratin [4]. Moreover, keratin can improve the mechanical properties of composites, which probably results from the formation of a common spatial network between keratin and silicone elastomer [3].

Wool, consisting of approximately 95 wt% pure keratin, is a kind of degradable natural biopolymer. It also contains about 11-17% cysteine, which serves as crosslinking sites to form water-stable fibers [5]. However, wool keratin is difficult to dissolve in conventional solvents, due to the tight packing of the secondary structures in the polypeptide. So efficient dissolution of keratin is the basis for the research of elastomer–keratin compositions [5].

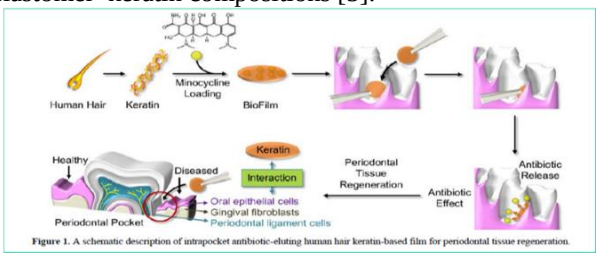

Figure 1. A schematic description of intrapocket antibiotic-eluting human hair keratin-based film for periodontal tissue regeneration.

As a new design solvent, ILs can dissolve a large number of biopolymers with high efficiency, due to their unique properties like high thermal stability, tunable properties, and good dissolving ability [5]. Although there have been extensive studies for dissolution of keratin in ILs, it is still a challenge to identify the best ILs for keratin dissolution. Experimental measurement of all these systems is not practically feasible; hence a rapid and a priori screening method to predict the keratin solubility capacity for ILs is needed. In this work, we designed three models containing disulfide bonds for describing wool keratin, and 462 ILs formed from 21 cations and 22anions were

selected for evaluation of their ability to dissolve wool keratin by COSMO-RS. It lays a foundation for the research of keratin elastomer composites later.

Specific Objectives

The objectives of this work were to design three keratin models based on our previous work and to select the best keratin model from three keratin models, and use COSMO-RS to screen the best ILs for keratin dissolution.

Results and discussion

We selected 462 ILs formed from 21 cations and 22 anions for evaluation of their ability to dissolve wool keratin by using COSMO-RS. The structure of cations and anions employed in this work can be seen in Fig.2 and Fig.3.

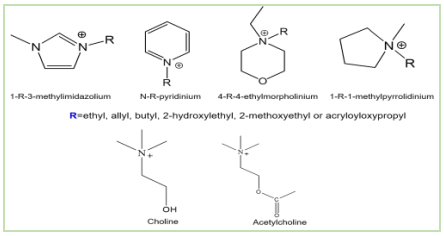

Fig.2 Structure of cations

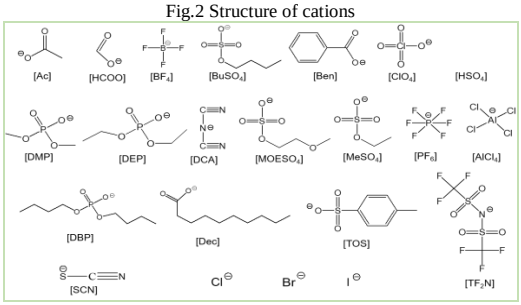

Fig.3 Structure of anions

Keratin has a complex structure, and there are a large number of inter- and intra-molecular strong hydrogen bonds and disulfide bonds. Moreover, keratin molecules have no regular repeating units, which led to it difficult to design a suitable model to describe keratin. In this work, three models containing disulfide bonds for describing wool keratin were designed. The chemical structures and charge surface regions are displayed in Fig. 4.

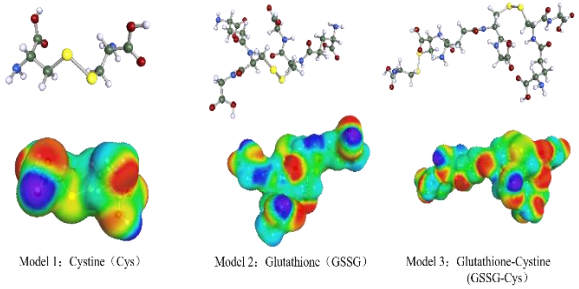

Fig.4 Chemical structures and charge surface regions of keratin models

The predicted logarithmic activity coefficients (ln γ) of the three keratin models in each of the 462 ILs are depicted in Fig.5. The cations and anions are listed according to their keratin dissolution ability. The ILs with high keratin dissolution capacities according to the predicted logarithmic activity coefficients are located to the left, while the ILs with lower keratin dissolution capacities are located to the right. From the prediction results of lnγ of the three keratin models, it can be concluded that keratin dissolution capacity is mostly determined by the anion while the cation only has a moderate effect on the dissolution process. Ac^-, Dec^-, $HCOO^-$, Cl^-, BEN^-, DMP^-, DEP^-, DBP^-, TOS^- and Br^- with various cations studied in this work exhibited particularly good properties for keratin dissolution.

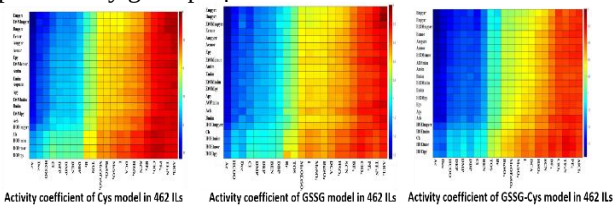

Fig.5 The logarithmic activity coefficients prediction of keratin models 1 in ILs. Conditions: the mole fraction of model was 0.5, the mole fraction of IL cations and anions was 0.25 each. The calculation temperature was 120 °C.

The excess enthalpies from the intermolecular interactions (H-bonds, misfits and van der Waals forces) between the keratin models and several kinds ILs were also calculated (Fig.6). The excess enthalpy calculations indicated that the main forces in the keratin dissolution in ILs are H-bonds, while the contribution of misfit forces and van der Waals forces are secondary.

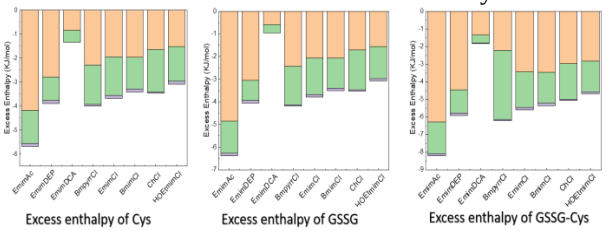

Fig.6 Excess enthalpies between the three cellulose models and seven ILs, H-bond (Orange), misfit (Green) and van der Waals force (Purple).

Conclusions

Three models containing disulfide bonds were designed for describing wool keratin, and 462 ILs formed from 21 cations and 22anions were selected for evaluation of their ability to dissolve wool keratin by COSMO-RS. From the predicted results, it can be concluded that in the process of keratin dissolution, the solubility of keratin in ILs is affected by cation and anion, but the anion plays a leading role. Ionic liquid with Ac^-, Dec^-, $HCOO^-$, Cl^- , DEP^-, DMP^-, DBP^-, BEN^- or Br^- has excellent solubility of keratin, and H-bond interactions between the three models and ILs have a high influence on the solubility of keratin.

Acknowledgements

The authors gratefully acknowledge the financial support of the department of chemical and biochemical engineering of DTU and key laboratory of green process and engineering of IPE.

References

1. R., Pelrine, R., Kornbluh, Q., Pei, J., Joseph, Science 287 (5454) (2000) 836-839.
2. C., Löwe, X., Zhang, G., Kovacs, Advanced engine-ering materials 7 (5) (2005) 361-367.
3. M., Van Dyke, U.S. Patent 2004, Application No. 10/606,279.
4. H., Lee, Y., Hwang, H., Lee, S., Choi, S., Kim, J., Moon, H. Bae, Macromolecular Research 23 (3) (2015) 300-308.
5. X., Liu, Y., Nie, X., Meng, Z., Zhang, X.,Zhang, S., Zhang, RSC Advances 7 (4) (2017) 1981-1988.

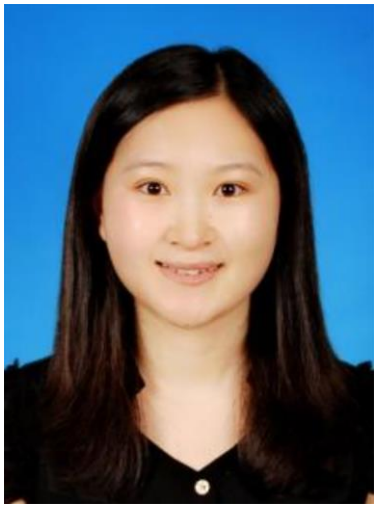

Yanrong Liu
Phone: +45 4525 6195
E-mail: yanrong.liu@ltu.se

Type: Joint KT-IPE
Supervisors: Anne S. Meyer
Kaj Thomsen
Suojiang Zhang
Yi Nie

PhD Study
Started: January 2015
Completed: December 2017

Predictive Screening of Ionic Liquids for Dissolving Cellulose and Conductive Fiber Spinning

Abstract
Cellulose is widely used in paper products, textiles, plastics, coatings, composites, laminates, optical film, pharmaceuticals and other applications. However, the multiple H-bonds between cellulose molecules form high order crystalline regions which makes cellulose insoluble in water and common organic solvents. Ionic liquids (ILs) as the green solvents have been investigated for dissolving cellulose recently. Numerous potential ILs composed of cations and anions can be synthesized. Thus, a rapid and a priori screening method to predict the cellulose solubility capacity for ILs is urgent needed, that is COSMO-RS. The objectives of this work are to use COSMO-RS to screen potential ILs for their ability to dissolve cellulose, select the best cellulose model and apply the cellulose to prepare the electroconductive fibers by spinning.

Introduction
Cellulose is a linear polymer consisting of several hundred to over ten thousand β-(1→4)-linked glucose repeating units, together with numerous intermolecular and intramolecular H-bonds [1]. The numerous applications of cellulose are attributed to its promising features, such as biocompatibility, biodegradability, thermal and chemical stability [2]. Some traditional solvent systems have been investigated for cellulose dissolution processes, for example, N-methylmorpholine oxide (NMMO) [3], N, N-dimethylacetamide/lithium chloride (DMAc/LiCl) [4], N, N-dimethylformamide/nitrous tetroxide (DMF/N_2O_4) [5], molten salt hydrates ($LiClO_4 \cdot 3H_2O$, $LiCH_3COO \cdot 2H_2O$, $LiCl/ZnCl_2/H_2O$, $NaSCN/KSCN/LiSCN \cdot 2H_2O$) [6] and aqueous NaOH or aqueous solutions of metal complexes (Cd-tren, Ni-tren and Cuoxam) [7]. However, drawbacks of these processes including high cost, high dissolution temperature, volatility, difficulty in solvent recovery and toxicity make them undesirable, and underlines the necessity for developing greener solvents for cellulose dissolution [8]. ILs were considered as green solvents in recent researches [9]. The increasing attraction to ILs is due to their remarkable properties such as immeasurably low vapour pressure, excellent chemical and thermal stability, electrical conductivity, and non-flammability [10].

The most fascinating property of ILs is the structural diversity, as numerous possible cations and anions can be combined freely [11]. It will be a tough work for acquiring the efficient ILs for dissolving cellulose. COSMO-RS (Conductor-like Screening Model for Real Solvents), integrates dominant interactions of H-bonds, misfits and Van der Waals forces in IL systems to summarize multiple solvation [12]. which can be used for performing mixture calculations at various temperatures. It has been considered by many as the most accurate model for the prediction and development of ILs for specific tasks currently available [13].

Carbon nanotubes (CNTs) have attracted tremendous attention because of their unique electronic and mechanical properties. Recent researchers have been reported that CNTs hybrid with the polymer can form conductive films and fibers by spinning, but little work based on natural polymers [14]. In this work, the potential ILs for dissolving cellulose were screened by COSMO-RS, then the potential ILs were used for dispersing CNTs and dissolving cellulose to prepare the electroconductive fiber by spinning.

COSMO-RS prediction

The COSMO-RS calculations were carried out using several procedures. First, the quantum chemical Gaussian09 package was used to optimize the structure of the studied compounds at the B3LYP/6-31++G (d, p) level. Second, the COSMO files of the optimized structures were opened by Gaussian03, and COSMO continuum solution models were calculated using the BVP86/TZVP/DGA1 level theory. Third, the logarithmic activity coefficients, excess enthalpies, σ-potentials and σ-profiles were determined using the model COSMO-RS (implementation: COSMOtherm version C3.0 release 14.01, applied with parameterization BP_TZVP_C30_1401, COSMOlogic, Leverkusen, Germany). The calculation temperature for COSMO-RS was set to 90 °C, the same temperature as used for the experimental determination of cellulose solubility. When conducting calculations in the COSMO-RS program, the molar fractions of the cations and anions of the ILs were treated as equal, i.e. $n_{cation}=n_{anion}=n_{IL}$ [15]. The logarithmic activity coefficients and excess enthalpies for solutions of cellulose in ILs were also investigated by COSMO-RS. Then the cellulose solubility experiment was used to verify the prediction results. The procedures of the ILs screening can be seen in Fig. 1.

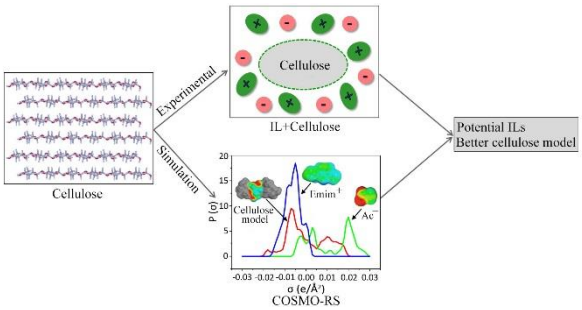

Fig. 1 The procedures of ILs screening

MWCNTs electroconductive fiber preparation

MWCNTs electroconductive cellulose-based fibres were prepared by spinning. First, a certain amount of MWCNTs were dispersed in IL by grinding. Second, a certain amount of pulp was dissolved in IL at 90 ℃. Third, hybrid these two solutions and mechanical agitation at 90 ℃. Finally, the homogeneous electroconductive solution was deaerated in vacuum oven at 35 ℃. Then the electroconductive solution was applied to spin at room temperature and used water coagulation bath. The wet fiber was washed by water at last 5 times and dried in atmospheric environment. The morphology, mechanical properties and conductive properties of the resultant MWCNTs–cellulose fibres can be investigated by scanning electron microscopy, tensile testing and electrical resistance measurement, respectively. The spinning process was shown in Fig. 2.

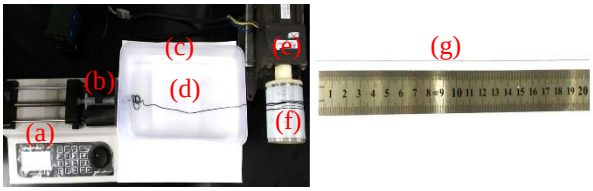

Fig. 2 The spinning procedures of carbon nano conductive fiber. (a) spinning pump, (b) 10 ml springe, (c) coagulating basin, (d) water, (e) rolling shaft, (f) wet conductive fiber, (g) dry conductive fiber.

Acknowledgements

The author acknowledges the financial support from Department of Chemical and Biochemical Engineering, Technical University of Denmark and Institute of Process Engineering, Chinese Academy of Sciences.

References

4. H. Wang, G. Gurau and R. D. Rogers, Chem. Soc. Rev. 41 (2012) 1519-1537.
5. C. Tsioptsias, A. Stefopoulos, I. Kokkinomalis, L. Papadopoulou and C. Panayiotou, Green Chem. 10 (2008) 965-971.
6. H. -P. Fink, P. Weigel, H. J. Purz and J. Ganster, Prog. Polym. Sci. 26 (2001)1473-1524.
7. C. L. McCormick, T. R. Dawsey, Macromolecules. 23 (1990) 3606-3610.
8. R. B. Hammer, A. F. Turbak, Abstracts of Papers of the American Chemical Society. 173 (1977) 8.
9. S. Fischer, H. Leipner, K. Thümmler, E. Brendler and J. Peters, Cellulose. 10 (2003) 227-236.
10. K. Saalwächter, W. Burchard, P. Klüfers, G. Kettenbach, P. Mayer, D. Klemm and S. Dugarmaa, Macromolecules. 33 (2000) 4094-4107.
11. Y. L. Zhao, X. M. Liu, J. J. Wang and S. J. Zhang, J. Phys. Chem. B. 117 (2013) 9042-9049.
12. A. R. Xu, J. J. Wang and H. Y. Wang, Green Chem. 12 (2010) 268-275.
13. Y. R. Liu, K. Thomsen, Y. Nie, S. J. Zhang, A. S. Meyer, Green Chem. (2016) DOI: 10.1039/C6GC01827K.
14. J. Palomar, J. S. Torrecilla, V. Ferro and F. Rodríguez, Eng. Chem. Res. 48 (2009) 2257-2265.
15. Z. Guo, B.-M. Lue, K. Thomsen, A. S. Meyer and X. Xu, Green Chem. 9 (2007) 1362-1373.
16. A. Klamt, Advanced Review. 1 (2011) 699-709.
17. H. Zhang, Z. G. Wang, Z. N. Zhang, J. Wu, J. Zhang and J. S. He, Adv. Mater. 19 (2007) 698-704.
18. A. Casas, S. Omar, J. Palomar, M. Oliet, M. V. Alonsoa and F. Rodrigueza, RSC Adv. 3 (2013) 3453-3460.

Hao Luo

Phone: +45 4525 2853
E-mail: haol@kt.dtu.dk

Type: DTU/SDC master
Supervisors: Kim Dam-Johansen
Hao Wu
Weigang Lin

PhD Study
Started: October 2016
To be completed: September 2019

CFD Simulation of Biomass Combustion in Fluidized Beds

Abstract

The project aims at developing an efficient and reliable computational fluid dynamics (CFD) model to simulate biomass combustion in fluidized bed systems. A multi-scale methodology (particle-scale, meso-scale, and reactor-scale) is adopted to simplify such a complex system. A heat transfer corrected isothermal model has been developed for CFD simulation of devolatilization of large biomass particles in fluidized bed.

Introduction

Biomass combustion in fluidized bed is a typical complex heterogeneous reacting system. Conventional chemical reaction engineering (CRE) models (e.g. plug-flow, ideal well-mixed etc.) oversimplifies the hydrodynamic behaviors in fluidized beds. Thus, the effect of hydrodynamic behaviors on biomass particles reaction is not fully understood. Compared to CRE models, CFD models have been widely considered as a useful tool to reveal both hydrodynamic and reaction behavers in detail, e.g. velocity, pressure and temperature profiles, as well as mixing in fluidized bed combustors. However, the following challenges remain in CFD modeling of biomass combustion in a fluidized bed at different scales, as shown in Fig. 1.

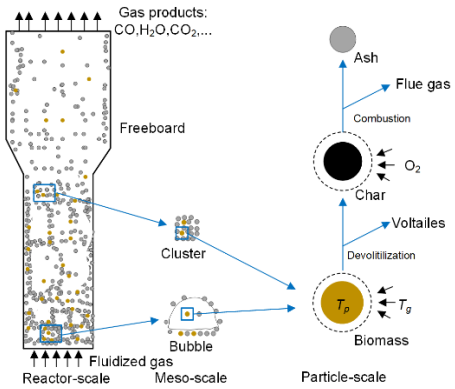

Figure 1: Different scales of CFD modeling biomass combustion in fluidized bed.

(1) Particle-scale: internal heat and mass transfer are usually neglected in CFD simulations, because a computational cell is larger than particles. However, internal transfer has significant effects on reaction at particle scale, especially for large particles [1].

(2) Meso-scale: the meso-scale structures (e.g. cluster or bubble) have significant effects on momentum, and heat and mass transfer between gas and solid phase [2,3]. Current meso-scale structure model should be validated for modeling biomass combustion in fluidized bed.

(3) Reactor-scale: CFD modeling coupled with chemical kinetic models is time-consuming for a large-scale fluidized bed. It is essential to develop reliable and efficient approaches to couple CFD models with chemical reaction kinetics.

Objectives

The objective of this project is to develop an efficient and reliable approach to simulate biomass combustion in fluidized bed systems. Through this project, we can have better understanding of biomass combustion in fluidized bed and the developed method can be used to model biomass combustion both at particle-scale and reactor-scale.

Heat transfer corrected isothermal model

An isothermal particle model is commonly used in CFD modeling of biomass devolatilization in fluidized beds. However, the model is only reasonable for small particles (Biot Number: Bi<1). For large particles, the internal temperature gradient has significant effect on devolatilization. Therefore, a non-isothermal model is favored for modeling biomass devolatilization. However, it is time-consuming when a non-isothermal model is directly coupled with CFD models. To solve the problem, a heat transfer corrected isothermal model

is developed by using correction coefficient defined as follows:

H_T: Correction coefficient for heat flux

$$Q_{cor-iso} = Q_{non-iso} = H_T Q_{iso} \quad (1)$$

$$H_T = \frac{Q_{non-iso}}{Q_{iso}} = \frac{h_c\left(T_g - T_{surf}\right) + \varepsilon_p \sigma\left(T_w^4 - T_{surf}^4\right)}{h_c\left(T_g - T_p\right) + \varepsilon_p \sigma\left(T_w^4 - T_p^4\right)} \quad (2)$$

H_R: Correction coefficient for reaction rate

$$R_{cor-iso,i} = R_{non-iso,i} = H_{R,i} R_{iso,i} \quad (3)$$

$$H_{R,i} = \frac{R_{non-iso,i}}{R_{iso,i}} = \frac{\int_0^R 4\pi f_{r,i}\, r^2 dr}{f_i V_p} \quad (4)$$

Based on the correction coefficients, a heat transfer corrected isothermal model is derived:

$$c_p \rho_p \frac{dT_p}{dt} = \frac{b}{r}\left(h_c\left(T_g - T_p\right) + \varepsilon_p \sigma\left(T_g^4 - T_p^4\right)\right) H_T - \sum_{i=1}^{n} \Delta H_{R,i} R_{cor-iso,i} \quad (5)$$

$$R_{cor-iso,i} = f_i V_p H_{R,i} \quad (6)$$

where Q is the heat flux between gas and particle, h_c is convection heat transfer coefficient, R is the reaction rate, f is kinteic model of reaction i. V_p is particle volume. T_w, T_p, T_g,T_{surf} are wall, particle, gas, and particle surface temperature, respectively, ΔH is heat of reaction.

In this way, the non-isothermal and corrected isothermal model can predict similar results and more importatly, the corrected isothermal model can be easily coupled to a CFD software with similar compuational time of isothermal model.

Fig 2. shows the conversion history predicted by different models and a comparison to experimental data [4] of a near-spherical particle devolitilized at the single particle combustor. Obviously, the mass loss history predicted by corrected isothermal and non-isothermal model are in good agreement with the experimental data, while the isothermal model underestimates the conversion at the beginning and overestimates the conversion at later time.

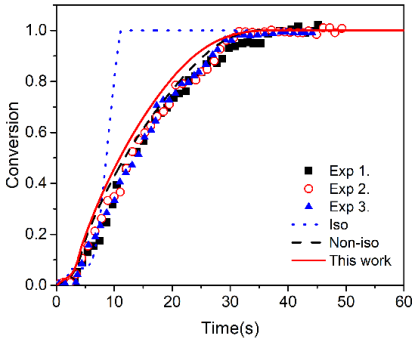

Figure 2: Conversion history of large particle (d_p=9.5mm, T_g=1050 K, Moisture=6 wt%, T_w=1276 K)

Fig 3 shows a comparison of CFD modeling of biomass particle pyrolysis rate by using corrected isothermal and isothermal model in a batch fluidized bed. At average particle temperature T_p~600 K, the particle outer layer temperature is high enough for biomass devolatilization, and this stage corresponds to H_R>1. Therefore, corrected isothermal model shows a higher pyrolysis rate as well as volatiles mass fraction than isothermal model. At average particle temperature T_p~800 K, the particle outer layer has high conversion or even totally converted, this stage corresponds to H_R<1. Therefore, the pyrolysis rate predicted by isothermal model larger than that of corrected isothermal model. In totally, the corrected isothermal model shows that biomass particle starts devolatilization at low particle temperature and ends at higher particle temperature, as compared to isothermal model. The result is consistent what we observed in single particle modeling.

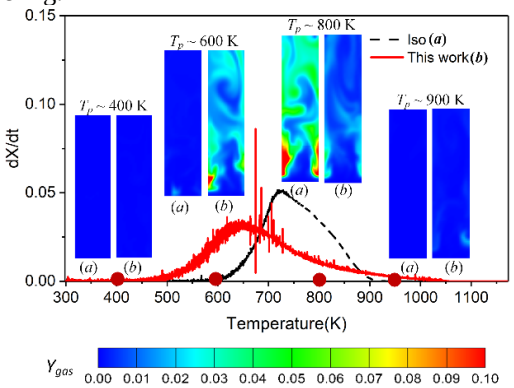

Figure 3: Comparisons of CFD modeling pyrolysis rates versus particle average temperature and contour plot of volatiles mass fraction by using isothermal model and this work.

Conclusion

CFD modeling biomass combustion in fluidized bed dependent on the development of models of different scales (particle scale, meso-scale, and reactor scale). A heat transfer corrected isothermal model is developed to model devolatilization of large biomass particle at particle scale. Two heat-transfer corrected coefficients, H_T-correction of heat transfer and H_R-correction of reaction rates are introduced and correlated as a binary function of heat convection coefficients and a dimensionless particle temperature. The model is validated by experimental data in literatures and implemented in a CFD software.

Future work

In future, it is planned to extend this method to describe char combustion in a fluidized bed. After that, the current meso-scale model (e.g. drag model, heat transfer model etc.) will be validated for CFD modeling biomass combustion in fluidized bed. Finally, we plane to develop a reliable and efficient approach to model large-scale fluidized by coupling CFD and CRE models.

References

1. A. Gómez-Barea, B. Leckner, Prog. Energy Combust. Sci. 36 (2010) 444–509.
2. W. Wang, B. Lu, N. Zhang, Z. Shi, J. Li, Int. J. Multiph. Flow. 36 (2010) 109–118.
3. K. Hong, Z. Shi, W. Wang, J. Li, Chem. Eng. Sci. 99 (2013) 191–202.
4. H. Lu, W. Robert, G. Peirce, B. Ripa, L.L. Baxter, Energy and Fuels. 22 (2008) 2826–2839.

Cuicui Lyu

Phone: +86 15522037532
E-mail: lvcuicui870818@163.com
Type: SDC (IPE)
Supervisors: Shufeng Ye
Anne Juul Damø
Hao Wu
Weigang Lin
Jytte Boll Illerup

PhD Study
Started: September 2013
Completed: June 2017

Characterization of elemental sulfur in chalcopyrite leaching residues from the FLSmidth® ROL Process

Abstract
A key component in the atmospheric leaching of metal sulfides is the oxidation of sulfide to either elemental sulfur or S(VI). The final oxidation state of sulfur significantly influences the economic viability of a leaching process. Thus, it is important to both quantify and characterize the sulfur oxidation products. In this work, a new method based on Simultaneous Thermal Analysis (STA) is established for the quantification and thermal characterization of elemental sulfur in chalcopyrite leaching residues from the FLSmidth® ROL process.

Introduction
To address the intractable technical problem of hydrometallurgically extracting chalcopyrite (CuFeS2), global engineering company FLSmidth® has developed a mechanochemical approach, i.e., the FLSmidth® Rapid Oxidative Leach (ROL) for atmospheric leaching of chalcopyrite in acidic ferric sulfate, which provides more than 97% copper recovery in 6 h or less [1]. Even though the generated extraction products can be tuned by changing the leaching operating conditions, the amount of produced sulfur during the leaching process is still unknown. In terms of its effect on oxygen consumption, acid generation, and surface passivation, it is of great significance to establish a method to identify the sulfur characterization [2].

In this paper, Simultaneous Thermal Analysis (STA) is used to analyze elemental sulfur in chalcopyrite concentrate leaching residue obtained from hydrometallurgical leaching of chalcopyrite. The STA method employs the simultaneous application of thermogravimetric analysis (TGA) and differential scanning calorimetry (DSC) [3]. The key point in this paper is to develop a STA method to quantify and characterize the sulfur in the chalcopyrite leaching residue.

Elemental composition and mineral phases in the leaching residue
According to the result of inductively coupled plasma-optical emission spectrometry (ICP-OES), X-ray diffraction (XRD) and scanning electron microscope-energy dispersive spectrometer (SEM-EDS), we assume that there are elemental sulfur (S_0), quartz (SiO_2), chalcopyrite ($CuFeS_2$), pyrite (FeS_2), carrollite ($CuCo_2S_4$), and muscovite ($KAl_2(AlSi_3O_{10})(OH)_2$) in the leaching residue. The content of each mineral phase in the leaching residue is calculated in Table 1.

Table 1. Calculated content of each mineral phase in leaching residue (wt %).

Content	**sulfur**	**quartz**	**chalcopyrite**
wt %	62.25	24.68	8.70
Content	**pyrite**	**Carrollite**	**muscovite**
wt %	1.61	2.31	0.45

Establishment of quantification and qualification method by STA
The STA of synthetic samples (marked by J1, J2, J3, J4, means the ratioes of S_0: $CuFeS_2$:SiO_2 to be 2.7:1:3, 4.8:1:3, 15.3:1:3, 1:0:0, respectively.) are shown in Figure 1, with the heating/cooling rates of 2 °C/min, N_2 flow of 100 mL/min, samples mass of 10 mg.

DSC curve
1st stage: Heating from 25 °C to 130 °C
There are two distinct endothermic peaks at around 110.0 °C and 121.0 °C for the four samples. The temperature position of peak T1 is reduced with the increase of the sulfur content in the synthetic samples, indicating that the conversion of sulfur proceeds slowly near the transformation temperature, which can be assigned to the α-sulfur to β-sulfur transformation [4]. It is believed that the transformation time is influenced by the purity of the sample [5]. The peak T2 at around 120.0 °C is likely the melting of β-sulfur.

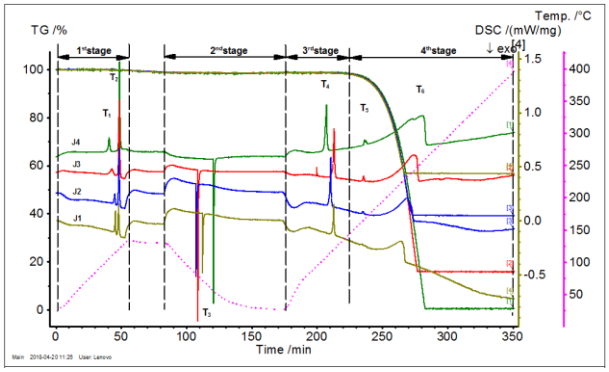

Figure 1: STA of synthetic samples with different sulfur contents.

2nd stage: Cooling from 130 °C to 25 °C

A distinct exothermic peak T3 is present at 54.9 °C, 78.4 °C, 81.0 °C, and 71.4 °C for different synthetic samples, respectively. The exothermic peak in synthetic samples may be attributed to the recrystallization of S_β (or a mixture of S_β and other cyclic molecules) [6].

3rd stage: Heating from 25 °C to 150 °C

The distinct endothermic peak T4 position at 108.9°C, 120.7 °C, 115.4 °C, and 120.4 °C for the four samples, respectively. As compared to the melting point of what is supposed to be monoclinic β-sulfur during the 1st stage heating (around 120.3 °C), the positions of the peak for J4 and J2 are shifted toward significantly lower temperatures. This strongly indicates that the re-crystallized sulfur during the 2nd stage is another (metastable) allotrope of sulfur than the monoclinic β-sulfur.

4th stage: Heating from 150 °C to 400 °C.

There are also small endothermic peaks at around 165.0 °C for the four samples, which could be assigned to the producing of λ-sulfur at 165 °C.

TGA curve

As for the TGA curves, the performance of the four synthetic samples are almost the same as the leaching residue, with small mass losses of 1.62% during the 130 °C isothermal stage and large mass losses above 150 °C. There are total mass losses of 98.13 %, 82.62 %, 59.31 %, and 41.82 % for J4, J3, J2 and J1, respectively, which are highly close to the theoretical sulfur content in samples (on the grounds of the sample ratios).

Based on the melting enthalpy of elemental sulfur, the quantification of sulfur can be done by STA measurements. The related function is calculated between sulfur melting enthalpy and mass change based on DSC data and TGA data. The linear function fitting is shown in Figure 2. With the fitting equation, the unknown amount of sulfur in leaching residue can be easily figured out.

Conclusions

In this work, an STA-based method for quantification and thermal characterization is developed and evaluated. It is found that STA, which refers to the simultaneous application of thermogravimetric analysis (TGA) and differential scanning calorimetry (DSC) in a single instrument, can be used conveniently for the quantification and thermal characterization of sulfur in leaching residues from the FLSmidth® ROL process.

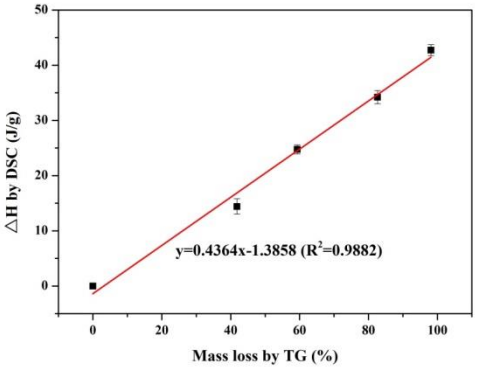

Figure 2. The linear fitting of TGA-based mass loss and DSC-based enthalpy.

Acknowlegements

This work is part of the Joint Doctoral Programme from Sino-Danish College (SDC). The work is also part of the advanced technology platform 'Minerals and Cement Process Technology - MiCeTech' funded by the Innovation Fund Denmark, FLSmidth A/S, Hempel and the Technical University of Denmark (Grant No. 39-2013-2). The financial and material supports of the work by the SDC and FLSmidth® Company are gratefully appreciated.

References

1. Chaiko, D., Baczek, F., Rocks, S., Walters, T., & Klepper, R., 2015. The FLS Rapid Oxidative Leach (ROL) Process. Part I: Mechano-Chemical Process for Treating Chalcopyrite. Conference of Metallurgists, Toronto, Ontario, 1-11
2. Sahu, S.K., Asselin, E., 2011. Characterization of residue generated during medium temperature leaching of chalcopyrite concentrate under CESL conditions. Hydrometallurgy, 110(1), 107-114.
3. Schindler, A., Neumann, G., Rager, A., Fuglein, E., Blumm, J., Denner, T., 2013.A novel direct coupling of simultaneous thermal analysis (STA) and Fourier transform-infrared (FT-IR) spectroscopy. Journal of Thermal Analysis and Calorimetry, 113(3), 1091-1102.
4. Donohue, J., 1974. Structures of the Elements. Wiley, New York, p324.
5. Steudel R., Passlack-Stephan S., Holdt G., 1984. Thermal polymerization and depolymerization reactions of 10 sulfur allotropes studied by HPLC and DSC. Zeitschrift Für Anorganische Und Allgemeine Chemie,517, 7-42.
6. Perrenot, B., Widmann, G., 1994. Polymorphism by differential scanning calorimetry. Thermochimica Acta, 234, 31-39.

Teng Ma

Phone: +86 18911512824

E-mail: mateng12@mails.ucas.edu.cn

Type: SDC (IPE)

Supervisors: Wenli Song, IPE, CAS
Weigang Lin
Peter Arendt Jensen

PhD Study

Started: September 2013

Completed: July 2017

Bed Agglomeration Mechanisms at Different Gas conditions

Abstract

Fluidized beds have been widely applied to gasification and combustion of biomass. However, biomass ash with high content of K and Si, such as agricultural straw may lead to a severe agglomeration problem in a fluidized bed. This study focuses on the rice straw ash induced agglomeration mechanism in various gas conditions. Significant differences are observed on the defluidization temperature (T_d) and agglomeration mechanisms in different gas atmospheres. T_d in the H_2- and steam-containing gas are much lower than that in the air. It appears that in the steam-containing gas, agglomeration mechanism is predominantly coating-induced and the coating is formed by the reaction between KCl and SiO_2. While in the H_2-containing gas, the agglomeration mechanism is melting-induced and K_2SO_4 in the ash samples disappears, caused by decomposition of K_2SO_4.

Introduction

Biomass gasification in dual fluidized beds is capable to produce fuel gas with a high heating value and with a high carbon conversion. However, biomass with a high content of alkali and silicon, such as agricultural straw, normally has low ash melting temperatures. The presence of molten ash may lead to bed agglomeration during combustion or gasification in fluidized bed[1]. Consecutive operation is severely hindered by agglomeration problem[2, 3]. Formation of agglomerates are closely related to melting properties of biomass ash[4]. Gas atmosphere in gasifier is completely different from that in combustor[5], but agglomeration mechanisms in different gas conditions are still unclear.

Specific Objectives

The main objective of this work is to study the effects of gas composition on the transformation of ash components and the agglomeration mechanism induced by rice straw ash. In the present research, the release ratio of ash-forming elements in various gas composition is firstly studied in fixed bed reactor. Then the characteristics of the agglomeration induced by rice straw ash are investigated in different gas composition.

Experimental

Rice straw ash (RS) is used as the feedstock to carry out the experiments. Defluidization experiments are carried out in a laboratory scale bubbling fluidized bed (BFB). The reactor is made of quartz with a total height of 900 mm, which is divided into three section: gas preheating, dense bed and freeboard sections. The dense bed section has a dimension of 32 mm in inner diameter and 240 mm in height. The freeboard section is 120 mm in the inner diameter and 150 mm in height. A filter is installed at the exit of the reactor to collect the elutriated ash. The reactor is electrically heated, with a maximum temperature of 1020°C. The defluidization temperature (T_d) is defined as a temperature at which the bed pressure suddenly decreases, as illustrated in Figure 1. The morphology and the element distribution of agglomerates formed in different gas atmospheres are examined by a Scanning Electron Microscopy (SEM, JSM-7001F) combined with Energy Dispersive Spectrometer (EDS, INCA X-MAX).

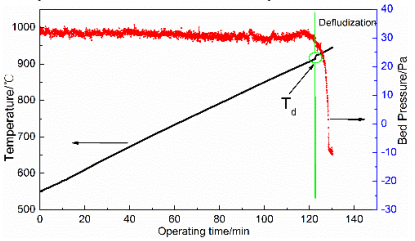

Figure 1: Illustration of definition of defluidization temperature from typical pressure drop and temperature curves in an agglomeration experiment

Results and Discussion

The results of element release ratio are summarized in Table 1. In H_2-containing gas, a large amount of sulfur

is released to the gas phase,which may be released to the gaseous phase in form of H_2S due to the reaction of K_2SO_4 and SiO_2. In steam-containing gas, a high release ratio of chlorine is observed. In rice straw ash sample, chlorine mainly exists in the form of KCl, which may be transformed to HCl and KOH at a high steam partial pressure[6].

Table 1: Release ratio of elements in biomass ashes, %.

Ash samples	Si	S	K	Ca	Cl
RS-H_2	0.27	76.72	13.12	8.16	20.87
RS-Steam	0.28	5.03	20.18	18.32	26.05
RS-Air	0.28	1.41	16.31	19.15	15.03

As illustrated in Figure 2, T_d in the CO_2 atmosphere and air are almost the same. However, T_d in both the H_2- and steam-containing gas are much lower than that in the air. To gain insights into the differences, the agglomerates formed in the H_2- and steam-containing gas are further analyzed by SEM-EDS.

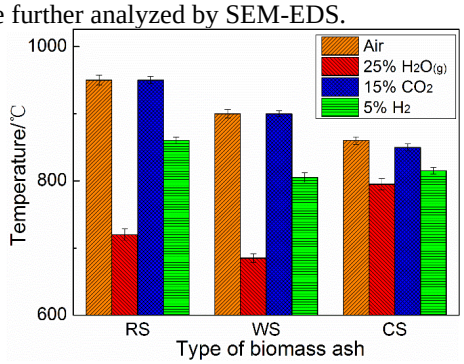

Figure 2: Defluidization temperatures in different gas conditions

In the steam-containing gas, the composition of agglomerate necks is similar to that of sand particle surface (shown in Figure 3). This result indicate that the coatings are formed on the surface of sand particles and agglomeration can be caused by the molten coatings. Thus, the coating-induced agglomeration may be the predominant mechanism in the steam-containing gas. The coatings, mainly consisting of Si and K, are probably K-silicates, which agree with the report in literature[7]. At a high partial pressure of steam, K-silicates may be formed by the reaction between KCl and SiO_2, which results in the release of HCl to gas phase.

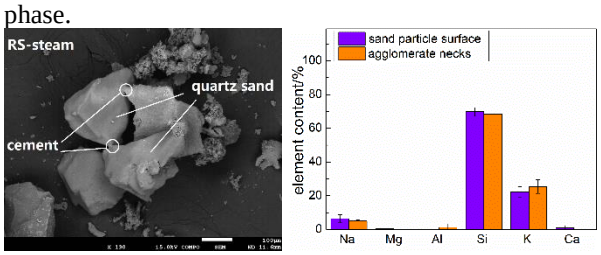

Figure 3: Surface morphology and composition of agglomerates formed in steam atmospheres

As shown in Figure 4, the surface of sand particles is mainly composed of Si, while the agglomerate necks consist of Si, K, Ca and Na. This indicates that the melting-induced agglomeration is the predominant mechanism for the formation of agglomerates in H_2-containing gas. Furthermore, the agglomerate necks has a large amount of K content, which may be caused by the transformation of K_2SO_4 to K-silicates in reducing condition.

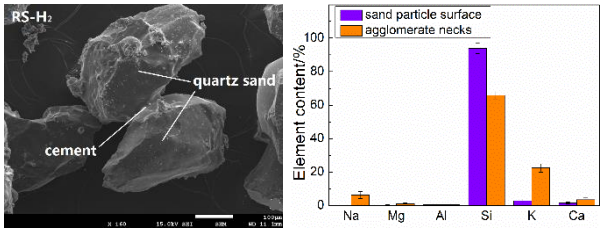

Figure 4: Surface morphology and composition of agglomerates formed in H_2-containing gas

Conclusions

The defluidization temperatures, in CO_2-containing gas and air are almost the same. In contrast, the defluidization temperature is significantly lower in H_2- and steam-containing gas than that in air. In steam-containing gas, the agglomeration induced by rice straw ash is coating-induced and the coating may be caused by the reaction between KCl and SiO_2. In H_2-containing gas, the agglomeration mechanism is melting-induced. The lower defluidization temperature in H_2-containing gas is partly attributed to the transformation of K_2SO_4 to K-silicates.

Acknowledgements

This study is supported by International S&T Cooperation Program of China (2013DFG62640) funded by MOST, Sino-Danish collaboration project (DANCNGAS) funded by Innovation Fund Denmark, and The National Natural Science Foundation of China (51104137).

References

1. W.G. Lin, K. Dam-Johansen,F. Frandsen. Chemical Engineering Journal. 2003. 96(1-3): p. 171-185.
2. E. Natarajan, M. Ohman, M. Gabra, A. Nordin, T. Liliedahl,A.N. Rao. Biomass & Bioenergy. 1998. 15(2): p. 163-169.
3. L.E. Fryda, K.D. Panopoulos,E. Kakaras. Powder Technology. 2008. 181(3): p. 307-320.
4. B. Gatternig,J. Karl. Energy & Fuels. 2015. 29(2): p. 931-941.
5. F. Kirnbauer, M. Koch, R. Koch, C. Aichernig,H. Hofbauer. Energy & Fuels. 2013. 27(6): p. 3316-3331.
6. R.J.F. David C. Dayton, and Thomas A. Milne. Energy & Fuels. 1995. 9: p. 855-865.
7. M. Zevenhoven-Onderwater, M. Ohman, B.J. Skrifvars, R. Backman, A. Nordin,M. Hupa. Energy & Fuels. 2006. 20(2): p. 818-824.

List of Publications

1. T. Ma, C.G. Fan, L.F. Hao, S.G. Li, W.L. Song,W.G. Lin. Thermochimica Acta. 2016. 638: p. 1-9.
2. T. Ma, C.G. Fan, L.F. Hao, S.G. Li, W.L. Song,W.G. Li. Energy & Fuels. 2016. 30(8): p. 6395-6404.

Xianglei Meng

Phone: +45 52909586
E-mail: xmen@kt.dtu.dk

Type: KT-IPE joint
Supervisors: Nicolas von Solms
Xiaodong Liang
Suojiang Zhang, IPE
Xiangping Zhang, IPE

PhD Study
Started: Dec. 2015
To be completed: Dec. 2018

Efficient Transformation of Atmospheric CO_2 to Carbonates by DBU Based Ionic Liquids under Mild Conditions

Abstract

1,8-diazabicyclo-[5.4.0]undec-7-ene (DBU) based ionic liquids (DBUILs) composed by a protonic acid and multi-nucleophilic sites were designed to catalyze the cycloaddition reaction of CO_2 with epoxides at atmospheric pressure and mild temperature. As a metal-free catalyst, DBUILs could support the transformation of CO_2 to carbonates in excellent yields with broad substrate scope, without the need for time-consuming and co-catalyst. The experimental evidences revealed a greatly improved activity via hydrogen bond activating epoxides by introduced extra hydrogen protons from water.

Introduction

The efficient transformation of CO_2 has attracted remarkable interests from viewpoint of sustainable chemistry, as these may reduce the greenhouse gas and mitigate the effects of climate change, whilst also producing various organic chemical commodity.[1] However, CO_2 activation requires electrolytic reduction processes or high-energy substrates, [2,3] due to its thermodynamic stability and kinetic inertness. One of the viable routes to overcome the thermodynamics is the synthesis of five-membered cyclic carbonates by cycloaddition of CO_2 with epoxides (Scheme 1).[4,5]

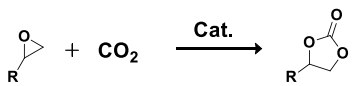

Scheme 1: Cycloaddition of CO_2 with epoxides

To date, various catalysts have been developed for the synthesis of cyclic carbonates from CO_2 and epoxides, such as metal catalysts, [6] salen complexes, [7] organocatalysts[8] and ionic liquids. [9,10] However, most of the catalyst systems often require high energy input, such as high temperatures (>100 °C) and/or high CO_2 pressures, which made this process not so "sustainability". Recently, great efforts have been focused on the development of more efficient and sustainable catalyst systems that can be carried out at atmosphere CO_2 pressure and ambient temperature conditions.

Specific Objectives

Therefore, the design of efficient, green and metal-free catalysts is still a great challenge toward effective CO_2 conversion under mild conditions. Herein, we demonstrated the use of DBU-based protic ionic liquids (DBUPILs) composed by protonic acid and multi-nucleophilic sites (Figure 1) for the convertion of atmospheric CO_2 with epoxides at mild conditions. The DBUPILs showed high activity in producing carbonates without the need for long reaction time and co-catalyst. Furthemore, the addition of suitable amount of water, a green sollvent and hydrogen proton, had a notable effect on the proceeding of the cycloaddition reaction. Thus, this work provides an efficient way for the development of green, low-energy consumption and sustainable process of transformation of CO_2.

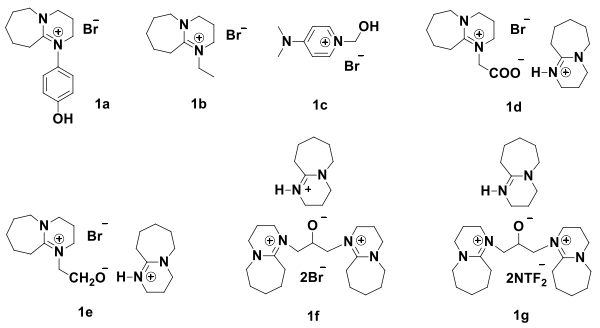

Figure 1: ILs used in this study.

Results and Discussion

We have been proved that Br^- is an excellent nucleophilic ion for the cycloaddition reaction in our previous work. [10, 11] Hence, Br- is chosen as the model anion. At the initial of our study, we prepared a series of DBUPILs in one-step by acid-alkali neutralizing reaction (Figure 1). The reaction could be completed in minutes at room temperature. The structures of the ILs DBUPILs were analyzed by NMR study and SEM (Figure 2). Then, the catalytic activity of various DBUPILs was carried out with epichlorohydrin and a balloon of CO_2 in schlenk tube at 30 °C. The results were shown in Table 1.

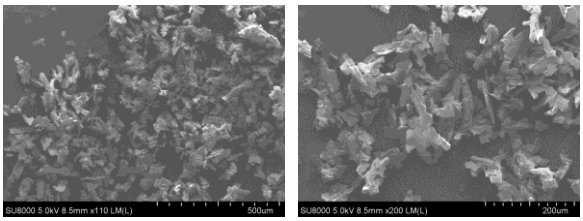

Figure 2: Photographs of **1f**

Table 1: Reaction of CO_2 with epichlorohydrin catalyzed by different ILs[a]

Entry	Catalyst	Time (h)	Yield[b] (%)
1	[Bmim]Br	6	23
2	TBAB	6	25
3	**1a**	6	14
4	**1b**	6	26
5	**1c**	6	47
6	**1d**	6	70
7	**1e**	6	79
8	**1f**	6	92
9	**1g**	10	4
10	**1f**	2	58

[a]Reaction conditions: epichlorohydrin (0.5ml), ILs (6mol%), CO_2 (balloon), Temperature (30°C) [b]Determined by 1H NMR using 1,1,2,2-tetrachloroethane as an internal standard. TBAB= tetrabutylammonium bromide.

.

It was found that the common ILs [Bmim]Br (entry 1) had a very low activity in catalyzing the reactions under this room temperature and atmospheric CO_2 condition. As a co-catalyst that regularly used in this cycloaddition reaction, TBAB was investigated a 25% yield of chloropropene carbonate (CPC) (entry 2). Interestingly, DBU-based ILs without protonic acid (**1b**) was observed similar activity with [Bmim]Br and TBAB (entry 4 vs 2 vs 1), which indicated that cation may have little effect on the reaction. However, the DBU-based ILs **1a** with a phenolic hydroxyl group showed lower activity than common ILs (entry 3 vs 1, 2, 4), even though the phenolic hydroxyl group could activate epoxide in prevous reports. The negative effects of phenolic hydroxyl group in this work may be induced by the stereo-hindrance. The 4-dimethylaminopyridine (DMAP) based ILs (**1c**) with a hydroxyl group was also studied (entry 5). **1c** showed promising yield of CPC (47%) for the hydroxyl group activating epichlorohydrin. To our delight, all of the DBUPILs demonstrated much higher activity than **1c** (entries 6-8 vs 5). Possibly because that the protonic acid site of DBUPILs could activate epichlorohydrin more efficiently at room temperature compared with hydroxyl group, besides, as a nucleophilic anion, alkoxy anion might play the same role with Br^-, which could increase the active site. Then, **1g** without Br^- was prepared to identify the catalytic activity of the alkoxy anion. But, the result shown in table 1 (entry 9) was only a 4% yield of CPC, which demonstated that the alkoxy anion could not catalytic this reaction. For DBUPILs, **1f** with two Br^- exhibited much higher activity (92%) than the other two DBUPILs that have only one Br^- (entry 8 vs 6, 7). The result illustrated that nucleophilic Br^- was very important to promote the reaction. To our surprise, the catalytic activity of **1f** was up to 58% in the initial of the reaction (entry 10). So, **1f** was chosen as benchmark catalyst to investigate influence of reaction parameters.

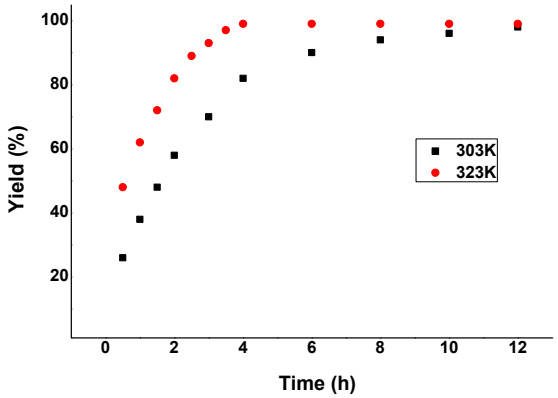

Figure 3: Effects of reaction time and temperature catalyzed by **1f**

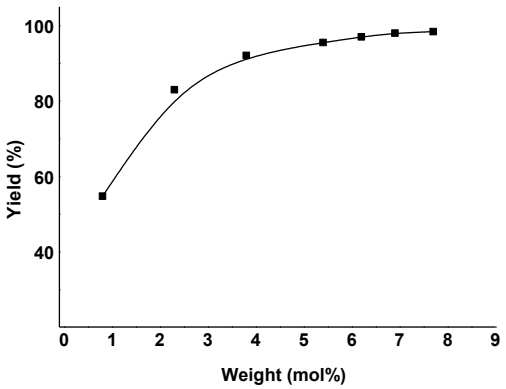

Figure 4: Effects of catalyst dose catalyzed by **1f**

It could be seen from figure 3 that the yield increased rapidly to 82% in the first 4 h at 30°C and then slowly increased to 99% in 12 h. The result indicated an obviously decrease of reaction rate. However, as temperature was 50°C, the yield increased

to 99% sharply in 4h without any obviously slow-growth stages. This might be caused by the increasing viscosity of CPC/**1f** reaction system with the producing of CPC during the reaction, thus affect the transferring effect of CO_2. The above mechanizm was confirmed by the same behavior of the catalyst loading study shown in figure 4, which also had a slow-growth stage with the increasing of **1f**.

Table 2: Reaction of CO_2 with substrates catalyzed by **1f**

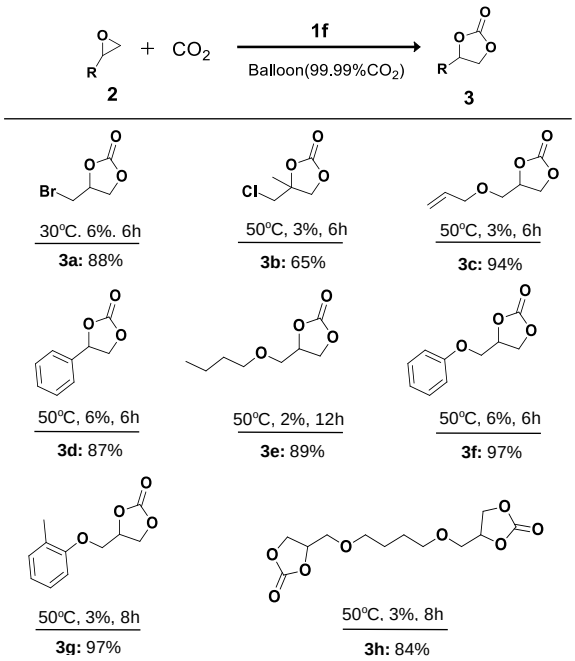

Subsquently, a range of different substituted terminal epoxides were examined under a balloon of CO_2 condition in the presence of **1f** ILs. The results were summarized in Table 2. Epibromohydrin (**2a**) could afford the product **3a** in a good yield of 88% at the optimal condition. Then, we found ILs 1f had a very low solubility in the other terminal epoxides at 30 °C. Taking into account of the industrial application, the loading of **1f** was reduced, and the reaction temperature was increased to 50°C. However, the carbonate **3b** showed much lower yield than **3c** at the same condition, which probably due to the high stereo-hindrance effect. Furthermore, Styrene oxide **2d** and glycidol derivatived **2e-2h** were examined, and all of these epoxides generated the corresponding cyclic carbonates in excellent yields (**3d -3h**).

Then, **2f** was chosen as an optimal terminal epoxide to study the cycling performance of DBUPILs **1f**, because **1f** could be easily separated from **3f** by adding water. Unexpectedly, when we tried to recycle **1f** after the reaction, we found that the yield of **3f** decreased obviously (See Figure 5) after it ran 4 times. This might be caused by the reaction of **1f** with **2f**.

In order to study the reaction mechanism, FT-IR spectra were employed to identify the possible intermediate under atmospheric CO_2 during the reaction. As shown in Figure 5, there appeared a new band at 1795 cm^{-1}, after the reaction of CO_2 with **1f**, which corresponded to the new asymmetric (C=O) vibration of the carbamate salt, presumably implying the activation of CO_2 by the alkoxy anion of **1f**.

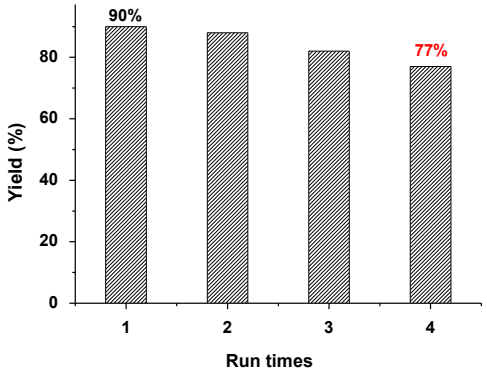

Figure 5: Reaction conditions: catalyst (6 mol%), CO_2 balloon, temperature (50°C).

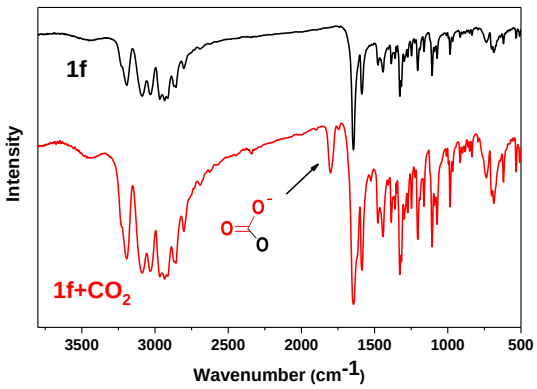

Figure 6: FT-IR spectra of the interaction between **1f** and CO_2

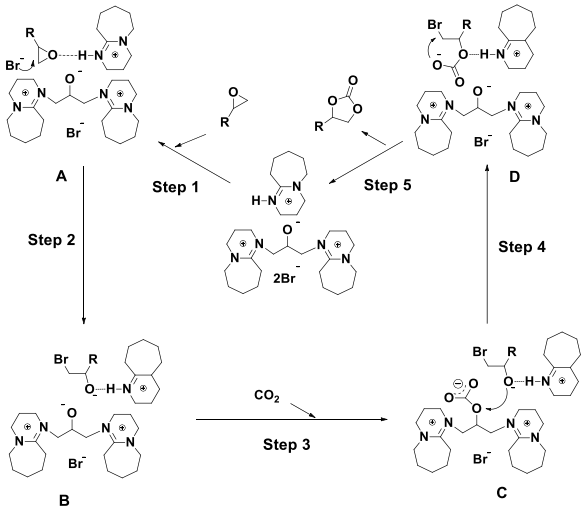

Scheme 2: Proposed Mechanism for Cyclic Carbonates Synthesis Catalyzed by **1f**

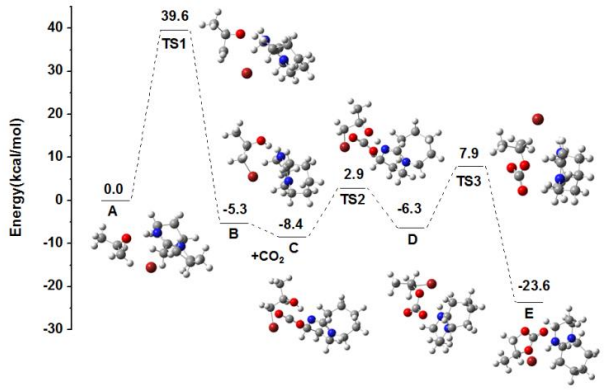

Figure 7: Potential energy surface profiles of **1f**-catalyzed process and the optimized geometries for the intermediates and transition states.

Based on these studies, we proposed a probable mechanism of **1f** catalyzed cycloaddition of CO_2 with epoxide. The detail was shown in Scheme 2. Subsequently, we investigated the mechanism of the **1f**-catalyzed process through DFT study. As shown in Scheme 2 and Figure 7, firstly, **1f** and **2f** interacted to form a complex **A**, and then epoxy ring-opening step made **A** convert into intermediate **B** via transition state TS1 with a barrier of 39.6 kcal/mol. A new complex **C** was formed, when CO_2 was added into the reaction system. Then, nucleophilic attack of the intermediate on the complex **C** produced the alkyl carbonate **D** through TS2 with a lower energy barrier of 2.9 kcal/mol. Finally, the cyclic carbonate was obtained by intramolecular ring-closure and the catalyst was regenerated with an energy barrier of 7.9 kcal/mol (TS3). The study illustrated that the epoxy ring-open step was the rate limiting step with the highest energy barrier of 39.6 kcal/mol (TS1).

Conclusions

In summary, DBU based protic ionic liquids with protonic acid and nucleophilic sites were successfully used as single and metal-free homogenous catalysts in the cycloaddition reaction of atmospheric CO_2 with epoxides at room temperature. DBUPILs showed excellent activity and good substrate compatibility. This work provides an excellent epoxy ring-open catalysts at room temperature conditions, which may be also promising in the other epoxy ring-open reactions.

Acknowledgements

This work is financially supported by National Key R&D Program of China (2017YFB0603301), The National Natural Science Fund for Distinguished Young Scholars (21425625) and Key Research Program of Frontier Sciences CAS (QYZDY-SSW-JSC011). The author is grateful to the support from the Department of Chemical and Biochemical Engineering, Technical University of Denmark.

References

1. X.B. Lu, D. J. Darensbourg, *Chem. Soc. Rev.* 41 (2012) 1462-1484.
2. T. Sakakura, J.-C. Choi, H. Yasuda, *Chem. Rev.* 107 (2007) 2365-2387.
3. P. Jessop, T. Ikariya, R. Noyori, *Chem. Rev.* 95 (1995) 259-272.
4. C. Bruckmeier, B. Rieger, W. A. Herrmann, F. E. Kühn, *Angew. Chem. Int. Ed.* 50 (2011) 8510-8537.
5. B. Schaffner, F. Schaffner, S. P. Verevkin, A. Borner, *Chem. Rev.* 110 (2010) 4554-4581.
6. J. W. Comerford, I. V. Ingram, M. North, X. Wu, *Green Chem.* 17 (2015) 1966-1987.
7. M. North, B.D. Wang, C. Young, *Energy Environ. Sci.* 4 (2011) 4163
8. J. Q. Wang, Y.G. Zhang, *ACS Catal.* 6 (2016) 4871−4876
9. B. H. Xu, J. Q. Wang, J. Sun, Y. Huang, J. P. Zhang, X. P. Zhang, S. J. Zhang, *Green Chem.*, 17 (2015) 108-122.
10. X. L. Meng, Y. Nie, J. Sun, W. G. Cheng, J. Q. Wang, H. Y. He, S. J. Zhang, *Green Chem.* 16 (2014) 2771-2778.
11. X. L. Meng, H. Y. He, Y. Nie, X. P. Zhang, S. J. Zhang, J. J. Wang, ACS Sustainable Chem. Eng., 5 (2017) 3081–3086

Seerup, Rasmus

Phone: +45 45 25 28 53
E-mail: rasee@kt.dtu.dk
CHEC Research Center
Type: SDC (KT)
Supervisors: Kim Dam-Johansen
Weigang Lin

PhD Study
Started: November 2013
Completed: July 2017

Modelling of Gasification of Biomass in Dual Fluidized Beds

Abstract
In fluidized bed gasification of biomass, tar may be problematic for downstream processing. Controlling of tar properties may make the gas cleaning process easier; thus, help to run the apparatus at optimal conditions. This project is aimed to investigate the formations of tars from biomass under gasification conditions in the dual fluidized bed, by modelling the development of tar in both particle scale and reactor scale.

Introduction
There is an increasing interest on the utilization of biomass as a renewable source for energy. Gasification of biomass in dual fluidized beds provides the possibility of producing synthetic gas with high hydrogen content and a high heating value.
The ash from biomass may cause a high tendency of agglomeration at elevated temperature. Consequently, biomass is usually gasified in fluidized beds at relatively low temperatures, which lead to a high yield of tars in the producer gas. Understanding tar formation and properties is of essential importance for optimizing the downstream cleaning or separation.

Tar produced at gasification conditions is mainly originating from monolignols released from lignin in the pyrolysis process before actual gasification proceed [1].

In situ removal of tar by catalysts may not be effective because of severe deactivation of the catalysts. The dual fluidised bed consists of a combustion and gasification chamber, where bed material is send between the chambers to provide energy for gasification without dilution with air. This opens op for a reactivation of catalyst and the use of tar removal in the gasification chamber.

Specific Objective
The objective of the project is to understand the tar development in dual fluidized beds gasification of biomass, by experimental and modelling studies at both particle and reactor scales.

Previous work
Experiments have been performed for pyrolysis of pulp lignin to study the influence of torrefaction. The results show that torrefaction primarily affects the methoxy groups which fits well with the lower bonding energy. Vanillin was furthermore show to be released at a much earlier stage than other tar components.

Model development

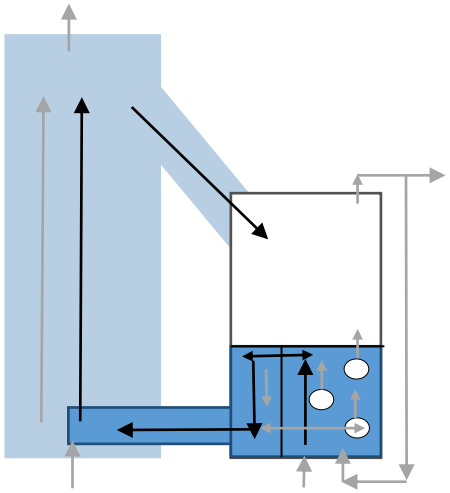

Figure 1: Illustration of the model of a dual fluidized bed. (black arrows: solid flow; gray arrows: gas flow; right side: gasification chamber, left side: combustion chamber).

The reactor model presented here is aimed at investigating the possibility of utilizing the deactivation of catalyst by adsorption of tar species, to remove tar from the gas and transport it to the combustion chamber for processing. The reactor model is based on bubbling bed model by D. Kunii and O. Levenspiel [2] and modified to include the transport of material from the

gasifier to the combustor, and include gas solid reactions.
The basic model with its transport of solid and gas is sketch in figure 1. Solid particles are transported up through the bed in the bubble wake, while moving downwards in the emulsion phase to counter the particles flow.
Solids are transported from the bottom of the bubbling bed to the entrained flow combustion reactor. here biomass is consumed and catalyst reactivated to heat the bed material which is send back to the bubbling bed.
For the bubbling bed most of the gas passes the bed in bubbles which makes it possible for tar species to bypass the bed. The gas inside the bubble convectively circulate in to the solid that is following the bubble in its wake, while the interchanged with the rest of the emulsion is based on a diffusion mechanism.
The downwards movement of particles furthermore drags gas down the emulsion phase creating a back mixing in the reactor.

The most important simplifications for the system is:

- The system is in steady state
- The reactor is isothermal and isobaric
- Gas formation directly contribute to the bubble phase
- Constant effective bubble size
- Neglectable bubble gas cloud

Results and discussion

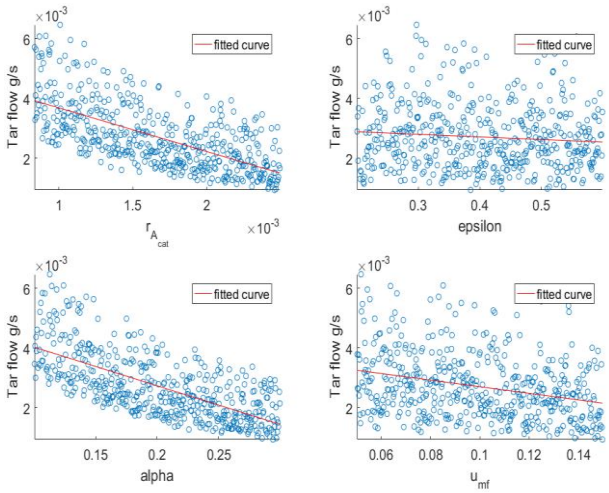

Figure 2: Scatterplot from model simulation

An initial Morris screening shows that the most influential parameters, except kinetics, are the hydrodynamic parameters. In order to investigate the effect of potential catalysts, the model is simulated with the estimated uncertainty of the wake fraction (alpha), the minimum fluidization velocity (u_{mf}), and the void between particles (epsilon), together with the possible range for the catalyst reactivity (r_{A_cat}), using a Monto Carlo scheme.

The result of the Monto Carlo scheme is shown in figure 2 where each circle is a result from a simulation. The spread of points is a consequence of the possible variation of other parameters value. The less uniform the result are, the more influence is attributed to the variable. From figure 2 it is seen that particular the reactivity of catalyst and the bubble wake fraction is significant for the tar output.
The wake fraction is thought to be influential, as this in particular affect the downward flow of particles in the reactor, which in turn drag gas down in the emulsion phase. Consequently, Tar is dragged down in the emulsion phase, where a good contact between gas and catalytic material exist, which will quickly remove tar from the gas phase.
The catalytic reaction rate is expected to have a significant influence as this is directly related to how fast the tar may adsorb to the catalyst, and thus be removed.
The hydrodynamic parameters like minimum fluidization and void fraction has an influence by affection the residence time in the reactor. Thus giving a higher contact time with the catalyst.
The model shows only a small amount of deactivation of catalyst which suggest that deactivation is not a considerable problem for the dual fluidized bed.

Conclusion

It may be concluded that, the removal of tar in the gasification chamber may be significantly increased by increasing the catalytic activity or increasing the wake fraction of the bubbles. The effect of catalytic activity is obvious. The effect from an increase in wake fraction is due to an increased drag of gas down the emulsion phase, by the emulsion particles.

Future work

Further work will focus on modeling of tar development in the gas phase under gasification environment of the dual fluidized bed. Changes in the gas phase composition is of interest as it may change the tar development.

Acknowledgements

This project is part of DANCNGAS. Financial support provided by Sino-Danish Centre for education and research and the Technical University of Denmark are gratefully acknowledged.

Reference

[1] T. Hosoya, H. Kawamoto, and S. Saka, "Cellulose–hemicellulose and cellulose–lignin interactions in wood pyrolysis at gasification temperature," *J. Anal. Appl. Pyrolysis*, vol. 80, no. 1, pp. 118–125, Aug. 2007.
[2] D. Kunii and O. Levenspiel, "Bubbling bed model," *I&EC Fundam.*, vol. 7, no. 3, pp. 446–452, 1968.

Peng Shen

Phone: +45 50391888
E-mail: psen@kt.dtu.dk

Type: CSC
Supervisors: Peter Szabo
Anders Egede Daugaard
Suojiang Zhang, IPE-CAS

PhD Study
Started: December 2016
To be completed: December 2019

Monolithic Thiol-ene Materials with Drastically Different Mechanical Properties

Abstract

Thiol-ene materials are a series of materials that can easily be crosslinked using suitable photo-initiator and UV light source. An advantage of thiol-ene materials is that they can be tailored, to have specific mechanical properties, by controlling the stoichiometry of the mixtures. By combination of different material systems it is therefore in principle possible to prepare monoliths with greatly varying mechanical properties, essentially from the same material.

Introduction

The possible application of polymer materials with distributed mechanical properties are many. Figure.1 illustrates one such example. Thiol–ene materials can be obtained through traditional thermal conditions with common azo-species such as 2,2-azobis(isobutyro-nitrile) (AIBN) or via with little or no added photoinitiators' photochemical thiol–ene reaction methods[1]. During the last century, thiol-ene material is a global focus because of the highly efficient reactions of thiols with reactive C=C bonds , has widely application in hydrogel drug delivery, coatings, adhesives, optical applications , dendrimer synthesis, all-solid-state electrolyte ,high strength laminates, dental resins and electroluminescent films[2]. In particular, two thiol reactions emerged, thiol–ene free-radical addition to electron-rich/electron-poor C=C bonds, and the catalyzed thiol Michael addition to electron-deficient C=C bonds [3]. Unlike typical chain-growth free-radical polymerizations or step-growth condensation polymeri-zations, thiol-ene polymers form in a stepwise manner but their formation is facilitated by a rapid, highly efficient free-radical chain-transfer reaction. Thus, crosslinked thiol-ene polymerizations proceed very rapidly but will not reach the gel-point until relatively high functional group conversions[4], which results in a material with very low shrinkage and inherent stresses.

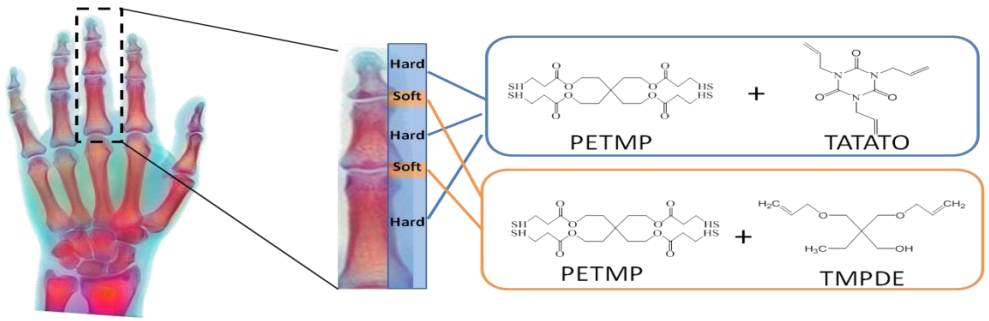

Figure.1 Artificial fingers with hard-soft alternate thiol-ene materials

Specific Objectives

In this project, the purpose is to prepare new monolithic thiol-ene materials with drastically different mechanical proportion, which is formed via a free radical based thiol-ene addition reaction. Products will show the different mechanical proportion by controlling the kind of reaction compound (thiol and ene with different number of functional groups), the ratio of reactants (the reaction conditions (ultraviolet light and heating)).

Through use of different reactants hard and brittle (H, TATATO and PETMP) to soft and flexible materials (S, PETMP and TMPDE) will be prepared as shown in Figure 1.

Results and Discussion

The mechanical properties of polymers are intimately related to their molecular structure, one of the most important mechanical properties is rheological behavior, which can be measured by shear rheometry and filament stretching rheometer (FSR).

The thermal properties of hard and soft polymer were characterized using the differential scanning calorimeter (DSC). The DSC measurement shows that the glass-transition temperature (Tg) of the hard segment (H) is 55.74℃and the soft(S) is -35.35℃, respectively. (Figure.2)

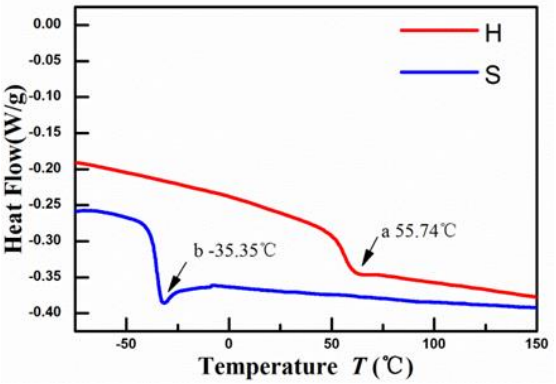

Figure. 2 DSC curve of (a) hard segment and (b) soft segment

To get the sandwich structure column shape sample, we made the hard segment and soft segment polymer, respectively. The hard polymer liquid was prepared by using the ratio (1:1) of PETMP to TATATO. Two chemicals were mixed by the SpeedMixer at the speed of 3000r/min for 2 mins, in addition, all processes should be carried out in total darkness for preventing the mixture prematurely polymerize. The soft liquid was obtained in the same way except for replacing the TATATO with PMDPE.

It is very important that the first two steps of the polymerization process should strictly control the reaction time, the hard polymer liquid and soft polymer liquid are mixed together in a shorter illumination time.(Figure.3)

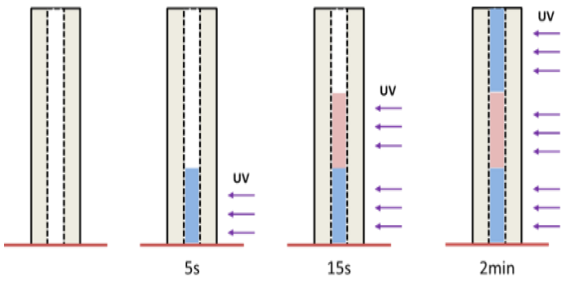

Figure. 3 The production process of hard-soft alternate sample

The extensional stress was measured by a filament stretching rheometer (FSR) to get the Force-Time curve (Figure.4) and the 40mm-soft segment material can be thought of as the total soft material, because it only has 3cm hard segment in the both end. It can be seen that the new structure materials improved tensile property by 20 percent.

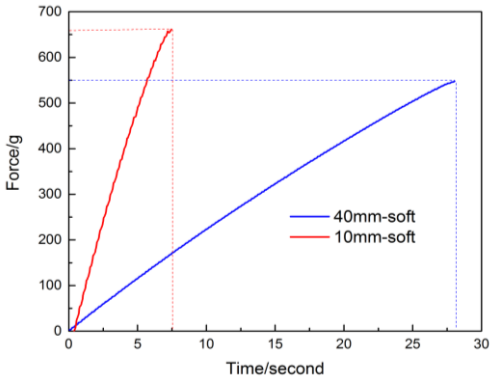

Figure.4 The Force-Time curve of 10mm soft segment and 40mm soft segment

The high-speed camera recorded the images of fracture process. (Figure.5), the crack was generated in the soft segment surface not in the interface of the hard and soft material, so it was the ductile fracture belong to the Mode Ⅰ crack.

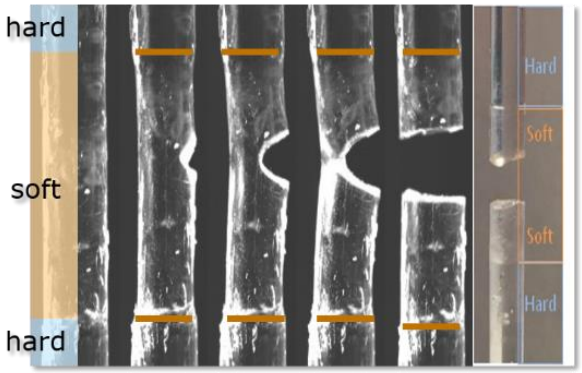

Figure.5 image of 10mm soft segment Hard-Soft material fracture process(bread bond is the interface of hard and soft materials)

Future work

- Future experiment with the different length soft segment materials such as 1mm, 2.5mm and 5mm will be made for the extensional stress test and studying the fracture behavior.
- The bending stress and fatigue test should be done by TA Instruments Electroforce 3200, the most suitable material, which has the optimal performance, will be selected.

References

1. P. Alagi, Y. J. Choi, J. Seog, S. C. Hong, Industrial Crops and Products 87(2016), 78-88.
2. K. Aoki, R. Imanishi, M. Yamada, Progress in Organic Coatings 100 (2016) 105-110
3. J. Bae, Y. Yang, Journal of Non-Crystalline Solids 357(2011) 3103-3107.
4. J. W. Bartels et al., Acs Applied Materials & Interfaces 3(2011)2118-2129

Ting Song

Phone: +45 50251205
E-mail: tison@kt.dtu.dk

Type: KT-IPE joint
Supervisors: Peter Szabo
Anders Egede Daugaard
Suojiang Zhang, IPE

PhD Study
Started: November 2015
To be completed: October 2018

The modification of PSf membranes with ionic liquids used for CO_2 separation

Abstract
The PhD project focuses on the separation of CO_2 from CH_4 or N_2 with ionic liquid-based membrane. Commercial PSf membrane is a good candidate to act as the substrate membrane due to its specific properties. This is the first time to polymerize ionic liquid on the surface of a commercial membrane through atom-transfer radical-polymerization (ATRP). In order to get better performance of CO_2 separation, the ionic liquid counter ion on the as prepared membrane can be exchanged to CO_2-philic anion, such as bis(trifluoromethylsulfonyl)imide ([NTf_2]), etc. The introduction of butyl acrylate helps improve the flexibility of the ionic liquid modified PSf membrane.

Introduction
Carbon capture and utilization are regarded as one of the major challenges in the 21st century. Carbon dioxide (CO_2) can be commonly found in natural gas streams, biogas, flue gas and product of coal gasification [1]. The presence of CO_2 and other acid gases reduce the thermal efficiency and make the gas streams become acidic and corrosive, which in turn reduces the possibilities of gas compression and the transport within the transportation systems [2]. Therefore, it is urgently necessary to develop new technologies for CO_2 separation with high efficiency, low energy consumption. Membrane separation is a promising technology for CO_2 capture due to its energy efficiency, simple process design, low cost and environmentally friendliness [3]. Recently, ionic liquids (ILs) have attracted great attention for their potential as alternative media for CO_2 separation due to their unique properties. However, it is difficult to realize industrialization using ILs to capture CO_2 due to their high viscosity. The high viscosity of ILs will lead to its low heat transfer and mass transfer performance, which may not only affect the speed of absorption regeneration, but also increase the cost of energy consumption of transport, and operation. Immobilization of ILs in membranes has been extensively investigated to combine the advantages of membranes and ILs and to overcome their disadvantages for CO_2 capture [2]. Polysulfone (PSf) membranes can be used as platform for gas separation because it has many excellent properties such as a high mechanical, chemical and thermal resistance. Moreover, its separation and plasticization properties are also in an acceptable range [4]. In order to obtain a membrane with high CO_2 permeability and selectivity, we plan to modify the surface of commercial polysulfone membrane with poly(ionic liquid)s (PILs).

Here, imidazole-based IL was polymerized and grafted on the surface of PSf membrane via atom-transfer radical-polymerization (ATRP). The thickness of the poly(IL) layer can be controlled by controlling the reaction time. In order to overcome the brittle property of imidazole grafted PSf membrane, butyl acrylate was introduced in and copolymerized with N-vinylimidazole on the surface of PSf membrane.

Methodology and results

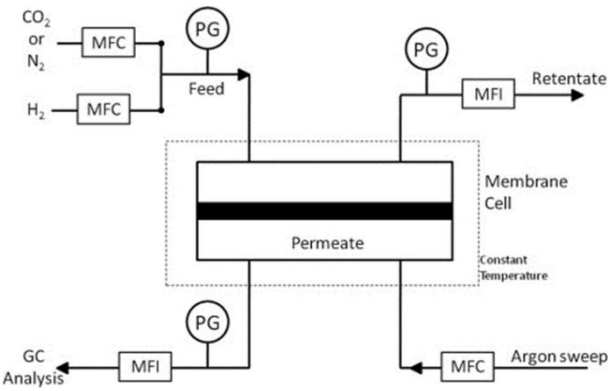

Figure 1. Brief diagram of the mixed gas constant pressure variable volume apparatus.

The mechanism of gas separation with membranes is showed in Figure 1. CO_2 can go through the membrane priority over other gases when the mixture gas of CO_2 and CH_4 or CO_2 and N_2. The permeate gas can be test by GC (Gas Chromatography). The membrane used for CO_2 separation is based on the solution-diffusion mechanism. There are two parameters, permeability and selectivity, to evaluate the performance of membranes used for gas separation.

IL is for the first time polymerized on the surface of PSf through Atom-transfer radical-polymerization (ATRP) (Figure 2a, 2b, 2c). The thickness of PILs layer can be controlled by controlling the ATRP reaction time. Additionally, membranes with different properties in terms of CO_2 affinity can be obtained by changing the counter ion of the ionic liquid as shown in Figure 2d.

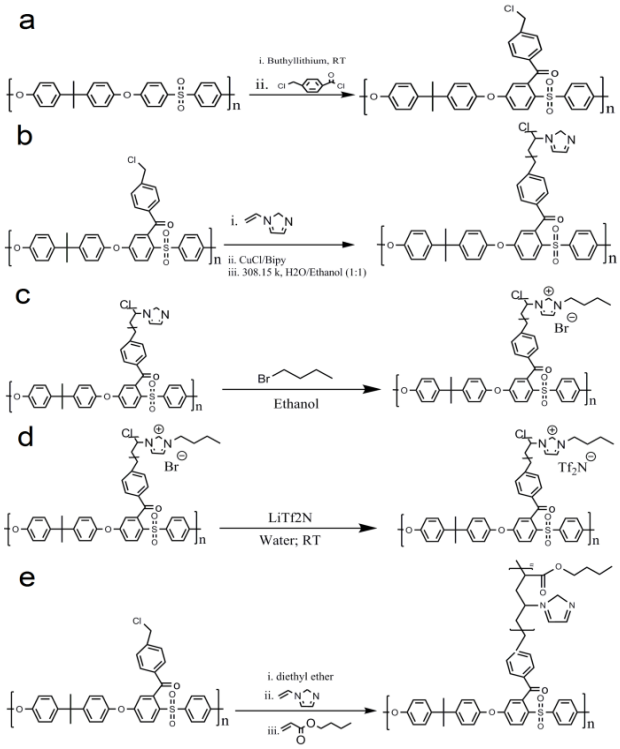

Figure 2. The synthesis of IL modified PSf membrane (a, b, c); anion exchange process (d); N-vinylimidazole and butyl acrylate copolymerized on the PSf membrane (e).

The as prepared N-vinylimidazole modified PSf membrane is brittle, since the poly(N-vinylimidaozle) is a glassy polymer. In order to overcome this problem, butyl acrylate, to provide softness, was introduced in (Figure 2e). The result turns out that the membrane becomes more flexible after the introduction of butyl acrylate.

FT-IR (Figure 3) and WCA (Figure 4) of membranes I prepared were tested to confirm that all the reactions here happened successfully.

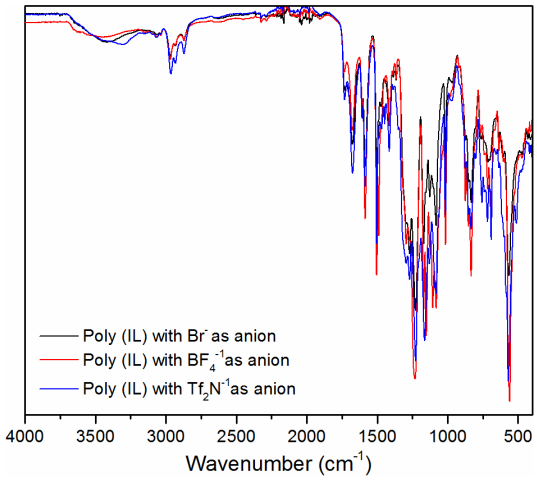

Figure 3. FT-IR of different kinds of membranes.

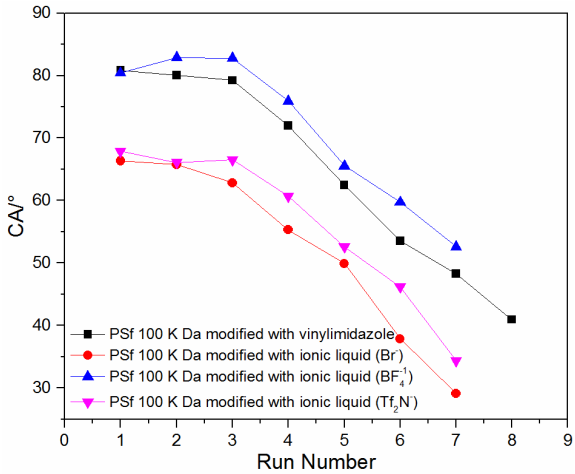

Figure 4. WCA of different kinds of membranes.

Conclusion

In order to improve the gas separation performance of commercial PSf membrane, N-vinylimidazole and butyl acrylate are copolymerized on its surface. The introduction of butyl acrylate helps overcome the shortcoming of the ionic liquid modified PSf membrane, which is very brittle. All the reactions have been confirmed by FTIR and WCA. The gas separation performance will be tested afterwards, and the experimental conditions can be optimized according to the results of gas separation test.

References

1. Y. Zhang, J. Sunarso, S. Liu, R. Wang, Int. J. Greenh. Gas Control. 12 (2013) 84–107.
2. J. Deng, L. Bai, S. Zeng, X. Zhang, Y. Nie, L. Deng, S. Zhang, RSC Adv. 6 (2016) 45184–45192.
3. S. Rafiq, L. Deng, M.-B. HäggChemBioEng Rev. 3 (2016) 68–85.
4. T. Chittrakarn, Y. Tirawanichakul, S. Sirijarukul, C. Yuenyao, Surf. Coatings Technol. 296 (2016) 157–163.
5. Matthew G. Cowan; Douglas L. Gin; Richard D. Noble, Acc. Chem. Res. 2016, 49, 724-732;

Jiahuan Tong
Phone: +45 5273 1884
E-mail: jito@kt.dtu.dk

Type: KT-IPE joint
Supervisors: Nicolas von Solms
Suojiang Zhang
Xiaodong Liang

PhD Study
Started: March 2017
To be completed: March 2020

Theory, Simulation and Models for Electrolyte Systems with Focus on Ionic Liquids

Abstract
The development of new electrolytes play essential roles in the capacity, life expectancy, and safety of the batteries, e.g. in the energy storage field, which support the development of green energies for a sustainable society. Ionic liquids are among the best candidates as additives or co-solvents used in batteries. This work is aiming to provide theorectical basis and understanding for developments of such ionic liquids.

Introduction

Electrolytes are an indispensable element in energy storage since the positive and negative electrodes are interconnected by an electrolyte that determines the charge transport during the charge/discharge process. Ideal electrolytes should fulfill the following requirements: i.e., wide voltage window, excellent electrochemical stability, high conductivity, high ionic concentration, small solvated ionic radius, low viscosity, environmental friendliness, low cost, and easy availability with high purity.[1,2]

The development of new electrolytes play essential roles in the capacity, life expectancy, and safety of the batteries, e.g. in energy storage field, which support the development of green energies for a sustainable society. Ionic liquids [3,4] are among the best candidates as additives or co-solvents used in batteries. Ionic liquids as an ionic electrolytes due to their unique physico-chemical properties such as wide potential window, high thermal stability, negligible vapour pressure (i.e., neither flammable nor volatile), relatively high ionic conductivity and good thermal and electrochemical stability.[5,6] In recent years, many researchers are focus on developing new types of ionic liquids to improve the performances of new lithium batteries.

In this project, in order to deeply understand the molecular mechanism of the ionic liquids electrolytes. Screen and design suitable ionic liquid for ionic liquid electrolytes using COSMO-RS method and develop a series of models of ionic liquid electrolytes with high electrochemical properties to help guide the experiment and application.

Project contents

This project will include the following contents (Fig.1):
1. Select several kinds of ionic liquids are which have excellent conductivity and electrochemical window for ionic liquids electrolyte via COSMO-RS simulations.
2. Design the structure of cations and anions for potential ionic liquids and optimize structures using the software of Gaussian.
3. Establish model of ionic liquid electrolyte that use different types of ionic liquids as solvent and add different lithium salts (LiPF6, LiTFSI, etc.).
4. Investigate the relationship between the type of ionic liquids and the performance of electrolyte by molecular dynamics simulation, and determine the optimal type of ionic liquid for ionic liquid electrolyte.
5. Develop the complex systems in ionic liquids electrolyte, containing different ratios and types of ionic liquids, different organic solvents (ethylene carbonate, dimethyl carbonate, diethyl carbonate, ethyl methyl carbonate, etc.) and lithium salts at different temperatures and concentrations.
6. Compare properties of electrolyte (conductivity, electrochemical window, transport property, etc.) in different kinds and content of ionic liquids by molecular dynamics simulation to determine the optimal content of ionic liquid for ionic liquid electrolyte.

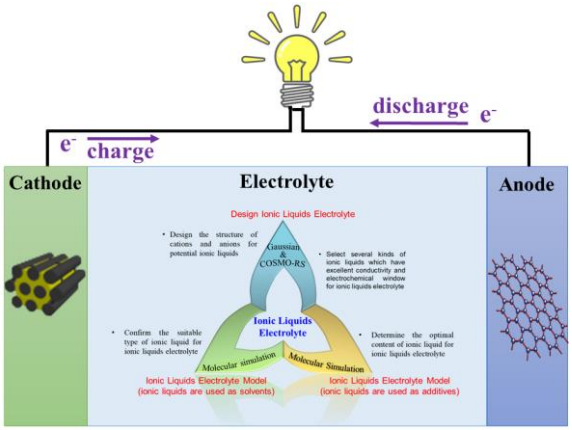

Figure 1. Illustrate of project content

Research Progress of Project

1. Model development of Pure Electrolyte system

The simulation system is constructed with 50 Li^+, 50 $TFSI^-$ ([bis (trifluoromethanesulfonyl) imide anion]) and 600 ACN (Acetonitrile) molecules (Fig. 2). The system is in a cubic box with a dimension of 44 Å in length, width and height.

Figure 2. Structures of electrolyte model

2. Simulation details

All molecular dynamic simulations were performed with the LAMMPS package. The OPLA force field was used in all simulation. The Lennard-Jones parameters and partial charges for Li^+, $TFSI^-$ and ACN were taken from the OPLA parameterization. Firstly, geometry optimization minimizes the energy of the system in just a few steps. Then, by applying 500 K temperature, total energy and potential energy suddenly increases due to the increase of kinetic energy. After a while, the average of total energy would be constant which means the system is located at its equilibrium point. Energy oscillation was related to the temperature oscillation. Shifting from NVT to NPT ensembles causes an increase in total energy. The reason is that the initial density is lower than the actual density, therefore, in NPT ensemble, the system tries to reduce the volume which leads to kinetic energy increases. After equilibrium was reached, the system would be cooled down and hold at 300 K for 2ns NPT and NVT respectively to be sure that minimum energy is achieved.

3. Diffusion Property

We simulated the property of different concentrations of LiTFSI on this process. In Fig. 3 and Fig. 4, the mean square displacement and self-diffusion coefficient of four different concentrations of LiTFSI are shown. The results indicated that the MSD of LiTFSI is similar to the result of $TFSI^-$, the diffusion property decreases as the concentration increases and diffusion rate are according to ACE > Li^+ > $TFSI^-$.

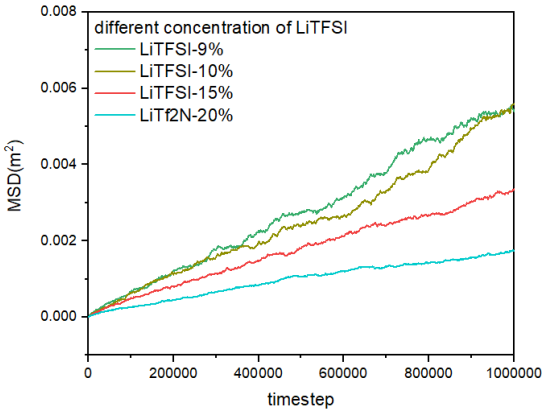

Figure 3. Mean square diffusion of four different concentrations of LiTFSI

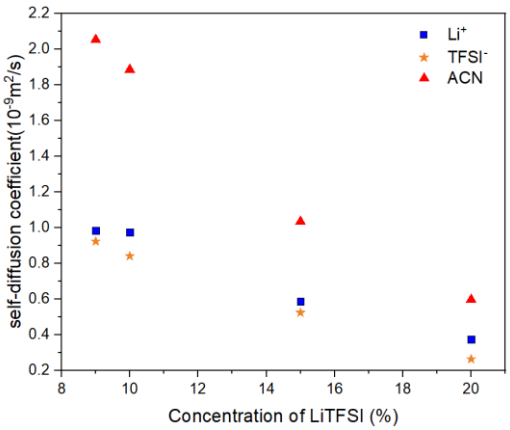

Figure 4. The self-diffusion coefficient ($10^{\wedge-9}m^2/s$) of four different concentrations of LiTFSI

References

1. I. Nezbeda, F. Moucka, W.R. Smith, Mol. Phys. 114 (2016) 1665-1690. J. Yu, S. M. Chen, W. J. Hao, S. J. Zhang, ACS Nano 10 (2016) 2500-2508.
2. C.G. Hanke, S.L. Price, R.M. Lynden-Bell, Mol. Phys 99 (10) (2001) 801–809.
3. J. Yu, S. M. Chen, W. J. Hao, S. J. Zhang, ACS Nano 10 (2016) 2500-2508.
4. J. N. Lopes, J. Deschamps, A. A. Padua, J. Phys. Chem. B 108 (6) (2004) 2038–2047.
5. Y. Zhu, S. Murali, M.D. Stoller, K.J. Ganesh, W. Cai, P.J. Ferreira, A. Pirkle, R.M. Wallace, K.A, Cychosz, M. Thommes, D. Su, E.A. Stach, R.S. Ruoff, Science 332 (2011) 1537−1541.
6. F. Beguin, V. Presser, A. Balducci, E. Frackowiak, Adv. Mater 26 (2014) 2219−2251.

Burak Ulusoy

Phone: +45 4525 2800
E-mail: bulu@kt.dtu.dk
Type: SDC (KT)
Supervisors: Kim Dam-Johansen
Weigang Lin
Wu Hao
Wei Wang, IPE

PhD Study
Started: September 2016
To be completed: August 2019

NO_x formation and reduction in fluidized bed combustion of biomass

Abstract
The focal point of this PhD project is to understand the NOx formation and reduction mechanisms in fluidized bed combustion of biomass. Comprehensive experimental and modelling work will be conducted on both laboratory- and pilot-scale with the ultimate goal of minimizing NOx emissions during combustion. The initial part of the project will mainly deal with the NOx formation and reduction during char combustion, which is lesser understood compared to the gaseous NOx chemistry. Following this, pilot-scale fluidized bed combustion experiments and full-scale CFD modelling will be performed to facilitate the minimization of NOx emissions.

Introduction
Fluidized bed combustion of biomass is a promising technology for heat and power production from biomass. Due to the possibility of fuel-flexibility, high combustion efficiency, and low pollutant emission, the application of fluidized bed technology in the gasification and combustion industry has increased at a fast pace [1]. However, incentives for further reducing the NOx emission from fluidized bed combustion are driven by the harmful environmental impact and strict emissions regulations. It has been well established that upon release to the atmosphere, NOx compounds contribute to global warming, photochemical smog production, and acid rain formation.

In a fluidized bed combustor, the final NO emission is determined by the competing formation and reduction reactions. The NO primarily stems from the fuel bound nitrogen either through volatile or char nitrogen oxidation. Analogous to the formation reactions, NO is reduced through homogeneous thermal DeNOx reactions or heterogeneous reduction over char [2]. Controlling the NO emissions requires a thorough understanding of the underlying mechanisms, which is the primary goal of this work.

Objectives
The main objective of this project is to minimize NOx emissions from fluidized bed combustion of biomass. To do this, a fundamental understanding of the underlying mechanisms in NOx formation and reduction will be acquired through experimental studies in laboratory- and pilot-scale. Mathematical and computational modelling work will also be conducted to describe the experimental data, which could then serve as predictive tools or as sub-models in large-scale simulations.

Experimental Work
Combustion and NO reduction reactivity of pine wood, straw (S), waste wood, bran (B), DDGS, and sunflower seed chars was investigated in a fixed bed reactor, shown in Figure 1. Prior to charring, the biomasses were demineralized (DM) using 1 M HNO_3 at 60°C for one hour. Subsequently, charring was performed in a horizontal oven at 800°C under a N_2 flow of 2.5 NL/min for 10 min.

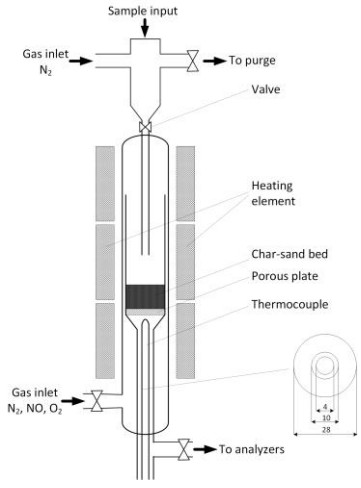

Figure 1: Schematic illustration of the fixed bed reactor.

The reactor is equipped with a solid feeding device, thereby allowing sample admission at a desired temperature and gas composition. In the reduction study, 50 mg char was mixed with 1.70 g silica sand and introduced into the reactor at 800°C and a NO inlet concentration of 400 ppmv. The combustion experiments were performed at 800°C at an inlet O_2 concentration of 10 vol%. In both experiments, the outlet concentrations of NO, O_2, CO, and CO_2 were continuously monitored.

Kinetic Modelling

The steady state fixed bed reactor design equation (Eq. 1) was employed to extract kinetic information from the NO reduction experiments. Assuming the carbon mass based reactivity, R_{NO} (mol/kgC/s), is first order with respect to NO, Eq. 1 integrates to Eq. 2.

$$dX_{NO}/dW = R_{NO}/F_{NO,0} \quad \text{Eq. 1}$$

$$- \ln(1-X_{NO}) = k_{NO} \cdot W/v_0 \quad \text{Eq. 2}$$

Here, X_{NO} (-) is the conversion of NO, W (kg) the instantaneous carbon mass in the bed, $F_{NO,0}$ (mol/s) the flow rate of NO at the inlet, k_{NO} (m^3/kgC/s) the first order carbon mass based reaction rate constant, and v_0 (m^3/s) the volumetric flow rate. Calculating the instantaneous mass of carbon in the bed using the CO and CO_2 outlet concentrations, the transient behavior of the first order reaction rate constant can be determined.

Results and Discussion

Figure 2 illustrates the selectivity of NO formation from combustion of the biomass chars. A decreasing tendency in the selectivity is observed for the DM chars as the char nitrogen content increases. This has previously been reported [3], however, the reasoning for this behavior remains unknown. Due to the underlying mechanism of NO release from combustion, the char nitrogen content conceivably affects the formation and reduction reactions of NO. The decrease in selectivity was more pronounced for the DM chars wherein the catalytic influence of ash forming elements was diminished.

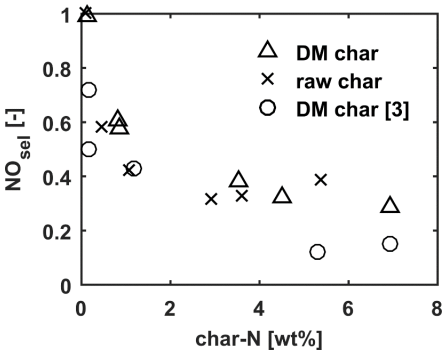

Figure 2: NO selectivity versus char nitrogen content for raw and DM biomass chars. Results of Karlström et al. [3] shown for comparison.

The reduction of NO over chars was examined, with selected results depicted in Figure 3, showing the transient first order carbon mass based reactivity. Of the raw chars, straw exhibited the highest reactivity towards NO, followed by DDGS and bran. On the other hand, the DM samples in general exhibited little discrepancy with DM straw being the most reactive followed DM DDGS and DM bran. No clear correlation was observed between reduction reactivity and char nitrogen content for both the raw and demineralized chars.

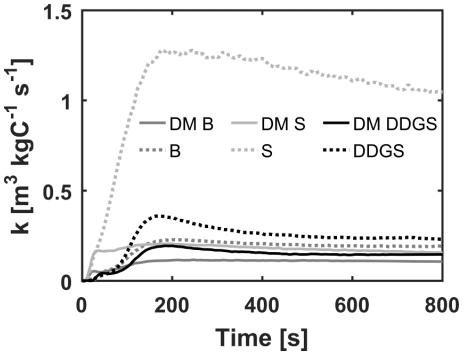

Figure 3: Transient first order reactivity of select chars towards NO. Conditions, T=800°C and $C_{NO,0}$=400 ppmv.

The explanation of the observed trends can be elucidated from the chemical compositions of the chars. Although, bran was noted to contain a larger potassium content (69610 mg/kg) relative to straw (50769 mg/kg), it exhibited a considerably lower reactivity towards NO. This could be caused by the high phosphor content in the bran (49429 mg/kg), thereby forming KPO_3, which is catalytically inactive in NO reduction.

Conclusion

It was noted that the char nitrogen content influenced the NO selectivity upon combustion of biomass chars. Examining the reduction behavior of the chars towards NO showed no clear tendency between reduction reactivity and char nitrogen content.

The observed reactivity difference between straw and bran chars indicated that the main controlling factor of reactivity is the content and chemical association of the ash forming elements.

Future work

Experiments will be carried out in a pilot-scale fluidized bed combustor to investigate the emission of NOx under well-defined operating conditions. To minimize NOx emissions, the influence of fuel type, secondary air inlet, bed material, and additives will be examined.

CFD simulations will be performed in combination with skeletal NOx models to describe the freeboard of an industrial-scale fluidized bed boiler, thereby providing a simplified gas phase model, useful in industrial applications.

References

17. R.I. Singh, A. Brink, M. Hupa, Appl. Therm. Eng., 52 (2) (2013) 585-614.
18. P. Glarborg, A.D. Jensen, J.E. Johnsson, Prog. Energy Combus. Sci. 29 (2003) 89-113.
19. O. Karlström, M. Perander, N. DeMartini, A. Bring, M. Hupa, Fuel 190 (2017) 274-280.

Song Xu

Phone: +8615238623728
E-mail: songx@ipe.ac.cn

Type: SDC (IPE)
Supervisors: Suojiang Zhang
Xiangping Zhang
Kaj Thomsen

PhD Study
Started: September 2015
To be completed: December 2018

Research of high-energy-density lithium-sulfur flow batteries

Abstract

The traditional aqueous redox flow batteries are suffering low energy density due to the low solubility of active species. Semi-solid suspension electrodes are not subjected to solubility limit of active materials and output higher volumetric energy density. We design and prepare a high-energy-density suspension catholyte based on a sulfur-Ketjenblack-reduced graphene oxide composite (S-KB-G@P). The special hyperbranched structure of KB enhances the stability of the suspension; rGO sheets which wrap the S-KB particles immobilize polysulfides migration, and meanwhile facilitate the electron transportation in the whole suspension. Li-S flow cell with this catholyte shows excellent cycle stability (more than 1000 cycles with 99% coulombic efficiency) and low self-discharge (1.1% loss per day). Continuous charge/discharge tests in different flow modes are demonstrated and the influence of the flow rate on the flow battery performance is discussed. The smooth operation in long-lasting flow mode further demonstrates the stability of the suspension catholyte.

Introduction

Electrochemical energy storage (EES) devices are crucial to the extensive utilization of the unstable and intermittent renewable energy, such as solar and wind systems. Among different chemistries, redox flow batteries are promising technologies owing to their operation flexibility, easy scalability and high cost effectiveness. Li-S flow battery is attracting great interest as it not only takes advantage of the properties of flow battery but also has the specialties of high energy density, low cost and non-toxic of Li-S battery. The long-term stability is undoubtedly the fundamental prerequisite for future development of sulfur suspension catholyte. To achieve stable suspension, active material should be suspending rather than precipitating; to improve the electrochemical stability, the shuttle effect which still exists in sulfur catholyte should be restrained as much as possible. [1-3]

We design and prepare a pie-structured Sulfur-Ketjenblack@reduced Graphene Oxide (S-KB@rGO) composite in which sulfur nanoparticles are loaded on the KBs; and the rGO sheets are wrapped around the S-KB particles.Li-S flow cell with this catholyte exhibited outstanding electrochemical performance. The sulfur utilization reached 91.4% (1532 mA h g-1) at 0.05C; upon 1000 cycles was achieved with high coulombic efficiency of 99%; the self-discharge rate was 1.1% per day.

Specific objectives

The main specific objiective of this work is to study the application of sulfur suspension catholyte in Li-S flow battery. Meanwhile we also verify the feasibility of Li-S suspension catholyte flow system in real work condition.

Results and discussion

Fig.1 shows the structure of S-KB@rGO, the KB and nano sulfur were wrapped by rGO sheets, a pie-structured S-KB@rGO composite was formed. It is difficult to distinguish the KB and sulfur particles in the S-KB or S-KB@rGO composites (Fig 2b and Fig. 2c), the possible reason is that the sulfur is well dispersed in the pores of the KB particles due to the excellent wettability between carbon and sulfur.

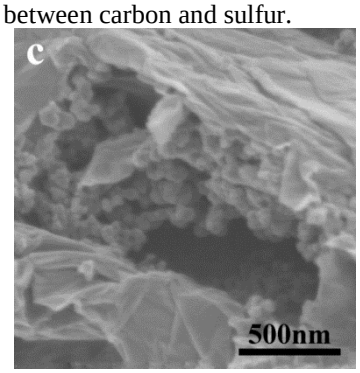

Fig.1 SEM of S-KB@rGO[1]

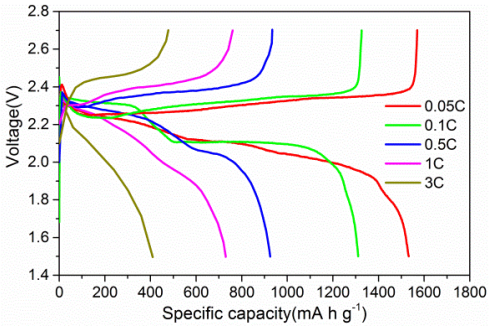

Fig.2 Charge/discharge profiles at varied rates.[1]

Fig. 3 shows the charge/discharge profiles of the S-KB@rGO suspension catholyte at different C rate. Two typical discharge plateaus were detected at 2.25 V and 2.05 V regions at 0.05 C rate. The discharge capacity of the suspension catholyte reached 1532 mA h g^{-1} at 0.05C with sulfur utilization of 91.4%, moreover, the suspension catholyte delivered high specific capacity of 749 mA h g-1 and 410 mA h g-1 at 1C and 3C, respectively. The high electrochemical activity of the S-KB@rGO catholyte derives from the synergistic contributions of KB particles and rGO sheets that form a 3D conductive network to support sufficient electrochemical reaction sites and fast electron/ion transfer channels.

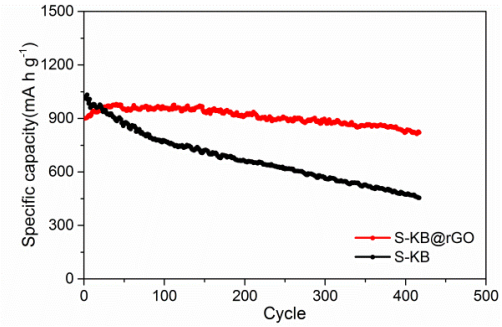

Fig.3 Cycling test at 0.5C

A long-term cyclic test was conducted in the potential range from 1.5 to 2.7 V at 0.5C (Fig. 3). The S-KB catholyte, as a whole, exhibited poor cyclic stability. The rapid decrease may be mainly attributed to the migration and loss of polysulfides during cycling. In a sharp contrast, the S-KB@rGO suspension catholyte showed more stable cyclic performances. It output an initial specific capacity of 899 mA h g-1, in the following cycles, the capacity of the S-KB@rGO suspension catholyte rose slowly to a maximum reversible value of 980 mA h g-1 (40th cycle) and maintained steady, this was mostly due to the gradual activation of internal sulfur well-wrapped by rGO. The S-KB@rGO suspension delivered a specific capacity of 837 mA h g-1 at the 400th cycle with a capacity retention ratio of 93.1%, which was about two times higher than that of S-KB catholyte (45.4%). Above evidences confirm that the outer rGO sheets do play an important role in improving the cycle stability of the sulfur suspension catholyte.

The flow cell was conducted continuous charge/discharge test at flow rates of 5, 25 and 45 mL min-1 at current density of 1 mA cm-2 (Fig. 5). The power capability was tested by linear sweep voltammetry. Fig.5f shows the power density of the S-KB@rGO suspension flow cell at the flow velocity of 5, 10, 30 ml min-1, and the achieved peak power density is 9.6, 12.9, 15.5 mW cm-2, respectively. The power density is improved by 61% when the flow rate is accelerated from 5 to 30 ml min-1.The continuous flow operation verify the feasibility of the Li-S flow battery in real work condition.

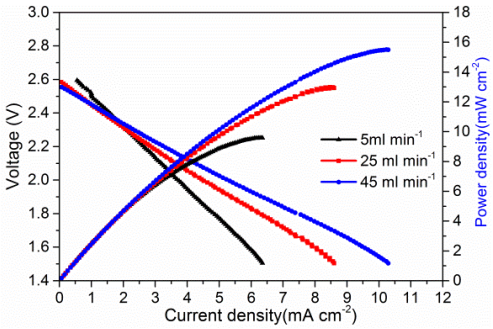

Fig.4 Power density of the flow cell at varied flow rate[1]

Conclusions,

In summary, a novel self-stabilized catholyte enabled by nano pie-structured S-KB@rGO composite for Li-S flow batteries was demonstrated here. The S-KB@rGO catholyte exhibited stable cycle performances (low capacity decay rate of 0.047% and high coulombic efficiency of 99% in 1000 cycles), high specific energy (400 W h L^{-1}) and low self-discharge rate (1.1% loss per day). The laboratory scale Li-S flow cell showed stable charge/discharge performance with high coulombic efficiency in intermittent-flow and continuous flow modes, which certify the feasibility of the S-KB@rGO suspension cathode in practical working conditions. The concept of sulfur suspension catholyte improves the cycle stability which is urgently needed for the large-scale application of Li-S flow batteries, and this strategy also offers a promising direction for the development of other flow batteries.

Acknowledgements

This work was supported by National Key Projects for Fundamental Research and Development of China , International Cooperation and Exchange of the National Natural Science Foundation of China), Key Program of National Natural Science Foundation of China, “Strategic Priority Research Program” of the Chinese Academy of Sciences), CAS/SAFEA International Partnership Program for Creative Research Teams .

References

1. 1. S. Xu, L. Z., X. Zhang , Y. Cai, S. Zhang.. J. Mater. Chem. A 2017,5, 12904-12913.
2. 1.M. Z. Jacobson, Energy Environ. Sci., 2009, 2, 148.
3. 2.Z. Yang, J. Zhang, M. C. Kintner-Meyer, X. Lu, D. Choi, J. P. Lemmon and J. Liu, Chem. Rev., 2011, 111, 3577.
4. 3.G. L. Soloveichik, Chem. Rev., 2015, 115, 11533.

Shaoqi Yang
Phone: +86 18811304213
E-mail: sqyang@ipe.ac.cn

Type: SDC (IPE)
Supervisors: Xingmei Lu
Suojiang Zhang
Anker Degn Jensen

PhD Study
Started: September 2015
To be completed: July 2019

Study on Biomass Pretreatment and Conversion in Ionic Liquids System

Abstract
High purity of cellulose I materials (≥ 90 wt%) was obtained from the treatment of corn straw by using polyhydric protic IL of 2-hydroxy-N-(2-hydroxyethyl)-Nmethylethanaminium methanesulfonate ([BHEM]mesy, about $1000/t). The cellulose material maintaining high degree of crystallinity could be further applied for manufacturing of biomaterials with superior mechanical properties. Meanwhile, [BHEM]mesy combined with Ru/C catalysis was also used for the fractionation of alkali lignin under mild conditions. The products were characterized by elemental analyzer and size exclusion chromatography (SEC).

Introduction
Biomass is relatively cheap sources of lignin, hemicelluloses and cellulose, which can be used as starting materials for biofuels and other commodity chemicals [1]. Cellulose, the most abundant carbohydrate polymer in lignocellulosic materials, has been applied to many aspects, such as, fuel ethanol production, amphiphobic cellulose-based material, cellulose gels and aerogels, and cellulose fibers for reinforcing composites [2]. Cellulose I material can be separated from biomass by using various solvent systems, such as dilute acid treatment, alkaline treatment, the sulphite pulping process, organosolv isolation and ionic liquids (ILs) [3]. The protic ILs with sulfonate anion are regarded as the most efficient types in terms of the relative impact on breaking down the largest lignin molecules for separation of cellulose and reducing the cost for multi-ton IL production [4]. Hence, polyhydric PIL has a better industrialization prospect on biomass pretreatment.

Lignin is an abundant natural renewable aromatic polymer, possessing about 15 to 35 wt% in the biomass resources [5]. Conversion of lignin to usable building blocks or platform molecules has been widely researched in recent years. However, many researchers mainly used lignin model chemicals as their feedstock for the investigated process and really a few of them employ real lignin [6]. Hydrodeoxygenation of real lignin to renewable aromatic chemicals and drop-in bio-fuels has great significance for advanced utilization of renewable lignocelluloses and the future bio-based economy.

Specific Objectives
Extraction of higher value products of cellulose I material from corn straw is of interest, which is meaningful for making the utmost utilization of biomass resources. The traditional strategies for separation of Cellulose I material from biomass usually cause serious environmental consequences. High cost of ILs system also limited its further utilization. Separation of cellulose I material from corn straw with low-cost protic ILs (about $1000/t: calculated according to the material price) was therefore conducted in this work.

Converting lignin to value-added platform molecules has attracted much attention in recent years. Among all the strategies, heterogeneous catalyst combined with ILs is one kind of promising method for hydro-liquefaction of lignin. Therefore, conversion of alkali lignin was investigated by using Ru/C catalyst in cooperation with 2-hydroxy-N-(2-hydroxyethyl)-Nmethylethanaminium methanesulfonate ([BHEM] mesy).

Experimental
Corn straw (cellulose 50.72%, hemicelluloses 31.35% and lignin 15.39%) was used as the raw material after washed with Neutral detergent solvent. ILs were synthesized by one step protonation reaction. Dried biomass materials (5 wt% of the ILs) and ILs (10 g) were added into a 50 ml tube with stir bar. The mixture was then heated and stirred at a given temperature and time in an electric heating module (IKA RCT basic). 10 ml of water was added into the tube till the end of heating to dilute the mixture and separate undissolved

cellulose components from ILs by centrifugation. Water and ethanol were used to wash the solid cellulose material three times respectively. Moreover, all of the cellulose materials were dried by the way of freeze-drying for about 24 h.

Catalytic Hydrogenolysis of alkali lignin by using Ru/C and [BHEM]mesy was conducted in ethanol medium. Alkali lignin (5 g), [BHEM]mesy (5 g), 5 wt% Ru/C (0.5 g) and ethanol (39.5 g) were added to the auto clave. Then sealing the autoclave and flushing with N_2 and H_2. The reactions were conducted at a given temperature for 3 hours. Distilled water and ethyl acetate were applied to extract the bio-oil products from [BHEM]mesy.

Results and Discussion

The results of the research showed that High purity of cellulose I materials (≥ 90 wt%) can be obtained from the treatment of corn straw by using [BHEM]mesy at 140 °C for 6 h. For the recent study, although most of lignin and hemicelluloses can be efficiently removed by PIL, the product of cellulose also loses its crystal structure [7].

The solubility of corn straw and contents of cellulose in the cellulose materials shows an obvious trend towards higher value with both elevated temperature and longer pretreatment time. Among the ILs, [BHEM]mesy shows the highest removal efficiency for both of hemicelluloses and lignin.

Figure 1 shows the XRD pattern of raw corn straw and the cellulose materials that obtained from treatment of corn straw by PILs at 130 °C for 6 h. The pattern confirms that the cellulose materials maintain the same crystal structure with cellulose I and no signs of cellulose II were found [8]. The crystallinity index (CrI) of the cellulose materials from the treatment of corn straw by [DMEA]mesy, [BHEM]mesy and [2-HTEAF]mesy are 44, 59 and 45%, respectively. Compared with corn straw (CrI 37%), the cellulose materials show an increasing CrI.

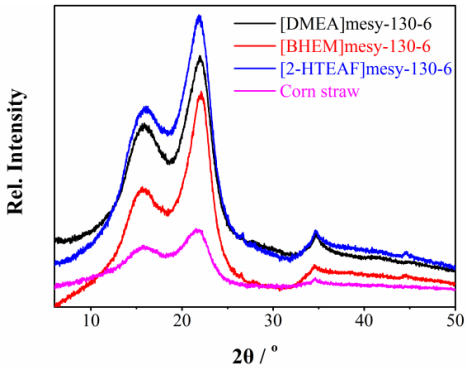

Figure 1: XRD pattern of raw corn straw and cellulose materials obtained from the treatment of corn straw by ILs at 130 °C for 6 h

The comparison of liquid products between using Ru/C and Ru/C incorporate with [BHEM]mesy at 275 °C for 3 h is shown in Figure 2. Significant degradation of alkali lignin can be attained by using Ru/C incorporate with [BHEM]mesy. There are lower molecular weight products for Ru/C incorporate with [BHEM]mesy comparing with just use Ru/C.

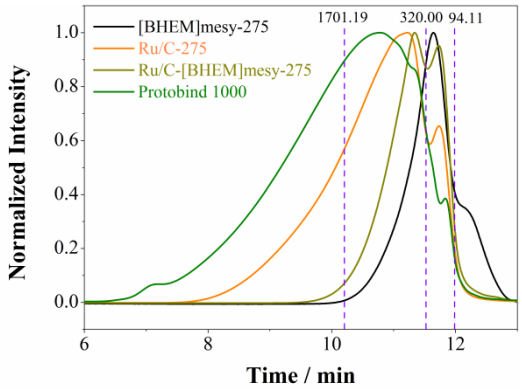

Figure 2: SEC spectrogram of Liquid products by using Ru/C and Ru/C incorporate with [BHEM]mesy.

Conclusions

High purity of cellulose I materials (≥ 90 wt%) can be obtained from the treatment of corn straw by using [BHEM]mesy. This work provides a high efficiency way to separate cellulose I material from biomass, which is a promising green technology of corn straw industrial application. In addition, Comparing with just using Ru/C as the catalyst, Ru/C incorporate with [BHEM]mesy shows excellent effects for degradation of alkali lignin.

Acknowledgements

This research was supported financially by the National Basic Research Program of China (973 Program) [2015CB251401] and the National Natural Science Foundation of China [Nos. 21476234, 21210006, 21336002, 21606240, 21406230]. Thanks very much for all the helpful suggestions and guidance from Assistant Prof. Jakob Munkholt Christensen and Dr. Soheila Ghafarnejad Parto.

References

1. A.J. Ragauskas, C.K. Williams, T. Tschaplinski, Science, 311 (2006) 484-489.
2. N. Mahfoudhi, S. Boufi, Cellulose, 24 (2017) 1171-1197.
3. S.Q. Yang, X.M. Lu, S.J. Zhang, Cellulose, 25 (2018) 3241-3254.
4. A. George, K. Tran, B.M. Holmes, Green Chem, 13 (2011) 3375-3385.
5. C.Z. Li, X.C. Zhao, T. Zhang, Chem Rev, 115 (2015) 11559-11624.
6. R. Rinaldi, R. Jastrzebski, B.M. Weckhuysen, Angew Chem Int Edit, 55 (2016) 8164-8215.
7. A. Brandt-Talbot, F.J.V. Gschwend, J.P. Hallett, Green Chem, 19 (2017) 3078-3102.
8. A. Isogai, M. Usuda, R.H. Atalla, Macromolecules, 22 (1989) 3168-3172.

List of Publication

1. S.Q. Yang, X.M. Lu, S.J. Zhang, Cellulose, 25 (2018) 3241-3254.

Shuai Yang
Phone: +86 15963218500
E-mail: yangs.qday@sinopec.com

Supervisors: Hongzhong Li
Qingshan Zhu
Hao Wu, DTU
Weigang Lin, DTU

PhD Study
Started: September 2012
Completed: June 2016

An Exploratory Study of MP-PIC based 3D Simulation of a Bubbling Fluidized Bed with and without Baffles

Abstract
In this study, the flow characteristics of Geldart A particles in a bubbling fluidized bed with and without perforated plates were simulated by multiphase particle-in-cell (MP-PIC) based Eulerian-Lagrangian method. A modified structure-based drag model was developed based on our early work [Lv et al. Chem. Eng. J. 236 (2014) 149-157]. Other drag models including the Parker drag model and the Wen&Yu-Ergun drag model were also employed to investigate the effects of drag models on the simulation results. Although the modified structure-based drag model gives better prediction of the gas-solid flow dynamics of a baffle-free bubbling fluidized bed in comparison with the experimental data, none of these drag models are good enough for prediction of the gas-solid flow in a baffled bubbling fluidized beds due to the baffle treatment method in Barracuda. For improving the simulation accuracy, the current Barracuda version should address the challenges of bed height incorporation and baffle treatment method.

Introduction
Baffled gas-solid bubbling fluidized beds are widely applied in industrial processes [1]. However, how the configuration of perforated plates affects the hydrodynamics of bubbling fluidized beds is still indistinct. With the rapid development of computational capability, the computational fluid dynamics (CFD) method provides an efficient approach to solve this problem. The MP-PIC based the Eulerian-Lagrangian method is appropriate to simulate hydrodynamics in fast, turbulent and bubbling fluidization regime with coarse and fine particles, but the applicability in baffled bubbling fluidized beds with fine particles still needs to be explored.

Simulation
Simulations were conducted using the CPFD software Barracuda VR 17.0. The simulation was based on the gas-solid bubbling fluidized system used in our previous work [2]. The part for simulation is a column of 140 mm in diameter and 1000 mm in height. The particles used were glass beads with the average particle size of 53 μm, density of 2450 kg/m^3. The baffles used in the experiment were perforated plates, as shown in **Figure 1**. In the two-compartment baffled bubbling fluidized bed, the perforated plates were mounted at the height of 0.135 m and 0.235 m above the distributor, respectively. The operating conditions in the experiment and setting parameters in the simulation are shown in **Table 1**.

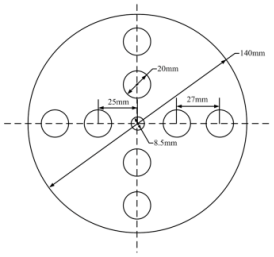

Figure 1: Configuration of the perforated plate.

Table 1: Summary of parameters used in Barracuda 17.0.

Parameters	Value
Initial bed height (m)	0.335
Initial solids concentration	0.56
Particle sphericity	0.8
Superficial gas velocity (m/s)	0.054，0.072
Initial fluid pressure (kPa)	106
Flow time (s)	35
Average time of results (s)	15

In CFD simulations, drag models are of vital importance for prediction of the hydrodynamics in gas-solid bubbling fluidized beds. To investigate the influence of drag models on the CPFD simulation results, three drag models were employed in the simulation, i.e. the modified structure-based drag model

reported in reference [3], the Wen&Yu-Ergun (Gidaspow) drag model [4] and the Parker drag model [5].

According to the independence test of grid and particle number per parcel, the appropriate grid size was 5 mm×5 mm×5 mm, and the particle number per parcel of 200 was selected in later simulations.

Results and Discussion

Baffle-free bubbling fluidized bed

Figure 2 illustrate the particle volume fraction profiles calculated by the three drag models at the superficial gas velocity of 0.072 m/s in the baffle-free bubbling fluidized bed. Slugging is observed from the Parker drag model and the Wen&Yu-Ergun drag model (see **Figure 2,** b and c), which is not realistic in a bubbling fluidized bed with Geldart A particles. As shown in **Figure 3,** all the drag models cannot predict accurately solid concentration distributions in top part of the bubbling fluidized bed. In the MP-PIC based Eulerian-Lagrangian method, a certain number of particles is treated as a parcel. This treatment may cause the homogenization of particles motion and influence the simulation accuracy.

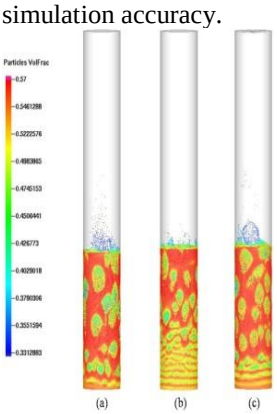

Figure 2: Particle volume fraction profiles at 35 s.

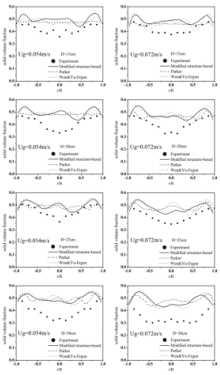

Figure 3: Radial solid concentration distributions.

Baffled bubbling fluidized bed

Similar to the results of baffle-free bubbling fluidized bed, there is unreasonable slugging at the bottom of the bed predicted by the Parker drag model (b) and the Wen&Yu-Ergun drag model (c), as shown in **Figure 4**. Although the gas-solid flow calculated by the modified structure-based drag model (a) is visually consistent with experimental phenomena, it cannot precisely predict the hydrodynamics at higher bed height neither, as shown in **Figure 5**.

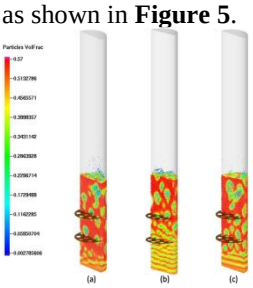

Figure 4: Particle volume fraction profiles at 35 s.

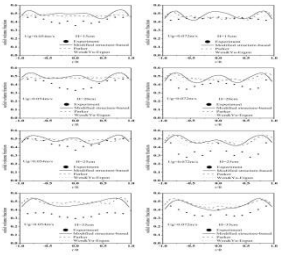

Figure 5: Radial solid concentration distributions.

Conclusions

Different drag models including the modified structure-based drag model, the Parker drag model, and the Wen&Yu-Ergun drag model have been applied to CPFD to explore the possibility for simulation of bubbling fluidized beds. Among these drag models, the modified structure-based drag model shows a better performance than other drag models. However, the results are not good enough for prediction of gas-solid flow compared with the experimental data. In addition, for comparison with experimental data, it is not sufficient to compare only the solid volume fraction profile data. Detailed fluid dynamics structure should be examined carefully as well. For increasing the simulation accuracy, the modified structure-based drag model should be improved to adapt the computational logic of CPFD. In addition, the baffle treatment method of Barracuda should be improved as well.

Acknowledgements

This work is supported by the Sino-Danish Center for Education and Research, the Sino-Danish collaboration project (DANCNGAS), the Innovation Fund Denmark, the State Key Development Program for Basic Research of China (973 Program) under Grant 2015CB251402 and the National Natural Science Foundation of China under Grant No. 21325628, which are gratefully acknowledged.

References

1. D. Kunii, O. Levenspiel. Fluidization Engineering, Wiley, New York, 1991.
2. S. Yang, H. Li, Q. Zhu, Chem. Eng. J. 259 (2015) 338-347.
3. X. Lv, H. Li, Q. Zhu, Chem. Eng. J. 236 (2014) 149-157.
4. D. Gidaspow, Multiphase Flow and Fluidization: Continuum and Kinetic Theory Descriptions, Academic Press, New York, 1994.
5. J.M. Parker, Improving Drag Correlations for Modeling of Real Particle Fluidization. Proceedings of the Inaugural Barracuda Virtual Reactor User' Conference, Santa Ana Pueblo, New Mexico, 2015.

List of Publications

1. S. Yang, H. Li, Q. Zhu, Chem. Eng. J. 259 (2015) 338-347.
2. S. Yang, L. Peng, W. Liu, H. Zhao, X. Lv, H. Li, Q. Zhu, Powder Technol. 296 (2016) 37-44.
3. S. Yang, H. Wu, W. Lin, H. Li, Q. Zhu, Particuology 2018.
4. W. Liu, S. Yang, H. Li, Q. Zhu, Powder Technol. 295 (2016) 122-132.

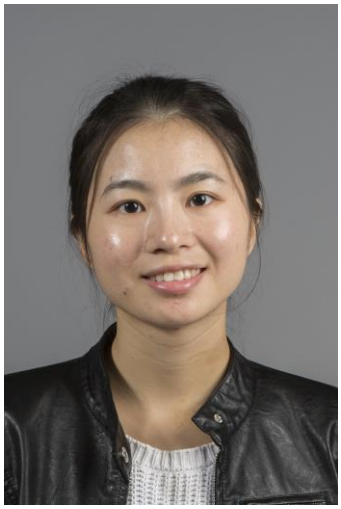

Ying Zeng

Phone: +45 4525 2952
E-mail: yzen@kt.dtu.dk

Type: KT/SDC master
Supervisors: Søren Kiil
Claus Erik Weinell
Kim Dam-Johansen
Louise Ring, Hempel

PhD Study
Started: October 2016
To be completed: October 2019

Novel testing methods for intumescent coatings

Abstract
The thermal shield of intumescent coatings is an effective way to protect the structural steel in the event of a fire. This project involves design and validation of a lab-scale setup for fast and reliable fire tests, and evaluation of the effect (or synergic effect) of different concentrations of the ingredients on the performance of intumescent coatings based on a basic hydrocarbon formulation. The evaluation is for understanding the roles of ingredients thoroughly by linking their responses in the fire tests with the char characterizations and mapping the intumescent mechanism.

Introduction
The protection of structural steel on exposure to a fire has become paramount to prevent the loss of lives and assets with increasing use of structural steel as a material to create the shape of construction projects. Structural steel only retains 60% of its original strength when its temperature reaches a critical value and loses it bearing ability under full design load [1]. For regular loaded structural components, such as onshore platforms, 550ºC has been selected as a standard critical temperature for steel. While for heavily loaded structural components, such as offshore platforms, 400°C has been selected as a standard. This critical temperature is also known as ‘‘failure temperature’’, and the time for reaching it in the event of a fire is called the “failure time” [2].

An efficient way to protect the building structure and prolong the time before the failure temperature is reached is by intumescent coatings. At elevated temperature, intumescent coatings swell to a multicellular char layer, which acts as a physical barrier to slow heat and mass transfer between gas and condensed phase and thereby protects the underlying substrate. The most effective intumescent coatings are the ones that have best fire-resistance performance and therefore can provide longest failure time for the substrate in the fire tests.

Instead of natural fire that has varied relationships between temperature and time, usually fire tests refer to the tests under standard fires for which the fixed temperature-time responses are imposed in order to roughly simulate the evolution of natural fires and meanwhile facilitate the normalization of fire test procedure. Depending on the source of fuel, most of the standard fires are classified into two types: cellulosic fire (ISO 834) and hydrocarbon fire (e.g. UL 1709). Their corresponding intumescent coatings are called cellulosic intumescent coatings and hydrocarbon intumescent coatings. The latter is the focus of the present project, as it is the most challenging type used for high-risk environments such as petrochemical complexes and offshore platforms.

Generally, intumescent coatings consist of three essential ingredients: acid source (e.g. ammonium polyphosphate), carbon source (e.g. dipentaerythritol), and blowing agent (e.g. melamine). Other ingredients are incorporated into the formulation as well to improve its function (e.g. composite fibers). All the ingredients are bound together by a polymeric binder. The physical and chemical interactions among these compounds are complex and have not been fully quantified in the literature, especially for the case of the hydrocarbon intumescent coatings [3]. To optimize the formulation of hydrocarbon intumescent coatings, it is fundamental to understand the effect (or synergic effect) of ingredients on the physical (expansion and strength) and chemical (thermal conductivity and thermal stability) properties of char.

Specific Objectives
This Ph.D. project aims at:

- Validation of equipment for fire tests and characterizations with two typical hydrocarbon intumescent coatings.
- Design a setup with motion system for continuous and reliable fire tests.

- Link varying levels of ingredients with different char characteristics.

Two hydrocarbon intumescent coatings (A and B) supplied by Hempel were investigated in terms of fire-resistance performance and variation of complex viscosity with temperature increasing. The formulations of A and B are confidential and not given here. The application of the intumescent coatings starts with mixing the two parts (base and curing agent) according to the specific ratio. Once it is mixed well, about 6 mm of the coating is applied on the surface of a grit blasted steel plate that are squares of 60*60 mm and 3 mm thick. The coatings are cured for 24 h at room temperature before being used.

The fire tests of A and B were carried out with a lab oven (Nabertherm, LHT 01/17D) according to UL 1709. A lab-made insulating model is used to hold the coated plate and a thermocouple is attached to the back of the plate to record the temperature – time (T-t) response. The repeatability of the oven was assessed by testing A thrice and the T-t curves recorded are almost the same. The relative standard deviations of failure time at 400ºC and 550ºC are less than 1%. It indicates that the results of fire tests from the oven are reliable and reproducible.

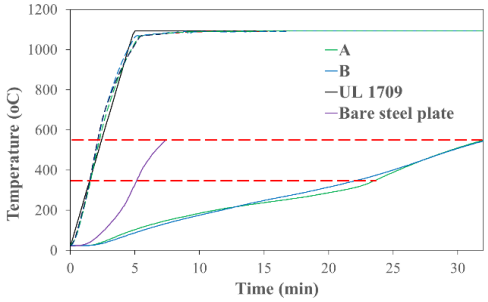

Figure 1: Temperature – time response of A and B tested with UL 1709.

Figure1 shows the T-t response of A and B under the fire tests of UL 1709. Table 1 lists the corresponding failure time and relative expansion calculated by dividing the coating thickness after the test by the counterpart before the test. The results of bare steel plate are also included for comparison. The dash lines in the figure are the experimental hydrocarbon curves performed with the oven, which show few differences compared with the standard UL 1709 (black solid line).

The bare plate reached its failure temperature (400ºC and 550ºC) rapidly within 8 minutes due to the lack of protection of intumescent coating. When A and B were applied on the plate, the failure time were greatly extended to around 32 minutes (550ºC). The performances of A and B are more or less the same according to the parameter of failure time. However, their T-t curves show an unneglectable difference considering the rather good repeatability of the oven. This difference may reflect the different reactions taking place during the fire tests, which give distinct composition of the incipient char. The XRD and EDS results (not shown here) confirmed that except for amorphous carbon the main components of the final char are zinc phosphate and boron phosphate (B), and composite of titanium phosphate doped with calcium (A). Their unique composition should result in different thermal conductivities as the unalike relative expansions give similar failure time (Table 1).

Table 1: The failure time and expansion of A and B.

Samples	Temperature (ºC)		Relative Expansion
	400	550	
Bare plate	5.5	7.4	-
A	25.45	32.05	9.17
B	25	32.35	4

The diverse expansions are expected in light of the variation of viscosity (see Figure 2). The viscosity measurement was done with the free-film coatings that have diameter of 25 mm and thickness of 3 mm. It was suggested that expansion of intumescent coatings occurs when the viscosity is lowest [4]. The lower minimum complex viscosity of A at around 360ºC permits less external stress for the degradation gases released from the blowing agents (or the reactions between other compounds), which thereby leads to substantial expansion.

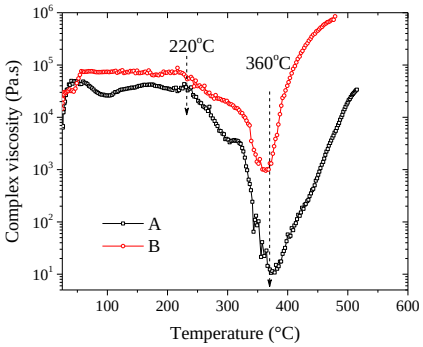

Figure 2: Dynamic viscosity of A and B varied with temperature increasing.

Conclusions

The failure time of steel plate coated with A or B is greatly increased compared with the bare steel plate. The performances of A and B in the fire tests are more or less the same with respect to the failure time. Nevertheless, the differences between both their T-t responses and relative expansions may indicate the divergent reactions occurring during the intumescence. Future work will provide more information about the underlying reactions with the aid of characterizations.

References

1. M. Jimenez, S. Duquesne, S. Bourbigot, Ind. Eng. Chem. Res. 45 (2006) 7475-7481.
2. M. Jimenez, S. Duquesne, S. Bourbigot, Ind. Eng. Chem. Res. 45 (2006) 4500-4508.
3. J. Alongi, Z. Han, S. Bourbigot, Prog. Polym. Sci. 51 (2015) 28-73.
4. M. Jimenez, S. Duquesne, S. Bourbigot, Surf. Coatings Technol. 201 (2006) 979-987.

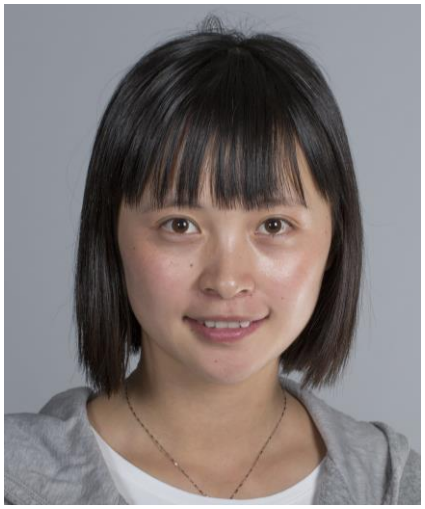

Yu Zhang
Phone: +45 9186 8186
E-mail: yuzha@kt.dtu.dk

Type: KT/SDC master
Supervisors: Peter Glarborg
Anker D. Jensen
Jakob M. Christensen

PhD Study
Started: September 2016
To be completed: August 2019

Catalytic Oxidation of Methane

Abstract
Natural gas is an interesting engine fuel for ships in coastal zones, where high sulfur marine fuels cannot be used. However, unburnt methane poses another severe emission problem. The current study seeks to develop a catalyst for methane emission abatement from natural gas engines. Among the catalysts studied for CH_4 oxidation, Pd based catalysts are recognized as the most active catalyst, while they suffer from deactivations caused by H_2O and more detrimentally, SO_2. A catalyst that remains sufficiently active under real exhaust gas conditions (350-550 °C, 5-10 vol.% H_2O and 1-2 ppm SO_2) is still being sought. The commercial catalyst from Haldor Topsøe and the home made catalysts were tested under different conditions. The homemade catalysts are more active than the commercial catalyst in the absence of SO_2, while they lost most of the activity with addition of 20 ppm SO_2.

Introduction
Dual-Fuel engine can switch flexibly between diesel mode and natural gas mode to lower NOx and PM emissions and meet the strict regulations [1]. However, the unburnt CH_4, which has a greenhouse impact of 25 times larger than that of CO_2, becomes another environmental issue for the Dual-Fuel engines. In order to solve this problem, a CH_4 catalytic oxidation unit, which could fully convert the unburnt CH_4 to CO_2 and H_2O, is necessary to be installed in the exhaust gas pipe. CH_4 has no C-C bond but four identical and strong (bond dissociation energy at 298 K: 439 kJ/mol) C-H bonds, making it difficult to be converted to CO_2 and H_2O compared with other alkanes. The catalysts studied in the literature for CH_4 oxidation can be divided into two groups, noble metals supported catalysts and non-noble metal catalysts. Among the catalysts, Pd based catalyst are most active for CH_4 oxidation with a mixed metal and oxidized phase as active site [2]. 1 wt.% Pd/H-ZSM-5 could fully convert CH_4 to final products at 320 ℃ and the activity was stable in the subsequent 3 runs even to a temperature as high as 800 ℃.[3]

The commercial catalyst from Haldor Topsøe and homemade catalysts are tested for methane oxidation in the temperature range of 250-550 ℃, in a simulated exhaust gas (2500 ppm CH_4, 5 vol.% H_2O, and 20 ppm SO_2 when present).

Specific objectives

The objectives of the PhD project focuses on developing a desired catalyst which can be used in practical engine exhaust conditions: low temperature (lower than 500-550 ℃), CH_4 concentration of 2000-2500 ppm, the presence of a large amount of H_2O (~ 10 vol.% H_2O) and low concentrations of SO_2 (~ 1 ppm). The scope of the PhD work includes:

- Test the activity, stability, and poisoning properties of the commercial catalyst supplied by Haldor Topsøe.
- Prepare and test the homemade catalysts (A) and (B).
- Investigate the thermal, H_2O and SO_2 deactivation mechanism of the prepared catalysts at different operating temperatures (400-550 ℃), and SO_2 concentrations (1-20 ppm).
- Investigate the influence of the promoter on the SO_2 resistance of the homemade catalysts.
- Characterization of catalysts (fresh and spent).
- Identification of the optimum conditions for the process and evaluation of the implications in the process on four-stroke maritime engines.

Results and discussion
As shown in Figure 1and 2, lab prepared catalyst (A) and catalyst (B) have better activity than the Haldor

Topsøe catalyst in the presence of 5 vol.% H_2O but in the absence of SO_2.

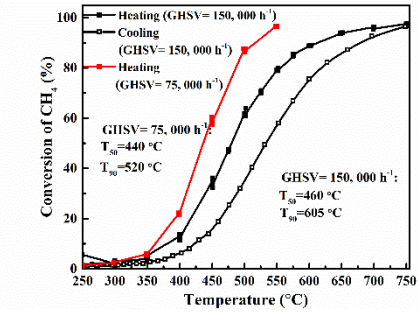

Figure 1: Activity of commercial catalyst from Haldor Topsøe (2500 ppm CH_4, 10 vol.% O_2, 5 vol.% H_2O.

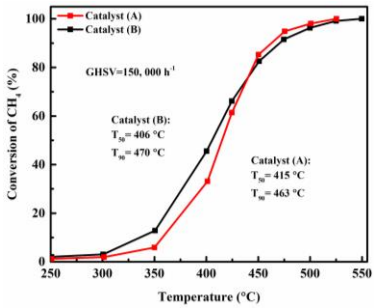

Figure 2: Activity of catalysts (A) and (B) (2500 ppm CH_4, 10 vol.% O_2, 5 vol.% H_2O.

As shown in Figure 3, catalyst (A) lost almost all the activity (50 % CH_4 conversion) immediately upon addition of 20 ppm SO_2. The activity could be partially restored to 46 % by heating to 550 ℃ after the first time poisoning. What's worse, the restored CH_4 conversion decreased to 26 % after the second time SO_2 poisoning. It indicates the weak SO_2 resistance of catalyst (A).

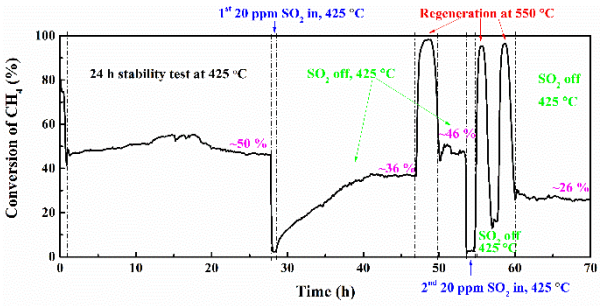

Figure.3 stability of catalyst (A) (425 ℃, 5 vol.% H_2O), SO_2 resistance (20 ppm SO_2).

As shown in Figure 4, the activity of Haldor Topsøe catalyst could maintain at a CH_4 conversion of 22 % after running in the presence 5 vol.% H_2O and 20 ppm SO_2 for around 10 days. After removal of SO_2 for 12 h, without any heating, the activity can be mostly self-regenerated to 46 %.

Lab prepared catalyst (B) showed high and stable low temperature activity in the presence of 5 vol.% H_2O. However, when 20 ppm SO_2 was added into the H_2O containing feed stream, the activity decreased significantly (Figure 5 curve a).

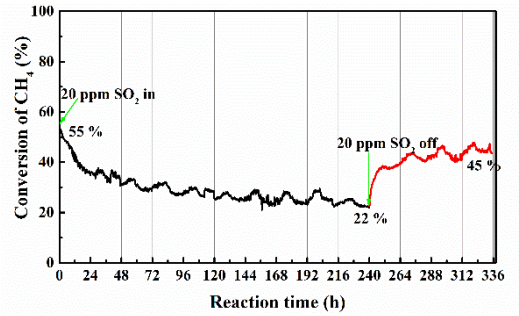

Figure 4: SO_2 resistance of commercial catalyst from Haldor Topsøe (450 ℃, 5 vol.% H_2O, 20 ppm SO_2)

Compared with the immediate activity loss for catalyst (A), catalyst (B) could maintain the original activity for about 20 min and finally the CH_4 conversion was stable at 5 %. Promoting catalyst (B) with adding the promoter in different manners shows no apparent improvement on the SO_2 resistance of catalyst (B). (Figure 5)

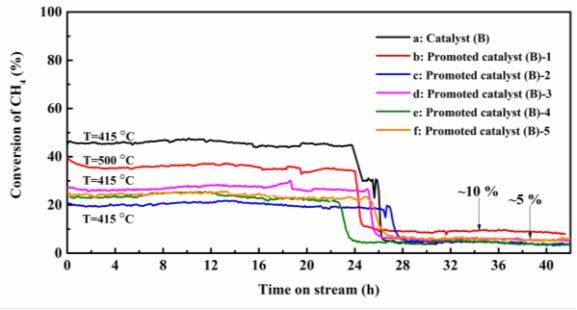

Figure 5: SO_2 resistance of catalyst (B) with and without promoter (5 vol.% H_2O, 20 ppm SO_2)

Conclusions and Future work

Catalyst (B) has comparable activity with catalyst (A) in the presence of 5 vol.% H_2O. Catalyst (A) lost all the activity as soon as 20 ppm SO_2 was introduced into the stream, while catalyst (B) can maintain at the original level for about 20 min and then dropped to 5 %. The promoter shows no enhancement on the SO_2 resistance of catalyst (B).

Future work will mainly focus on the performance of higher loading catalysts.

Acknowledgments

This work is funded by the Blue INNOship project and DTU.

References

1. A. Gremminger, P. Lott, M. Merts, Applied Catalysis B: Environmental 218 (2017) 833-843.
2. J.H. Chen, H. Arandiyan, X. Gao, Catal Surv Aisa 19 (2015) 140-171.
3. Y. Lou, J. Ma, W.D. Hu, ACS Catal 6 (2016) 8127-8139.

Zhibo Zhang

Phone: +45 52695821
E-mail: zhiz@kt.dtu.dk

Type: KT-IPE joint
Supervisors: Manuel Pinelo
Suojiang Zhang
Nicolas von Solms

PhD Study
Started: December 2015
To be completed: November 2018

Ionic Liquids as Bifunctional Cosolvents enhanced CO_2 Conversion Catalysed by NADH-dependent Formate Dehydrogenase

Abstract

The PhD Project focuses on improving conversion of CO_2 catalyzed by formate dehydrogenase. The main bottleneck of enzymatic reaction is the low solubility of the substrate (CO_2) in the liquid media and the low stability of NADH in the presence of CO_2 (acid gas). In order to overcome these problems, a new novel solvent (Ionic liquids) is evaluated. Enzymatic conversion of CO_2 was improved – as compared to the reaction conducted in buffer- after evaluating different kinds of ionic liquids as co-solvents and the reaction mechanism was studied and proposed.

Introduction

To minimize environmental problems and produce clean energy, efficient utilization of CO_2 and carbon regeneration has been the focus of a tremendous amount of research.[1] Enzymatic conversion of CO_2 to formate, formaldehyde, and methanol has inspired many researchers in the past several years.[2] However, enzymatic hydrogenation of CO_2 to formic acid (CH_2O_2), formaldehyde (CH_2O) and methanol (CH_3OH) is hampered by the low concentration of CO_2 that is available for the enzyme (formic acid dehydrogenase) in the reaction mixture. Increasing CO_2 concentration could result in an increased conversion, as reported by Liu.[3] CO_2 is highly soluble in ionic liquids (ILs), and such high solubility is explained via electrostatic forces, van der Waals forces, hydrogen bonds and other physical effects.[4] One serious limitation of conducting the reaction in carbon dioxide is to maintain the stability of NADH, as it is easily affected by the solution's pH. The investigations on the interaction between ILs and coenzyme (NADH) could then play a key role in the conversion of CO_2. NADH is used not only as hydrogen donor to catalyse reduction of CO_2 but is also employed to follow the progression of the reaction and thus it can be used to quantify the produced formate. The objective of present work was to investigate the activity of NADH in ILs to improve the efficiency of enzymatic reaction and to increase enzymatic conversion by capturing CO_2 with ionic liquids.

Specific Objective

The objective of this work is to improve the enzymatic conversion of CO_2 in the contained-IL buffer. In order to achieve such a goal, three requirements have to be met: First, ionic liquids must have great ability to absorb CO_2. Second, the coenzyme (NADH) must keep its activity in the presence of the ionic liquids. Last, formate dehydrogenase should be able to keep its activity in the ionic liquid.

Results and Discussion

Table 1. Stability of NADH in aqueous ILs.

Entry	IL	$Residue_{(NADH)}$ (%) (SD)	pH (SD)
1	IL1	100.0 (± 0.1)	7.8 (± 0.20)
2	IL2	12.8 (± 3.1)	5.3 (± 0.12)
3	IL3	3.1 (± 0.5)	2.8 (± 0.18)
4	IL4	4.7 (± 0.6)	2.6 (± 0.18)
5	IL5	11.1 (± 2.6)	2.3 (± 0.16)
6	IL6	99.7 (± 0.6)	9.3 (± 0.14)

Screen ionic liquids for absorb CO_2.

Six different ILs were selected for enzymatic reaction. These ILs were selected based on the great ability to absorb CO_2 with similar structure in cation and expect to find structure-performance relationship. Besides, these ILs' pH are range from acid to alkali. Therefore, NADH stability will firstly be evaluated in these ILs.

Stability of NADH in ILs

To verify if NADH stability in all kinds of ILs, five ILs were subsequently screened under identical conditions in terms of their respective reactivity with NADH (Table 2, entries 1~5). The results showed that the stability of NADH was found to be highly dependent on the pH value of the system. Under neutral-basic conditions, almost no degradation of NADH was detected (entry 1). In contrast, the concentration of NADH diminished markedly under acidic conditions (entry 2). Notably, under strongly acidic conditions, the absorption at 340 nm assigned to NADH disappeared coincidently with the appearance of a blue-shifted peak at 332 nm. Finally, when IL6 at known to be a strong basic IL was employed rather than imidazolium-based ILs (entry 6), only traces of degradation of NADH were observed. In the following degradation mechanism investigation, the analysis tools UV, NMR were used for identifying degradation procedure. According to experimental results, there are two possible degradation pathways, which were further confirmed by molecular simulation (DFT calculation).

Activity of Formate dehydrogenase (FDH) in ionic liquids.

Table 2. Enzymatic Conversion of CO_2 to Formate

Entry	Solvent(v/v)	Yield of formate (%) (SD)
1	Phosphate buffer	1.1 (± 0.5)
2	10% IL4	0.2 (± 0.3)
3	20% IL4	2.9 (± 0.4)
4	40% IL4	2.3 (± 0.4)

After evaluating these ILs for NADH stability above, IL4 was used for running enzymatic reaction. In the case of IL4, CO_2 conversion reached the maximum at 20% IL4 (2.9%), which is more than two folds as compared with conversion in phosphate buffer (1.1%). As is known, water with small amounts of salts was considered to be the best media for proteins. Normally, high concentration of ILs (salts) will cause conformational changes of peptide chains and cause enzyme denaturation, due to electrostatic unbalance between peptide chains. Crystallization and aggregation of proteins dramatically occurred upon increasing the concentration of ILs. Furthermore, in pure ILs, enzymes can hardly be dissolved in homogenous phase without causing denaturation.

Conclusion

We demonstrated that degradation of NADH occurs during carbon dioxide hydrogenation at low pH The mechanism of NADH degradation was investigated by UV, NMR, and DFT. By selecting neutral-basic ionic liquids and adjusting concentration of the ionic liquids in the buffer, 20% IL4 was the one found to be optimal for conducting the reaction. Finally, CO_2 conversion was more than twice as compared with the enzymatic reaction in the phosphate buffer (traditional buffer). This study is a significant contribution to improve yields formate dehydrogenase catalysed reactions in a novel medium (ionic liquid) and paves the way for improving biocatalysts using ionic liquids.

Acknowledgements

The PhD project is funded by Technical University of Denmark (DTU) and institute of process Engineering, Chinese Academy of Science (IPE, CAS).

References

1. Xu, B. H.; Wang, J. Q.; Sun, J.; Huang, Y.; Zhang, J. P.; Zhang, X. P.; Zhang, S. J., Fixation of CO2 into cyclic carbonates catalyzed by ionic liquids: a multi-scale approach. *Green Chem* **2015,** *17* (1), 108-122.

2. (a) Obert, R.; Dave, B. C., Enzymatic conversion of carbon dioxide to methanol: Enhanced methanol production in silica sol-gel matrices. *J Am Chem Soc* **1999,** *121* (51), 12192-12193; (b) Shi, J. F.; Jiang, Y. J.; Jiang, Z. Y.; Wang, X. Y.; Wang, X. L.; Zhang, S. H.; Han, P. P.; Yang, C., Enzymatic conversion of carbon dioxide. *Chem Soc Rev* **2015,** *44* (17), 5981-6000.

3. Wang, Y. Z.; Li, M. F.; Zhao, Z. P.; Liu, W. F., Effect of carbonic anhydrase on enzymatic conversion of CO_2 to formic acid and optimization of reaction conditions. *J Mol Catal B-Enzym* **2015,** *116*, 89-94.

4. D'Alessandro, D. M.; Smit, B.; Long, J. R., Carbon Dioxide Capture: Prospects for New Materials. *Angew Chem Int Edit* **2010,** *49* (35), 6058-6082.

Liyan Zhao

Phone: +45 50271099
E-mail: liyzh@kt.dtu.dk

Type: CSC
Supervisors: Kim Dam-Johansen
Weigang Lin
Hao Wu

PhD Study
Started: May 2018
To be completed: May 2021

Mechanisms of High Temperature Agglomeration in Fluidized Beds

Abstract
This PhD project focuses on the mechanisms of high temperature agglomeration in fluidized bed combustion/gasification of biomass. In this project, a series of experiments will be performed to achieve a systematic understanding of the bed agglomeration mechanisms in fluidized bed combustion/gasification, including the influence of operational parameters, biomass composition and bed materials, and so on. The differences and connections between the agglomeration mechanisms of combustion and that of gasification in fluidized bed at high temperature also be investigated. Based on the experimental results, an applicable model will be developed to predict the agglomeration tendency in fluidized beds, and some countermeasures can also be put forward. The understanding of the mechanisms of formation and breakage of agglomerates in a fluidized bed is important for effectively control of the agglomeration problem in combustion/gasification of biomass.

Introduction
The fluidized-bed combustors/gasifier are applied in large scale operations extensively due to their advantages of better temperature distribution, higher conversion efficiency, lower investment and maintenance costs, and better heat and mass transfer[1,2]. However, bed agglomeration is a vital problem in biomass fluidized bed combustion/gasification, which can strongly influence the performance of combustors/gasifier and eventually leads to the defluidization and unscheduled plant shutdown[3].

In order to control the agglomeration in the fluidized bed combustion/gasification, the mechanisms of agglomeration are studied broadly[4,5]. Bed agglomeration phenomenon is attributed to the high alkaline content contained in biomass, such as K and Na, will be released during combustion/gasification and a eutectics with low melting point is formed by alkaline metals and bed materials at high temperature. The homogeneous phase formed on the surface of bed materials enhances the stickiness of bed particles, results in increasing number of particles attaching together and the agglomeration occurs in the end. The interaction between bed particles and inorganic compounds in biomass can be distinguished into two different mechanisms: chemical reaction and decomposition of ash[6,7].

It is found that for different biomass, the agglomeration mechanisms are various[8]. It is owing to the constitute of biomass are different, especially the content of alkali metal (K, Na, Ca), sulfur and chlorine[9,10]. In addition, the operation temperature, gas velocity also seriously affect the performance of reactor[11]. Therefore, the influence of operational parameters, biomass composition and bed materials[11,12] on the agglomeration mechanisms are important to the systemically understanding of the process.

Even for the same kind of fuel, the characteristics and mechanisms of agglomeration during combustion and gasification also may be different. On the other hand, there are some connections between the agglomeration during combustion and gasification[13]. The understanding of the mechanisms of formation and breakage of agglomerates in a fluidized bed is important for effectively control of the agglomeration problem in combustion/gasification of biomass.

Specific Objectives
This PhD project focuses on the mechanisms of high temperature agglomeration in fluidized bed combustion/gasification of biomass. The objectives are to:

- Investigated the influence of operational parameters, biomass composition and bed materials on the agglomeration mechanisms

- Investigated the differences and connections between the agglomeration mechanisms of combustion and that of gasification in fluidized bed at high temperature
- Develop an applicable model to predict the agglomeration tendency in fluidized bed combustion/gasification
- Put forward some countermeasures for the agglomeration in fluidized bed combustion/ gasification

Approaches

The experimental work of this project will be operated on a laboratory-scale fluidized bed reactor in DTU Chemical Engineering. This setup will be applied to systematic investigate the bed agglomeration behaviors during combustion/gasification of various biomass under a serials of experimental conditions. The influences of biomass compositions, operational parameters (including different temperature, excess air ratio, superficial velocity etc.), various additives and alternative bed materials on combustion/gasification performance will be investigated.

During the whole experiment, the temperature and pressure distribution in the fluidized bed are on-line monitored in order to control the whole process and detect the occurrence of agglomeration phenomenon. In addition, various ex-situ measurements (e.g. scanning electron microscopy coupled with energy-dispersive x-ray spectroscopy (SEM/EDS), x-ray diffraction (XRD), thermogravimetric analysis (TGA), inductively coupled plasma optical emission spectroscopy (ICP-OES)) will be used to characterize and analyze the fuel/char samples and the bed materials before/after combustion/ gasification.

Acknowledgements

This project is funded by China Scholarship Council and Technical University of Denmark.

References

1. S. Palzer, Powder Technol. 206(1–2) (2011) 2–17
2. M. M. Saad, A. Barkouti, E. Rondet, T. Ruiz, and B. Cuq, Powder Technol. 208(2) (2011) 399–408
3. W. Lin, K. Dam-Johansen, F. Frandsen, Chem. Eng. J. 96(1–3) (2003) 171–185
4. F. Scala, Fuel Process. Technol. 171 (2018) 31–38
5. M. Bartels, W. Lin, J. Nijenhuis, F. Kapteijn, and J. R. van Ommen, Prog. Energy Combust. Sci. 34(5) (2008) 633–666
6. M. Öhman, A. Nordin, B. J. Skrifvars, R. Backman, and M. Hupa, Energy and Fuels 14(1) (2000) 169–178
7. H. J. M. Visser, H. Hofmans, H. Huijnen, R. Kastelein, and J. H. A. Kiel, Prog. Thermochem. Biomass Convers. (2008) 272–286
8. E. Brus, M. Öhman, and A. Nordin, Energy and Fuels 19(3) (2005) 825–832
9. H. J. M. Visser, S. C. van Lith, and J. H. a. Kiel, J. Energy Resour. Technol. 130(1) (2008) 11801
10. A. E. Ghaly, A. Ergüdenler, and E. Laufer, Bioresour. Technol. 48(2) (1994) 127–134
11. P. Chaivatamaset and S. Tia, Appl. Therm. Eng. 75 (2015) 1134–1146
12. A. E. Ghaly, A. Ergüdenler, and E. Laufer, Biomass and Bioenergy 5(6) (1993) 467–480
13. M. Öhman, L. Pommer, and A. Nordin, Energy and Fuels 19(4) (2005) 1742–1748

Sino-Danish Center for Education and Research (SDC),
University of Chinese Academy of Sciences (UCAS)

Technical University of Denmark

中国科学院大学
University of Chinese Academy of Sciences

SDC
The university partnership
Denmark – China